GDI-Mediated Cdc42 Recycling at Polar Cortex in Dynamic Maintenance of Cell Polarity in *Saccharomyces cerevisiae*

Thesis

UNRESTRICTED

GDI-mediated Cdc42 recycling at polar cortex in dynamic maintenance of cell polarity in *Saccharomyces cerevisiae*

A Thesis Submitted for the Degree of

Doctor of Philosophy

by

Arupratan Das, MSc

Stowers Institute for Medical Research,

an Affiliated Research Centre of the Open University

October 2011

Date of Submission: 28 October 2011
Date of Award: 14 February 2012

ProQuest LLC.
789 East Eisenhower Parkway
P.O. Box 1346
Ann Arbor, MI 48106 – 1346

Acknowledgement

I heartily thank Dr. Rong Li. She has been my inspiration as my excellent mentor. Her constant support, encouragement and guidance allowed me to progress steadily. Her guidance allowed me to thrive as an independent researcher and her constant teaching on how to approach new problems, boosted my knowledge, confidence and skills, which allows me to enjoy science even more.

I would like to thank my collaborator Brian D. Slaughter for his support, discussions and training in several microscopic and spectroscopic based techniques that I routinely used in my doctoral research, Jay R. Unruh and Boris Rubinstein for their assistance in data analysis. I sincerely thank my committee members: Drs. Sue Jaspersen, Paul Kulesa and Winfried Wiegraebe for all the suggestions and guidance during my doctoral research. I am thankful to Dr. Leanne Wiedemann, my UK experienced supervisor for her constant monitoring and assistance during the doctoral research and Shelly Hornbuckle for keeping all the meetings and documents on track. I am grateful to Stowers for giving me an opportunity to do my doctoral research in such a wonderful institute. I would like to thank the Stowers' core facilities such as Microscopy and Molecular biology, without their constant help my doctoral research would not have been accomplished.

I am thankful to my lab members for creating a wonderful work atmosphere. Frequent discussions with lab mates and their inputs during lab meetings improved my doctoral research in many ways. I would like to thank Mary Toth, senior administrative assistant in Rong Li lab for her help in organizing meetings, reminders and for all the fun discussions.

Finally, I am grateful to my parents Ranu Das and Gaya Prasad Das and my sister Bandana Das. Without their constant support and encouragement I would not have reached this point. I also thank my fiancée Parama Paul for being supportive and encouraging in all the difficult phases of such a long endeavor.

ARC12
(August 2011)

The Open University

RESEARCH SCHOOL

Affiliated Research Centre Programme

Library Authorisation

Please read and complete this form in conjunction with the ARC\S11G Examination Guidelines for Students. You should return this form to the Research School, The Open University, Walton Hall, Milton Keynes, MK7 6AA with the two bound copies of the thesis and any non-book component, if applicable to be deposited with the University Library. Please note that only theses which comply fully with the binding and presentation criteria as set out in the research degree regulations and the ARC\S11G Examination Guidelines for Students will be accepted for deposition in the University Library. All candidates should complete parts one and two of the form. Part two only applies to PhD candidates.

Part One: Candidate Details

Name: Arupratan Das PI: Y920821X

Degree: Ph.D. Affiliated Research Centre: Stowers Institute for Medical Research

Thesis title: GDI-mediated Cdc42 recycling at polar cortex in dynamic maintenance of cell polarity in *Saccharomyces cerevisiae*

Part Two: British Library Authorisation [PhD candidates only]

If you want like a copy of your PhD thesis to be available on loan to the British Library Thesis Service as and when it is requested, please tick Section A of this form.

The University has agreed that your participation in the British Library Thesis Service should be voluntary. Please tick either (a) or (b) to indicate your intentions.

a) [X] I am willing for The Open University to loan the British Library a copy of my thesis.

b) [ ] I do not wish The Open University to loan the British Library a copy of my thesis.

Part Three: Open University Library Authorisation

I confirm that I am willing for my thesis to be made available to readers by The Open University Library, and that it may be photocopied, subject to the discretion of the Librarian.

Signed: _____ Date: 08 March 2012

An electronic version of this form can be downloaded from http://www.open.ac.uk/research/research-degrees/affiliated-research-centre-programme/affiliated-research-centres.php

Thesis abstract

Cell polarization is a fundamental requirement for development and many physiological processes such as cell motility, stem cell differentiation, immune response and neuronal polarity. Small G-protein Rho GTPase, Cdc42 has long been shown to be the key regulator of the polarization process. In this study we aim to understand how cell maintains an optimum Cdc42 concentration at the polar cortex, and how distinct polarized Cdc42 distribution is achieved based on its recycling pathways taking budding yeast as a model system.

Our in depth study revealed that Cdc42 at yeast polar cortex is dynamically maintained via two redundant pathways of distinct response time. A slow pathway dependent on actin-mediated endocytosis and exocytosis and a fast response pathway dependent on Rdi1, yeast GDI (guanine dissociation inhibitor) for Rho GTPases. Quantitative imaging and mathematical modeling found both the pathways to be spatially overlapping in order to have physiological Cdc42 distribution. We further demonstrated Cdc42 GTPase cycle as the common regulator of actin and Rdi1 mediated pathways, a process supports their concentric localization.

We further focused on gaining mechanistic insight of Rdi1-mediated Cdc42 recycling at polar cortex. Using a high throughput genetic screen, imaging, spectroscopy and mathematical modeling we found that phospholipid asymmetry at the polar cortex regulated by lipid flippase complex (Lem3-Dnf1 and Lem3-Dnf2) plays a key role in Rdi1 mediated fast dissociation of Cdc42 from the polar cortex. Our finding suggests that flipping of phosphatidylethanolamine (PE), a phospholipid with a positively charged head group, reduces the charge interaction between a Cdc42 C-terminal cationic region with the inner leaflet of the polar cortex, a key step for fast Rdi1 mediated Cdc42 extraction. In *Δlem3* cells the negatively charged phospholipid phosphatidylserine (PS) is enriched in the inner leaflet of plasma membrane, as demonstrated by analysis of Cdc42 mutants with altered charge properties and biosensor for PS. Increase in PS in the inner leaflet increases Cdc42 and plasma membrane charge interaction antagonizing Rdi1-mediated Cdc42 extraction. Using an in vitro assay with reconstituted supported lipid bilayers, we further demonstrated that relative composition of PE versus PS directly modulates the rate of Cdc42 extraction from the membrane by GDI.

Table of Contents

Table of Figures

Table of Tables

Abbreviations

FRAP	Fluorescence recovery after photobleaching
iFRAP	inverse of fluorescence recovery after photobleaching
FCS	Fluorescence correlation spectroscopy
FCCS	Fluorescence cross-correlation spectroscopy
APD	Avalanche photodiode
PM	Plasma membrane
PS	Phosphatidylserine
PE	Phosphatidylethanolamine
PC	Phosphatidylcholine
PIP2	Phosphatidylinositol 4,5-biphosphate
PIP3	Phosphatidylinositol 3,4,5-triphosphate
SLB	Supported lipid bilayer
GEF	Guanine nucleotide exchange factor
GDI	Rho GDP dissociation inhibitor
ER	Endoplasmic reticulum
TGN	trans-Golgi network

Chapter 1. Introduction

Cell polarity in biology is the ultimate example of symmetry breaking; it is a natural process that evokes many beautiful patterns as it orchestrates several essential processes at the cellular or organismal level. By definition, a spherically symmetrical cell that creates a specialized domain at the plasma membrane in the presence of spontaneous or external cues, is called a polarized cell (Drubin and Nelson, 1996). The study of cell polarity became the central focus of cell and developmental biologists as they became aware that it is essential for many biological processes such as cell motility, active absorption in epithelial cells, neuronal growth, and immune response. A broad range of cell types (for example: budding yeast to mammalian epithelial cells) undergo cell polarity. These cell types, while each having unique molecular players, share many conserved mechanistic modules, including the Rho GTPase Cdc42 module, that has been established to be the central regulator of cell polarity (Etienne-Manneville, 2004).

In a quest to understand the process in depth, extensive studies have been undertaken using traditional genetic, biochemical and modern imaging approaches (Li and Bowerman, 2010). The study of cell polarity can be divided into two steps: 1) symmetry breaking, which leads to the establishment of cell polarity and 2) maintenance of the polarized distribution of molecules. Together these two processes give rise to polarized morphogenesis, which is required for the developmental or physiological responses of the cells (Li and Gundersen, 2008). While the symmetry breaking process has been well elucidated recently, knowledge of maintenance is still not fully enriched.

Stable cell polarity is critical for cellular morphogenesis and differentiation. The Cdc42 small GTPase localizes to the site of polarized growth in yeast and orchestrates the structural and signaling events required for budding and formation of mating projections (Etienne-Manneville, 2004; Pruyne and Bretscher, 2000a; Slaughter and Li, 2006). Prior work has shown that a polarized Cdc42 distribution is maintained dynamically through two colocalizing pathways of recycling to counter Cdc42 diffusion (Marco et al., 2007; Slaughter et al., 2009; Wedlich-Soldner et al., 2004). Whereas a slower pathway works through actin-based membrane trafficking; a more rapid Cdc42 recycling pathway is mediated through Rdi1, the yeast guanine nucleotide dissociation inhibitor (GDI) for Rho family GTPases (Masuda et al., 1994). GDI is known to extract Rho

GTPases from the plasma membrane by forming a complex that involves both protein-protein contacts and the binding of GDI to the prenyl lipid anchor at the COOH terminus of the GTPases (DerMardirossian and Bokoch, 2005; Johnson et al., 2009). We found that in vivo, the rate of the Rdi1-mediated Cdc42 dissociation can be tuned to shape Cdc42 distribution at the polar cortex during distinct morphogenetic processes (Slaughter et al., 2009).

A combination of high-throughput genetic screening, molecular biology, cutting edge microscopy, spectroscopy and *in vitro* techniques are used in this research to decipher molecular players ranging from polarized plasma membrane to cytosol which are involved in the maintenance of polarized Cdc42 distribution in budding yeast *Saccharomyces cerevisiae*. The introduction chapter will discuss several aspects of a cell's intrinsic ability to break symmetry through polarity establishment and then maintenance, while successive chapters will explore our understanding of the maintenance process through our research.

1.1. Cdc42 Rho-GTPase signaling module in establishment and maintenance of cell polarity

Over the last two decades, the study of cell polarity became one of the important areas in cell biology. Our understanding at the molecular level began with the discovery of Rho-GTPase Cdc42 in budding yeast (Adams et al., 1990). The Cdc42 ts-mutant is unable to form a bud and it grows into a large unbudded cell at restrictive temperatures, while the nuclear cycle continues (Adams et al., 1990). This observation showed Cdc42 as the key player required for polarity establishment and leads to the hypothesis of budding (polarity) and nuclear division being independent processes in the cell cycle. Earlier, similar observations were also found regarding Cdc24 ts mutants (Hartwell et al., 1974; Hartwell et al., 1973). Cdc24, a yeast protein originally found as an upstream effector of Cdc42 (Bender and Sprague, 1989; Ron et al., 1991) shares sequence similarity with mammalian GEF (Guanine nucleotide exchange factor), Dbl (Eva and Aaronson, 1985; Hart et al., 1991) and subsequently found to be a yeast Cdc42 GEF (Hart et al., 1994). Above observations indicate Cdc42 is essential for polarity establishment and its polarized localization is probably regulated by Cdc42 GTPase cycle involving Cdc24 GEF activity. After two decades, a series of interesting studies established that both the hypothesis were correct (Etienne-Manneville, 2004). Cdc24p was found to be sequestered inside the nucleus in complex

with Far1p during G1 phase (Nern and Arkowitz, 2000). At the end of the G1 phase, the cyclin-Cdk complex (Cdc28-cln2) activates and degrades the nuclear Far1p which then leads to Cdc24 nuclear exit and recruitment to the presumptive bud site (Shimada et al., 2000). These observations conclude that bud formation is linked through Cdc24. The localized accumulation and activation of Cdc42 at the site of polarization was believed to be through Cdc24; however, a constitutively active form of Cdc42 mutant can still accumulate at the plasma membrane in G1 arrested cells when Cdc24 should be inactive, albeit randomly (Caviston et al., 2002; Wedlich-Soldner et al., 2003). This indicates Cdc42 is activated at the polar site and the spatial regulation is Cdc24 dependent. Polarized morphogenesis during spontaneous budding or formation of mating projection (shmoo) requires directed growth of plasma membrane and cell wall in budding yeast and depends upon several structural and signaling events which are orchestrated through active Cdc42 (Fig. 1) (Etienne-Manneville, 2004; Pruyne and Bretscher, 2000b; Slaughter and Li, 2006). Mathematical simulation has shown that stochastic accumulation of active Cdc42 at the plasma membrane amplifies Cdc42 concentration through a positive feedback loop possibly through polarized growth of actin cables (see below) (Wedlich-Soldner et al., 2003). Active Cdc42 at the site of polarization interacts directly or indirectly with downstream effectors to establish and successively maintain the polarized morphogenesis (Fig. 2). Once active Cdc42 determines the site of polarization, it interacts and promotes septin assembly which forms an hourglass structure that separates the budding site from the mother. Successive interactions with other effectors like p21 activated kinase (Ste20p, Cla4p) initiates actin structure formation at the polarized site which provides a route for membrane trafficking and polarized accumulation of polarity ingredients.

1.2. Polarization from yeast to mammalian cell

1.2.1. Yeast Polarization

Budding yeast has long been proven to be an excellent model system for polarity study as it is a unicellular eukaryotic organism with relative ease of genetic manipulation, biochemistry and live cell imaging which helped to understand the process in depth and many of the mechanisms found to be conserved. Yeast cells display an ideal system for studying both spontaneous and

external cue dependent polarity as it breaks symmetry during cell division (budding) or in the presence of mating pheromone (Slaughter and Li, 2006) (Fig. 1).

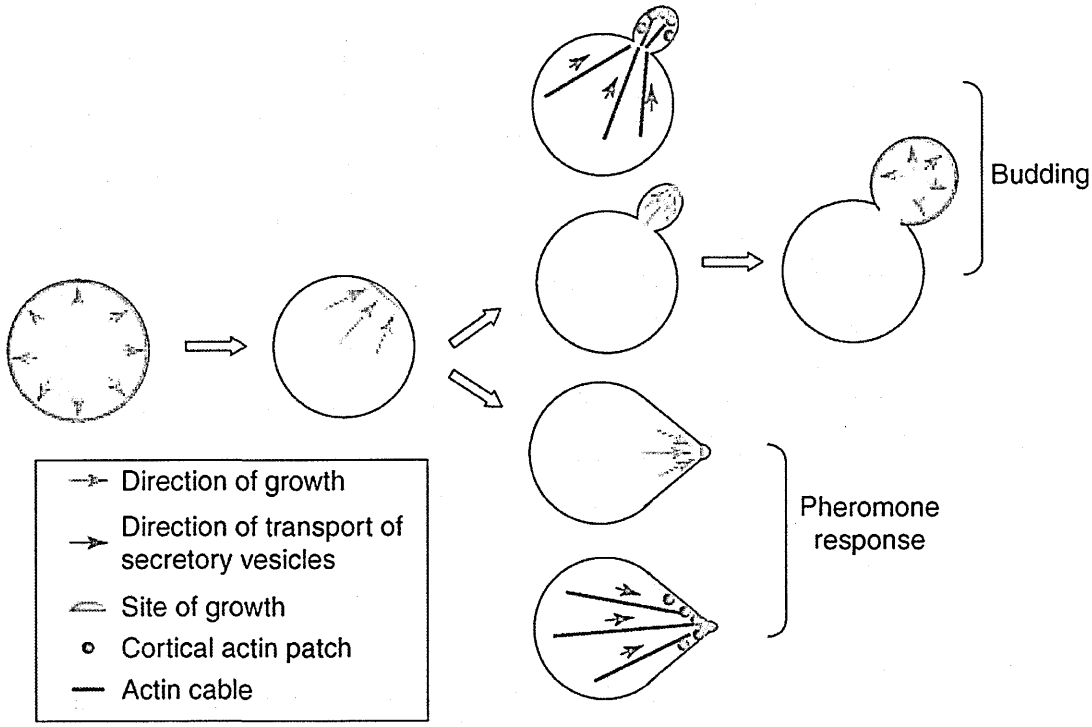

Figure 1-1. Polarized morphogenesis during spontaneous budding or in the presence of external stimuli pheromone.

Polarized secretion, direction of actin cable growth and actin patch assembly as depicted in the figure will be further explained in this chapter. This figure is taken from (Slaughter and Li, 2006).

Based on intrinsic and spatial cues, yeast cells can break symmetry in three different ways; axial, bipolar and unipolar (Drubin and Nelson, 1996) (see Fig. 3 a, b, c and therein references), each with unique molecular components. Genetic analysis revealed GTP binding protein Rsr1p (also known as Bud1p) is required for bud site selection, and Rho GTPase Cdc42p for bud site assembly; both are common for axial and bipolar budding (Drubin and Nelson, 1996) while Axl1p (Fujita et al., 1994) is unique for axial budding.

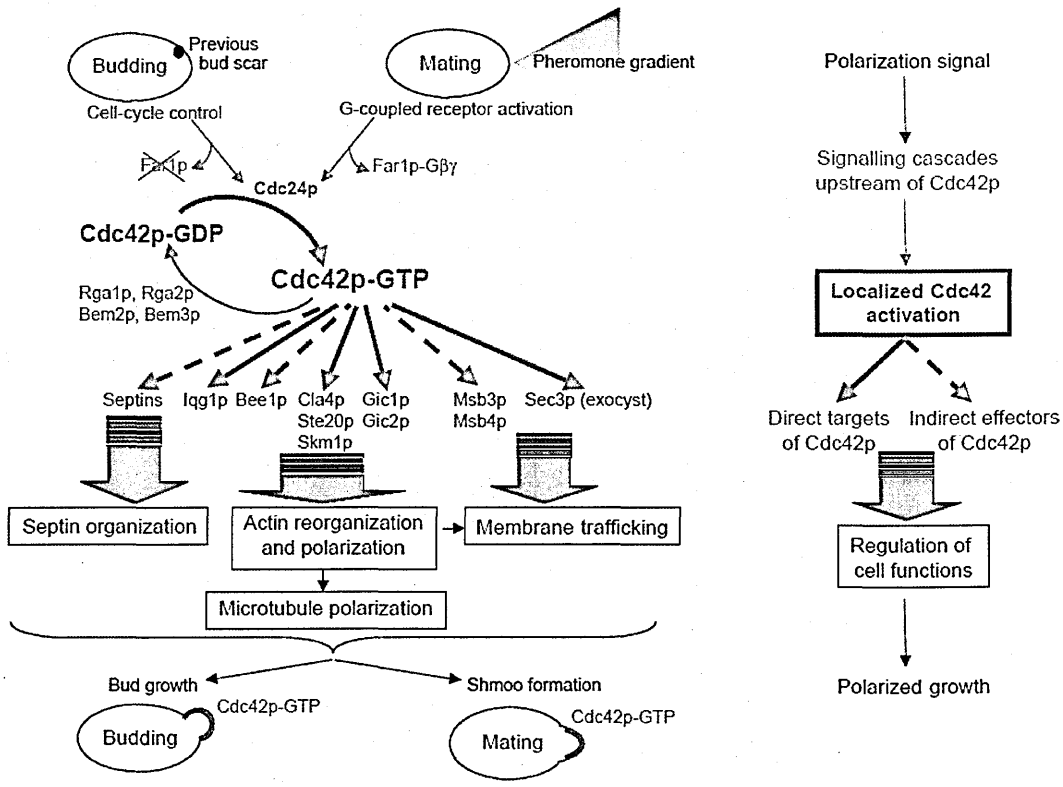

Figure 1-2. Cdc42 accumulation and initiation of different signaling cascades during spontaneous budding or in the presence of pheromone.

Active Cdc42, GTP bound (green) is shown to interact directly (solid green line) or indirectly (dashed line) with downstream effectors which in turn promotes septin organization or actin polarization that helps to accumulate polarity proteins through membrane trafficking. This figure is taken from (Etienne-Manneville, 2004).

1.2.2. Positive feedback loops in polarity establishment

Decades of genetic analysis have revealed many molecular players and advanced the understanding of how cells determine the axis of polarity and the molecules that drive the polarized assembly; however, it was still unclear how a spherically symmetrical cell recognizes and amplifies a stochastic signal which leads to polarized morphogenesis, especially in the cellular milieu of noisy signals. Intriguingly, it was found that a cell can polarize independent of the bud scar, albeit in random orientations (Butty et al., 2002; Irazoqui et al., 2003). An influx of quantitative imaging and mathematical modeling during last decade has helped us to understand that cell polarity is dependent on coupled positive feedback loops (Brandman et al., 2005; Wedlich-Soldner et al., 2004). In the absence of any preexisting cues the constitutively active form of $Cdc42^{GTP}$

($Cdc42^{Q61L}$) can form a polar cap in random orientation. Mathematical modeling showed that a positive feedback loop comprised of actin based transport of $Cdc42^{GTP}$ and $Cdc42^{GTP}$ mediated

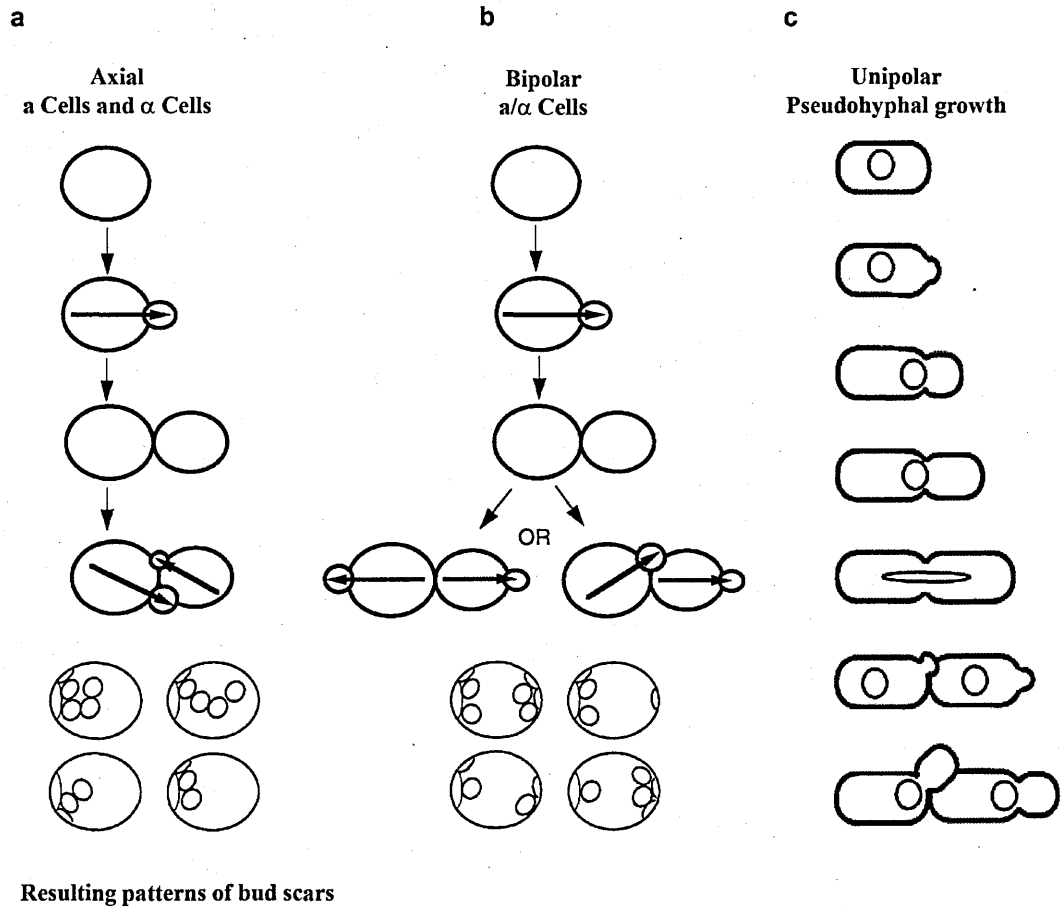

Figure 1-3. Bud formation pattern relative to the previous cell division site (marked by the bud scar)

(a) Axial budding pattern, where *MATa* and *MATα* cells form bud adjacent to the previous cell division site. (b) Bipolar budding pattern, where diploid yeast cells (*MATa/MATα*) form bud either closer to the previous bud site or to the opposite end of the cell (c) Unipolar budding pattern, during nitrogen starvation yeast cell growth switches to pseudohyphal (PH) form from yeast form (YF) (Kron et al., 1994). Under PH growth, cell buds always form the opposite end of the previous cell division site. Arrows within the cells indicate axes of polarity. (a) and (b) are taken from (Chant, 1999) and (c) is from (Kron et al., 1994).

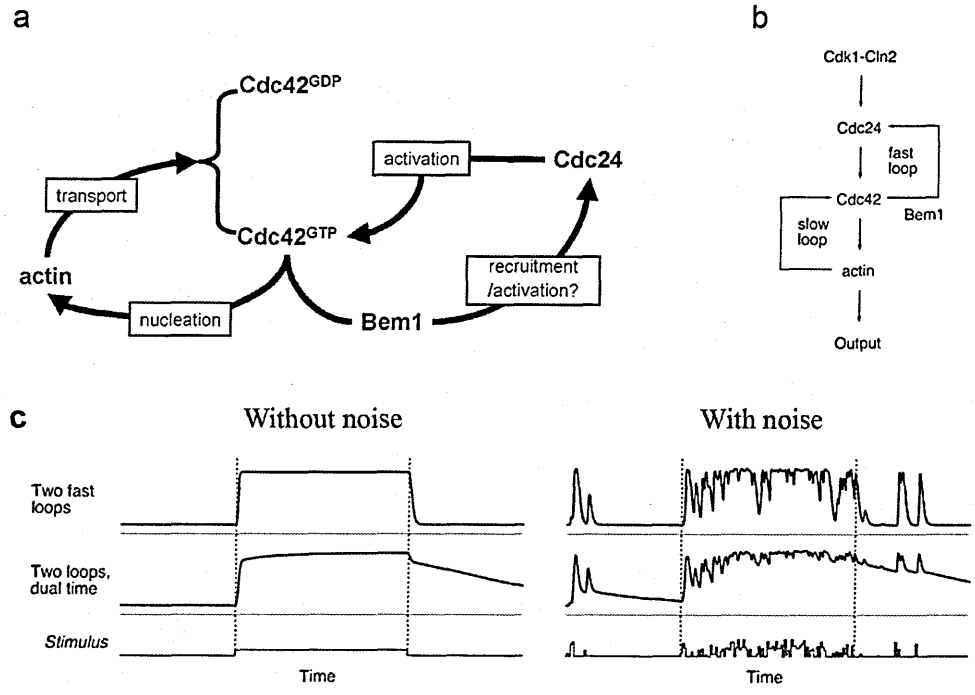

Figure 1-4. Cdc42 recycling with two pathways of dual response time.

(a) Schematic diagram explains how two positive feedback loops are coupled to give rise to robust cell polarity on yeast plasma membrane. Actin based feedback loop increases Cdc42 concentration at plasma membrane. Active Cdc42 activates and/or recruits GEF Cdc24 via Bem1 to the site of Cdc42 accumulation which in turn increases active Cdc42 concentration. (b) Schematic diagram of positive feedback loops with dual response times in yeast polarity, input for the mathematical simulation in **c**. (c) Simulated response in presence of stimulus. Two fast positive feedback loops turn on and off the switch very quickly with high susceptibility to noise. In contrast, in systems with coupled fast and slow positive feedback loops, the output turned on rapidly and turned off slowly. Importantly, the dual time switch eliminated the stimulus noise while in on state. (a) is taken from (Wedlich-Soldner et al., 2004), (b) and (c) are from (Brandman et al., 2005).

actin polymerization is sufficient to form a stable polar cap from stochastic accumulation of $Cdc42^{GTP}$ at the plasma membrane (Wedlich-Soldner et al., 2003). It was found that cells still can form a polar cap in the presence of Latranculin A (LatA), an inhibitor of actin polymerization, via a mechanism involving Bem1 which interacts with $Cdc42^{GTP}$ and Cdc24 (GEF, of Cdc42) directly on the plasma membrane (Irazoqui et al., 2003). Crucial pieces of evidence came from our lab when

cell polarization kinetics was measured in synchronous culture released from G1 at different conditions. Delayed polarization was observed in the presence of LatA and Δ*bem1* individually; however, in the presence of both LatA and Δ*bem1*, polarization was completely abolished (Wedlich-Soldner et al., 2004). This observation indicates actin and Bem1 operate within two parallel positive feedback loops, and each of them can independently amplify and stabilize a stochastic accumulation of Cdc42, generating stable output of Cdc42 polarized distribution. However, direct evidence of Bem1, as a component of positive feedback loop is still to be obtained. In the presence of only actin-dependent pathway (i.e., in Δ*bem1* cell) bipolar cellular morphology often observed however, in the absence of actin pathway (Wt + LatA), the polar cap tends to flicker and the population divides into polarized and non-polarized groups which was never observed in the wild-type cell (Wedlich-Soldner et al., 2004). Therefore, to have cell polarity with robust spatial and temporal stability, it was assumed to have a coupling between actin based and Bem1 based feedback loops (Fig. 4a and Wedlich-Soldner et al., 2004).

Immediately after this observation, mathematical modeling elegantly demonstrated that coupling two positive feedback loops, one with slow response (actin) and the other with fast response (Bem1), the output of Cdc42 polarized distribution turned on quickly due to the kinetics of fast pool and remained stable for a prolonged period of time due to the kinetics of slow pool, eliminating the stimulus noise while its "on" (Fig. 4 b, c and Brandman et al., 2005).

The Role of actin-mediated positive feedback loop in yeast cell polarity was well understood; however the involvement of other cytoskeletal filament microtubule in yeast polarity is not clear till now. Microtubule found to be an important cell polarity regulator in other eukaryotes such as fission yeast *Schizosaccharomyces pombe* and in complex animal systems (see below). In S. *pombe* polarity regulator tea1p binds to growing microtubule plus end and associates with the cell cortex when microtubule reaches to the cell cortex (Snaith and Sawin, 2003) which is required for polarized growth. It was also found polarized localization of tea1p is dependent on mod5p which is also polarized and in the absence of one other gets depolarized, this indicated the existence of microtubule-mediated positive feedback loop involving tea1 and mod5 in regulation of fission yeast polarity (Snaith and Sawin, 2003).

1.3. Cell Polarization in animal systems

In multi-cellular organisms, cells polarize primarily due to sensing the external environment through contact receptors such as integrins, cadherins, or external stimuli such as chemokines through chemokine receptors (Etienne-Manneville, 2004). One example for cell-cell contact-induced polarity is the formation of a polarized adhesive surface in T cells when they are in contact with an antigen-presenting cell. The polarized T cell surface is generated through the engagement of the T cell receptor (TCR) which accumulates Cdc42 and initiates polarized secretion through actin cables (Cannon and Burkhardt, 2002). Cell motility in migrating fibroblasts relies upon polarized and coordinated activation of GTPases, Rac1, RhoA and Cdc42 which regulate cytoskeleton dynamics at the leading edge (Machacek et al., 2009). A biosensor based study revealed the spatio temporal activation pattern of above GTPases at the leading edge. RhoA is activated and initiates protrusion at the leading edge while Cdc42 and Rac1 activates 2μm behind the edge with 40sec delay (Machacek et al., 2009). This suggests that activation of RhoA initiates leading edge protrusion, while Cdc42/ Rac1 stabilizes and maintains the protruded end. Such patterns of Cdc42 activation reflect its role in sustained polarized morphogenesis, contrasting rapidly moving cells which require rapid protrusion contraction at the leading edge. Indeed, it was observed that in fast moving cells like neutrophils, the absence of Cdc42 does not affect protrusion formation but rather inhibits formation of a stable leading edge of a single cell (Etienne-Manneville, 2004).

1.3.1. Diverse regulatory processes in symmetry breaking and polarity maintenance in animal cell polarity

Polarization in mammalian cells follows the similar principle steps as in yeast that is symmetry breaking which leads to polarity establishment and then maintenance. In animal cells a coordinated crosstalk between cytoskeletal filaments actin, microtubule, associated myosin motor proteins and signaling molecules renders initial symmetry breaking and polarity maintenance (Li and Gundersen, 2008).

Polarization through contractile actomyosin network

A classic example of symmetry breaking driven by contractile actomyosin (myosin-II) network is the anterior-posterior (A-P) polarity of *Caenorhabditis elegans* (C. *elegans*) zygote (Munro et al., 2004). Asymmetric distribution of PAR (partitioning defective proteins) undermines the A-P polarity. PAR-3, PAR-6 along with atypical protein kinase C (aPKC) asymmetrically localize to the anterior cortex of the zygote while PAR-1 and PAR-2 localize to the posterior cortex (Li and Gundersen, 2008). Upon sperm entry at the presumptive posterior cortex actomyosin network gets weaken, resulting in asymmetry in the contraction force and the net contraction of the network drives towards anterior site (Fig. 5). PAR-3 and PAR-6 move toward the anterior site while PAR-2 remains at the posterior site inhibiting myosin recruitment hence posterior directed contractile movement (Li and Gundersen, 2008). The anterior localization of PAR-3-PAR-6-aPKC and posterior localization of PAR-2 further antagonize the ability of mutual localization at the cortex (Hao et al., 2006; Watts et al., 1996), a process further enhances the maintenance phase.

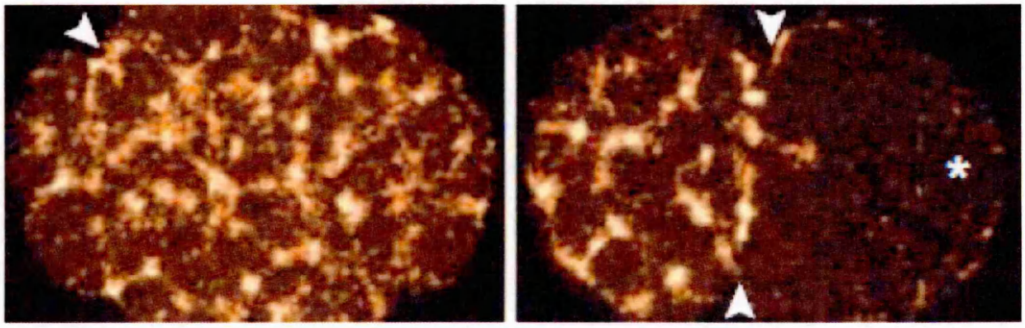

Figure 1-5. Anterior-posterior (A-P) polarity in C. *elegans* zygote.
The images show cortical network of myosin-II, left panel (before) and the right panel (after) symmetry breaking. Arrows indicate cleavage furrows on the egg surface while the asterisk marks the site of sperm entry. This figure is taken from (Li and Gundersen, 2008).

The above example of A-P polarity is seemed to be via affected Rho GTPase signaling upon sperm entry (Cowan and Hyman, 2004; Motegi and Sugimoto, 2006) as Rho-GTP can stimulate both myosin-II activation and formin proteins required for actin nucleation (Piekny et al., 2005).

Polarization through microtubules

While actin often plays a key role in the initial symmetry breaking process, neurons display an exception where microtubule drives the initial symmetry breaking (Li and Gundersen, 2008). Neurons are highly polarized cell with multiple undifferentiated neurites, cultured embryonic rodent hippocampal neurons showed that one of the neurites breaks symmetry and starts growing rapidly to form axon and over time the shorter neurites begin to grow and differentiate into dendrites (Arimura and Kaibuchi, 2007; Wiggin et al., 2005). The differentiated axon and dendrites can be detected from corresponding markers, microtubule associated dephosphorylated tau protein and microtubule associated protein 2 (MAP2) (Binder et al., 1985; Matus et al., 1981). It is well documented that microtubules in the neuronal processes are more stable compared to the proliferating cells, from experiments that showed neural microtubule resistant towards microtubule depolymerizing drugs and higher level of post translationally modified tubulin (Baas and Black, 1990; Ferreira and Caceres, 1989).

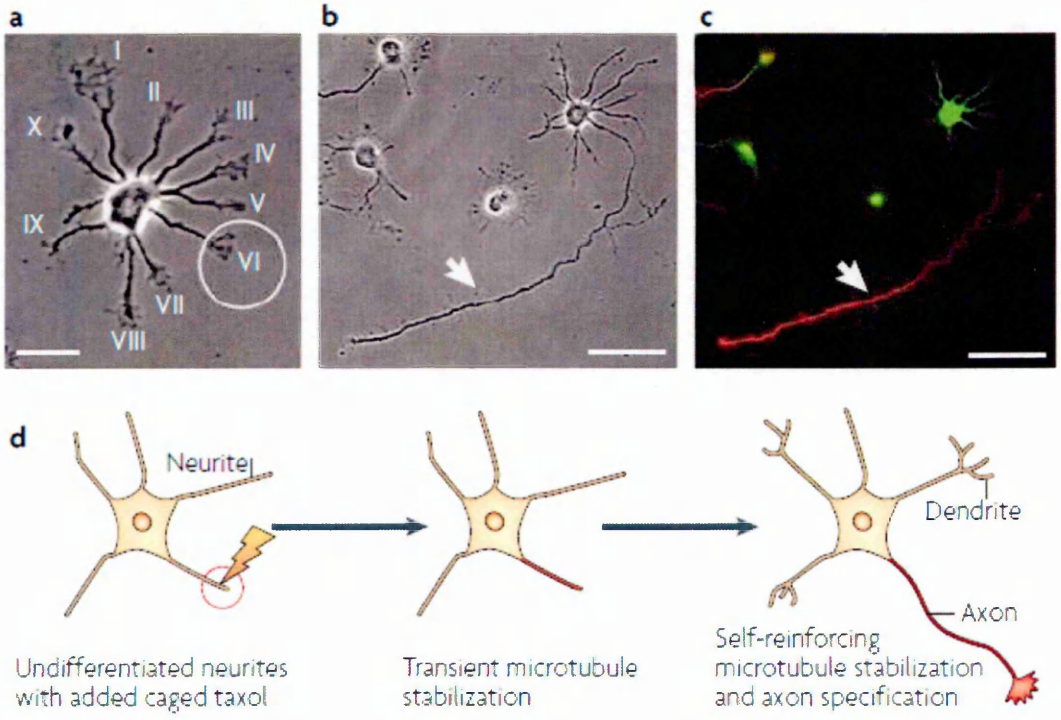

Figure 1-6. Microtubule driven symmetry breaking in neurites.
(a-c) transient activation of taxol stabilizes microtubule in a single undifferentiated neurite, which is sufficient to differentiate into axon. (a) Circled neurite just before photoactivation

of the shielded taxol at the tip of the neurite. (b) 2 days after the taxol treated neurite transformed into axon. (c) Immunofluorescence (Vazquez et al., 2006) of the neurons shown in (b). Green: MAP2, dendritic marker and red: dephosphorylated tau, axonal marker. (d) Summary of the result shown in a-c, transient stabilization of microtubule is sufficient to differentiate a neurite into axon. This figure is taken from (Li and Gundersen, 2008).

It was elegantly shown that local activation of microtubule in an undifferentiated neurite is sufficient to form an axon by photoactivating a taxol analogue, microtubule stabilizing agent locally in an undifferentiated neurite which strongly biased the neurite to form axon over the untreated ones (Fig. 6) (Witte et al., 2008).

Apart from symmetry breaking in neuronal cell microtubule driven asymmetric localization of centrosome and selective stabilization of a subset of microtubule plays important role in polarity maintenance in migrating cells such as macrophages, fibroblasts and astrocytes (Li and Gundersen, 2008). In asymmetric centrosome positioning centrosome localizes in between the nucleus and the leading edge regulated by signaling molecules like Rho GTPase Cdc42, PAR-6, aPKC and dynein (Etienne-Manneville and Hall, 2001; Palazzo et al., 2001; Solecki et al., 2004). Microtubule polarization is also observed through stabilization of a subset of microtubules directed towards the direction of cell migration by post translational modification of the tubulin, a process observed in migrating fibroblasts (Gundersen and Bulinski, 1988; Palazzo et al., 2001).

Phospholipid driven animal cell polarization

Recent studies revealed extensive information regarding the link between phospholipid asymmetry and the cell polarization. Asymmetric localization of PI(3,4)P2 (PIP2), PI(3,4,5)P2 (PIP3) and PIP3 phosphatase PTEN along plasma membrane has proven to be key regulator of cell polarizations such as neutrophils under chemotaxis, polarizing neurons and more recently in MDCK kidney epithelial cells (Leslie et al., 2008). Among these molecules PTEN seems to play a prominent role as it can asymmetrically localize to the plasma membrane and hydrolyze PIP3 to PIP2, a process required for asymmetry in PIP2 and PIP3 distribution (Leslie et al., 2008). Studies showed that membrane localization of PTEN largely depends upon the charge interaction between the basic membrane binding domain of the protein and the negatively charged polar head group of PS and PIP2 and the later interaction also enhances PTEN activity by many fold (Das et al., 2003; Lee et al., 1999; Redfern et al., 2008; Vazquez et al., 2006).

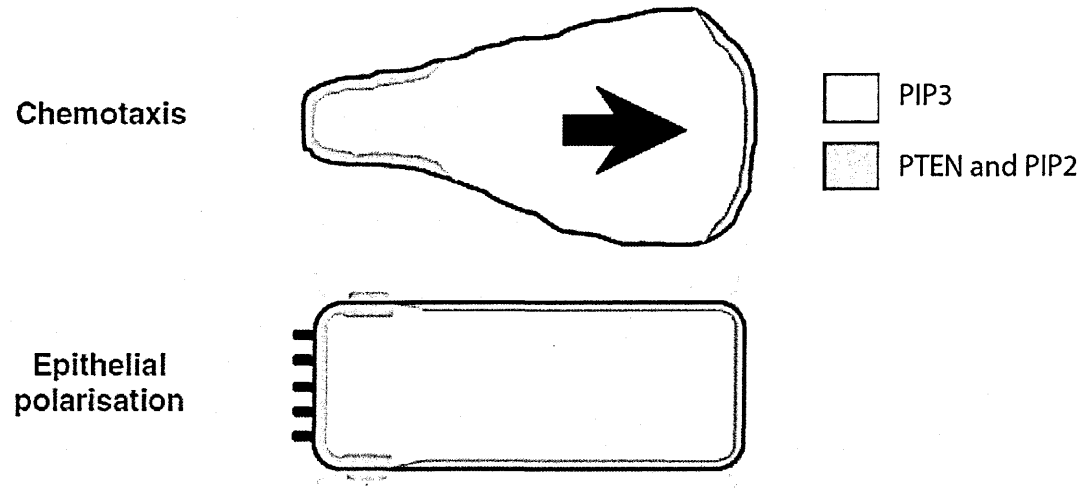

Figure 1-7. PTEN, PIP2 and PIP3 polarization

PIP3 is enriched at the leading edge while PTEN and PIP2 at the back of a migrating neutrophil. Kidney epithelial cell polarizes PTEN and PIP2 at the apical surface while plasma membrane enriched with PIP2 at the basolateral surface. This Figure is taken from (Leslie et al., 2008)

In migrating neutrophils under chemotaxis it is observed PIP3 enriches at the leading edge while PTEN at the back (Servant et al., 2000) (Fig. 7). MDCK kidney epithelial cell apico-basal polarity depends on asymmetric localization of PTEN. It was found that PTEN, PIP2 along with Cdc42 are polarized at the apical membrane while PIP3 at the basolateral membrane (Martin-Belmonte et al., 2007). A role for PTEN in epithelial polarization is also supported from its loss of function in epithelial-derived tumors which enhances the metastasis process (Wodarz and Nathke, 2007).

1.4. Polarized state is dynamic

So far, this discussion has been centered around a cell's ability to break symmetry intrinsically, or in the presence of external stimuli, and how structural and signaling events can be coupled to generate robust polarity. It was unclear whether the polarized state in yeast, marked by GFP-Cdc42, was dynamic or static until a FRAP (fluorescence recovery after photobleaching) based study showed rapid GFP-Cdc42 recovery ($t_{1/2} \sim 4$sec) at the polar cortex (Wedlich-Soldner et al., 2004) suggested that the polarized state is dynamic. It was also observed polarized distribution of the plasma membrane protein is strongly affected by the lateral diffusion along yeast plasma membrane (Valdez-Taubas and Pelham, 2003). Cdc42 on yeast plasma membrane diffuses with a

diffusion rate of 0.036 $\mu m^2/s$, found from $Cdc42^{Q61L}$ mutant which strongly binds to the plasma membrane and defective in entering into cytosol (Marco et al., 2007). This indicates a dynamic recycling of Cdc42 at polar cortex is required to counter diffusion along the plasma membrane to maintain a polarized distribution of the protein. Cdc42 mutant that is resistant towards GDP to GTP exchange, $Cdc42^{D57Y}$ (locked in GDP bound form) reduced the recovery kinetics drastically ($t_{1/2} \sim 37$sec). Wt Cdc42 recycling in presence of LatA, disassembling the actin structures was reduced albeit was less severely ($t_{1/2} \sim 7$sec) (Wedlich-Soldner et al., 2004). This experiment raised an intriguing possibility that Cdc42 concentration at the polar cortex was stably maintained through a fast recycling involving GTPase cycle and a slow actin based pathway.

Successive studies from our lab focused on understanding the mechanism underlying this fast Cdc42 recycling pathway. Interestingly, we observed that in the absence of the guanine nucleotide dissociation inhibitor (GDI, in yeast called Rdi1) which solubilizes Cdc42 in its inactive form in cytosol, reduced recovery kinetics ($t_{1/2} \sim 20$sec) to an extent similar to $Cdc42^{D57Y}$ (Slaughter et al., 2009). Live cell protein interaction studies between Cdc42 and Rdi1 in cytosol showed the interaction reduced drastically in $Cdc42^{D57Y}$ or $Cdc42^{Q61L}$ (locked in GDP or GTP bound form), comparable to the $Cdc42^{R66E}$ mutant which disrupts Rdi1 interaction (Gibson and Wilson-Delfosse, 2001; Slaughter et al., 2009). These results suggest that the Cdc42 fast recycling at the polar cortex is achieved through coupling between the GTPase cycle and Rdi1.

The above observations led us to hypothesize that Cdc42 concentration at the polar cortex is stably maintained through a slow actin mediated pathway which includes endocytosis and exocytosis and a fast recycling involving Rdi1 in cytosol (Fig. 8).

1.5. Thesis Goals

At the beginning of my thesis it was evident that dual modes of Cdc42 recycling as explained in Fig. 8 give rise to a stable polar cap in yeast. However, several important issues still needed to be determined: 1) how the two recycling mechanisms fine tune Cdc42 distribution at the

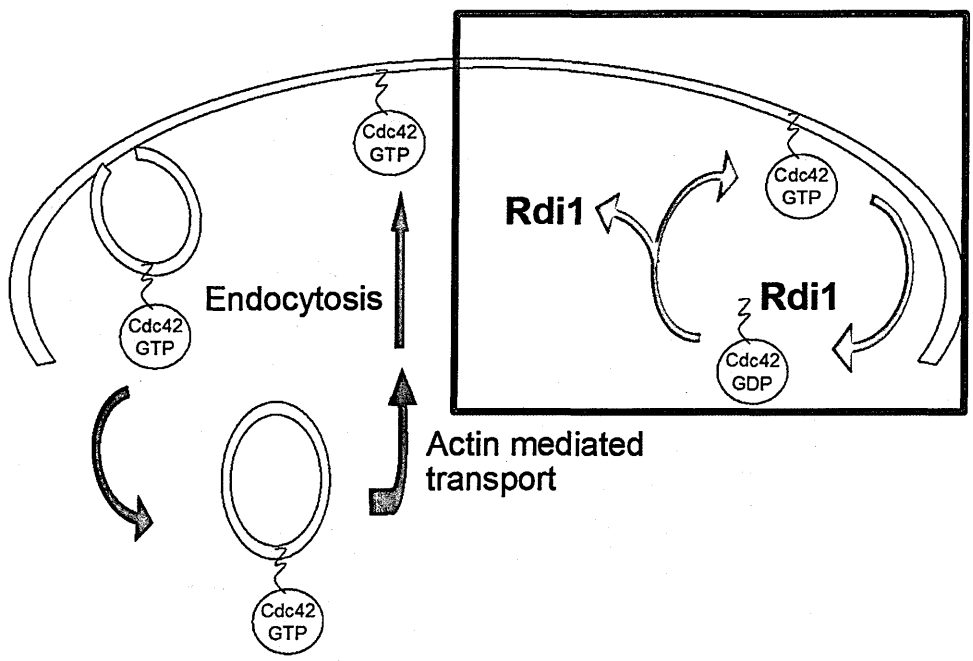

Figure 1-8. Dual modes of Cdc42 recycling.

Blue filled line represents polarized plasma membrane. Solid arrows (dark blue) describing Cdc42 recycling through membrane trafficking that involves actin mediated endocytosis and exocytosis. Brown box highlights cytosolic component of Cdc42 recycling that involves GTPase cycle and Rdi1.

polar cortex to give rise to distinct shapes like round bud or pointed shmoo, 2) how Cdc42 dissociates from the plasma membrane via Rdi1 during its recycling at the polar cortex, and 3) how Cdc42 is retargeted to the polar cortex from the cytosolic Cdc42-Rdi1 complex.

So far in my research, I have focused mostly on the first two points and the findings will be described in successive chapters. To study Cdc42 recycling at the polar cortex, I used fluorescent microscopic techniques like FRAP and iFRAP on GFP-Cdc42 while Cdc42 diffusion; interaction with Rdi1 in cytosol was measured by FCS (fluorescence correlation spectroscopy) and FCCS (fluorescence cross correlation spectroscopy). Details of these fluorescent techniques are explained in Chapter 2.

Chapter 2. Microscopy based methodology commonly used in this research

Experimental procedures explained in this chapter are frequently performed by Arupratan Das in his doctoral research in assistance with Brian D. Slaughter and Jay R. Unruh. FCS data fitting using weighted non-linear least squares and errors in the fitted parameters were estimated by the Monte Carlo method using algorithm written by Jay R. Unruh.

Live cell imaging

Live cell images were acquired with an inverted Zeiss 200 microscope equipped with a spinning-disc confocal system (Yokagawa) and a 100X, 1.45NA Plan-Fluor oil objective. GFP emission was collected through a BP505-540 nm filter onto an EM-CCD (Hamamatsu C9100). For most of the still images high signal to noise was obtained by summing up 20 middle confocal slices unless otherwise mentioned. ImageJ software was used to analyze and data extraction from images, data plotting and statistical analysis was performed using OriginLab Pro software.

FRAP (Fluorescence recovery after photo bleaching)

To study the Cdc42 recycling at polar cortex we performed fluorescence recovery after photobleaching (FRAP) experiments of GFP-Cdc42 at the polar cortex (Fig. 1). FRAP reflects the overall recycling process. Following photobleaching at the cortex, the bleached molecules at the polar cortex dissociate while the fluorescent molecules from the cytosol associate (Slaughter et al., 2009). Fluorescence recovery at the cortex is followed over time and the recovery curve is fit to an exponential equation to obtain the recovery rate.

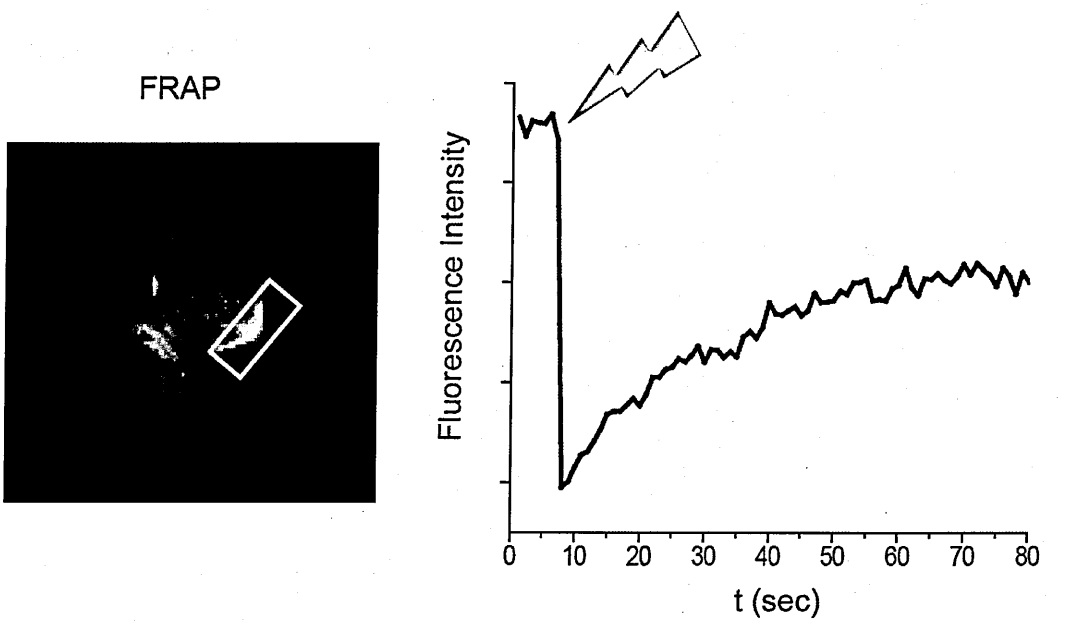

Figure 2-1 Demonstration of FRAP experiment

Example of a yeast cell expressing GFP-Cdc42. Red area depicts area at polar cortex to be photobleached. Fluorescence Intensity trace shows recovery at the polar cortex after photobleaching.

iFRAP (Inverse of Fluorescence recovery after photo bleaching)

iFRAP is similar to FRAP except the fluorescence intensity at the plasma membrane, cytosol and internal membrane but not the polar cortex is bleached. Dissociation of the bright molecules from the polar cortex is measured as the intensity decays at this region. Similar to FRAP, intensity decay at polar cortex is fit to an exponential model to extract decay rate. iFRAP measures the direct dissociation rate of Cdc42 from plasma membrane whereas FRAP measures overall recycling dynamics at polar cortex.

Fluorescence Correlation spectroscopy (FCS)

Using FCS we can measure protein concentration in cytosol and average diffusion time of fluorescent molecules through focal volume in live cells. Combination of confocal microscope and FCS setup a tiny area of interest (here cytosol) can be excited using laser beam (Fig. 2a). Fluorescent molecules diffuse in and out of focal volume give rise to fluctuation in emission intensity (Fig. 2b, c). An autocorrelation curve can be obtained from recorded intensity fluctuation using autocorrelation software. For slow diffusing molecules the intensity fluctuation remains alike (correlation) for longer period of time while for faster diffusing it decays fast (Fig. 2d). In case of both kind of diffusing molecules the correlation curve contains two part one with larger decay time and the other with faster. The autocorrelation curve can be fit to different diffusion model to extract molar concentration from the amplitude of the curve (G_0) and the diffusion time (τ_D) from the shape of the curve (Slaughter and Li, 2010).

FCS experiments were performed as described by Slaughter et al (Slaughter et al., 2007). In brief, live yeast cells were mounted on coverslips and FCS measurements were taken in the cytosol. GFP-Cdc42 was excited with the 488nm laser line of a Zeiss Confocor 3 through a HFT 488/561 dichroic. HFT565 was used as an emission dichroic and BP 505-540 as an emission filter to collect fluorescence data. Autocorrelation curves generated from the data were fitted to a two component (GFP-Cdc42) or one component (Rdi1-mCherry) diffusion model (Please see Chapter 4 method for model comparison) (Kim et al., 2007) with a triplet blinking component of 250μs (Haupts et al., 1998). Fitting was performed using weighted non-linear least squares (Bevington, 2003). The autocorrelation curves from many short (4 second) data acquisitions were averaged for

analysis. Curves that demonstrated bleaching or nondiffusive dynamics as judged by visual inspection of the binned trajectories and individual correlation traces were eliminated from the analysis. Weights were estimated from the standard error in the mean at each time lag point.

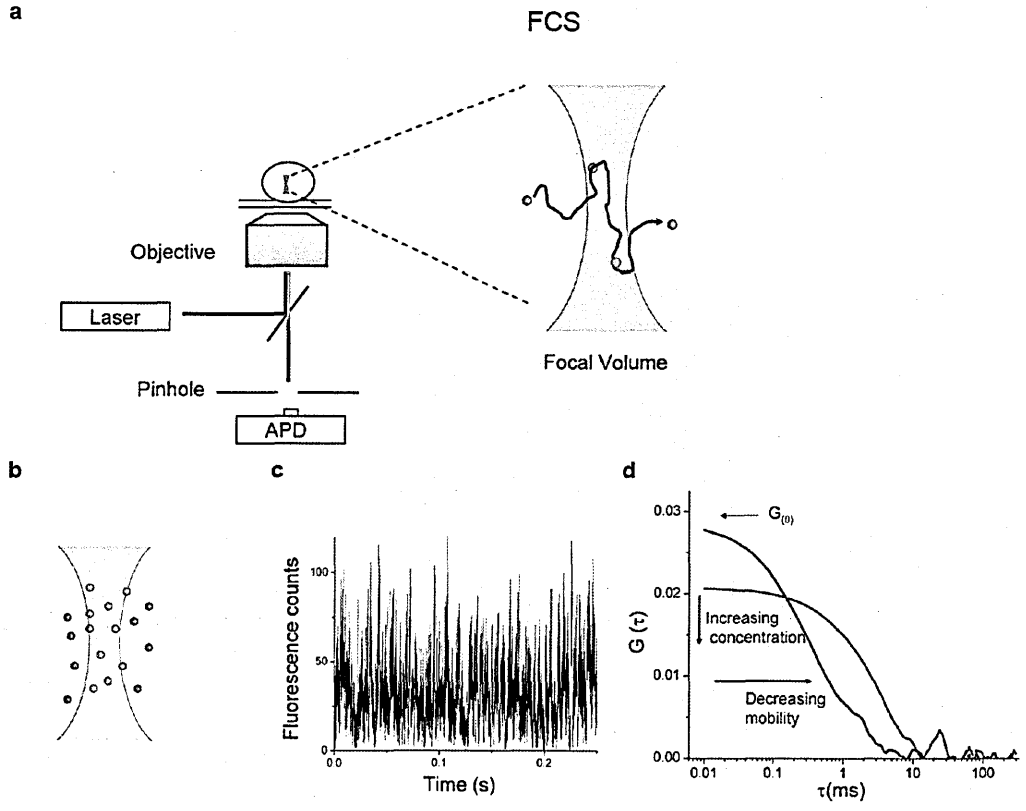

Figure 2-2 Principles of fluorescence correlation spectroscopy

(a) A laser source is focused on a tiny area of a sample through an objective with high numerical aperture. The fluorescence intensity emitted from the sample is collected through the same objective in the opposite direction of the laser source and passes through a pinhole prior to its detection by an avalanche photodiode (APD). Inset shows the shape of the focal volume and a single diffusing fluorescent molecule. (b) Focal volume with many diffusing fluorescent molecules. (c) Simulated fluorescence intensity fluctuation trace, arising from single channel excitation. (d) Autocorrelation curve obtained from the intensity fluctuation shown in (c), G_0 is the initial amplitude of autocorrelation curve which inversely proportional to the concentration of diffusing molecules. Average diffusion time of the molecules can be extracted from the decay of the correlation curve. Two correlation curves are shown with two different mobility. This figure is taken from (Slaughter and Li, 2010).

Errors in the fitted parameters were estimated by the Monte Carlo method as the standard deviation in fits of 500 simulated correlation curves with Gaussian random errors corresponding to the estimated weights and the observed χ^2 parameter (Bevington, 2003). These errors represent the estimated standard error in the fit parameters.

From the fitting we obtained G_0, amplitude of correlation function at zero time lag, and the average diffusion time τ_D required for the molecules to traverse the focal volume. The average number of molecules (N) present in the focal volume was calculated from the following equation 1:

$$N = \gamma / G_0 \qquad (1)$$

where γ, is the shape factor of the focal volume. For one photon excitation, the γ factor is 0.36 (Thompson, 1991).

Focal volume determination for FCS. To determine the size of the confocal focal volume, we examined the diffusion (τ_D) of fluorescein in 0.1 M NaOH, which has a published diffusion coefficient (D) of 320 $\mu m^2/s$ (Coles and Compton, 1983; Daly et al., 1983). The radial dimension, r_0, of the focal volume was found from the transit time, τ_D, of fluorescein through the focal volume using Equation 2

$$r_0^2 = 4 \cdot D \cdot \tau_D \qquad (2)$$

We used a value of 5 for the ratio of axial, z_0, and radial dimensions(Hess and Webb, 2002). The focal volume was then calculated using Equation 3 as

$$V = \left(\frac{\pi}{2}\right)^{3/2} \cdot r_0^2 \cdot z_0 \qquad (3)$$

With the size of the focal volume, it was straightforward to convert from molecules per focal volume to the concentration of mobile particles in nM.

Fluorescence Cross-Correlation spectroscopy (FCCS)

Fluorescence cross-correlation spectroscopy is an extension of FCS where protein-protein interaction is measured by dual color fluorescent tag. In case of complex formation two proteins diffuse together through focal volume causing similar intensity fluctuation over time (Fig. 3a, b).

Cross-correlation experiment gives three curves, two autocorrelation curves for each binding partners and one cross-correlation curve (Fig. 3c). Total protein concentration for each partner is calculated from the individual autocorrelation curve and extend of complex formation from the amplitude of cross correlation curve (Rigler et al., 1998).

$$N_{bound} = N_{GT}(N_{RT} + Q.N_{GT}) / N_{CC} - N_{GT}.Q \quad (4)$$ (Rigler et al., 1998)

N_{GT}, N_{RT} are the number of particles in the respective focal volume obtained from inverse of initial amplitude of the fitted correlation curves (see equation1). N_{CC} similarly obtained from the fit of cross correlation curve. Correction factors for the slight focal volume differences between green and red channels, bleed through (Q) between the channels are used similarly as estimated in (Slaughter et al., 2007).

We applied FCCS experiment to study Cdc42 and Rdi1 interaction in cytosol. Green (488nm) and red (561) laser channels were parked at a tiny portion of cytosol in Cells expressing GFP-Cdc42 and Rdi1-mCherry of a Zeiss Confocor 3. Emission intensity was collected using BP 505-540 for green and LP 580 for red channels respectively.

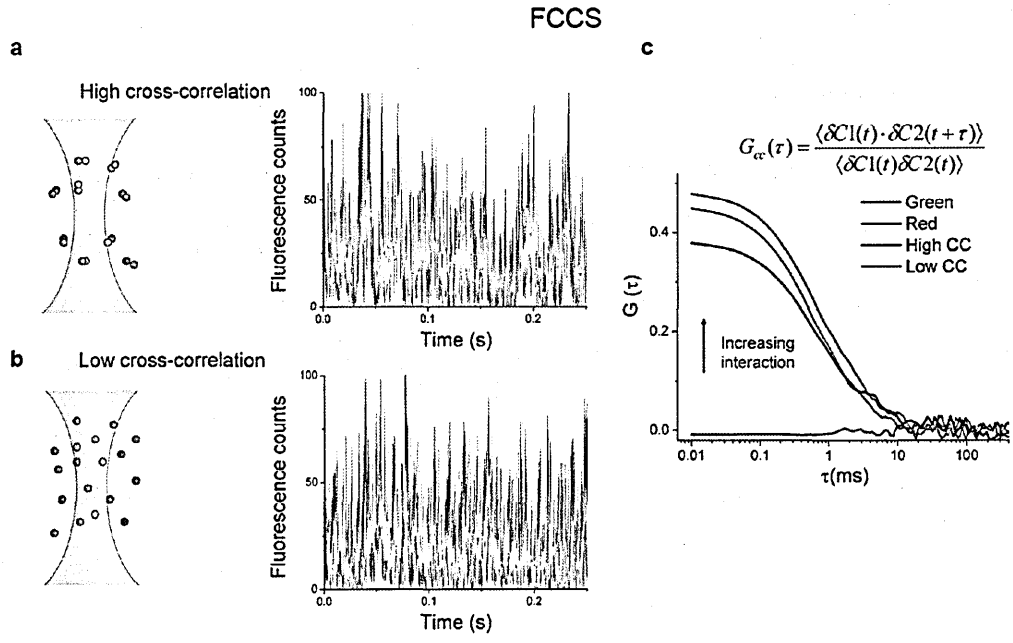

Figure 2-3 Principles of fluorescence cross-correlation spectroscopy

(a) Fluorescence cross-correlation spectroscopy, where two spectrally distinct fluorescent molecules co-diffusing through the focal volume. Adjacent intensity fluctuation traces

show high similarity between the channels. (b) Example of two less interacting molecules, resulting in less similarity in intensity fluctuations between two channels. (c) Autocorrelation and cross-correlation curves obtained from these experiments. The amplitude of the cross-correlation curve is proportional to the strength of the interaction as shown by the arrow. This figure is taken from (Slaughter and Li, 2010).

Chapter 3. Polarity maintenance in budding yeast depends upon two Cdc42 recycling mechanisms

Results (Figure 1-3) shown in this chapter are published in the following journal.

Developmental Cell

Article

Dual Modes of Cdc42 Recycling Fine-Tune Polarized Morphogenesis

Brian D. Slaughter,[1] Arupratan Das,[1] Joel W. Schwartz,[1,3] Boris Rubinstein,[1,*] and Rong Li[1,2,*]

[1]Stowers Institute for Medical Research, 1000 East 50th Street, Kansas City, MO 64110, USA
[2]Department of Molecular and Integrative Physiology, University of Kansas Medical Center, 3901 Rainbow Boulevard, Kansas City,
KS 66160, USA
[3]Present address: Department of Neurobiology, Duke University Medical Center, Box 3209, Bryan Research Building, Research Drive,
Durham, NC 27710, USA

*Correspondence: bru@stowers.org (B.R.), rli@stowers.org (R.L.)

Authors' contribution

Arupratan Das contributed in preparing plasmids, strains and did experiments along with Brian D. Slaughter. Mathematical modeling was solely done by Brian D. Slaughter and Boris Rubinstein.

Abstract

The highly conserved Rho GTPase Cdc42, accumulates at the cell cortex where orchestrates polarized cell growth during formation of bud or mating projection (shmoo) in budding yeast (Brandman et al., 2005; Wedlich-Soldner et al., 2004). Membrane diffusion of Cdc42 is rapid, and thus mechanisms must be in place to recycle Cdc42 molecules actively at the polar cortex in order to maintain a polarized distribution. Quantitative imaging and mathematical modeling revealed Cdc42 diffusion at polar cortex is balanced by a fast Guanine nucleotide dissociation inhibitor (GDI) mediated recycling and a slow actin dependent mechanism that consists of endocytosis and exocytosis. The recycling mechanisms are restricted to overlapping regions of the polar cortex, as we find both mechanisms are coupled to the Cdc42 GTPase cycle. I have focused on experimental findings I made along with Brian D. Slaughter to understand the dual mode of Cdc42 recycling and their regulation in maintaining a stable Cdc42 polarized distribution (Slaughter et al., 2009).

Introduction

Several physiological processes such as cell motility, embryogenesis relies upon polarized morphology at the unicellular level. Symmetry breaking as the first step of cell polarization accumulates protein and polarized cytoskeletal components at the cell surface which eventually leads to polarized morphogenesis. A significant amount of work has already been invested to understand symmetry breaking and establishment of polarization (Li and Gundersen, 2008; Onsum and Rao, 2009) while the maintenance of key polarity molecules at the site of polarization is not well understood.

Cdc42, a Rho GTPase first discovered in yeast (Johnson, 1999), has proven to be a key regulator of cell polarity in many eukaryotes (Etienne-Manneville, 2004). Please see the Introduction chapter Page 2-8 for a detailed explanation of the Cdc42 mechanistic module in polarity establishment and maintenance in budding yeast.

Previous FRAP based studies revealed Cdc42 is dynamic at the yeast polar cortex and Wt Cdc42 recycles with several order of magnitude higher rate compared to its GTP locked mutant

$Cdc42^{Q61L}$ (Wedlich-Soldner et al., 2004). Guanine-nucleotide dissociation inhibitor (GDI), Rdi1 in yeast is known to solubilize Cdc42 through interaction with its COOH-terminal prenyl group and also can extract Cdc42 from the polar cortex and increases its cytosolic concentration (DerMardirossian and Bokoch, 2005; Johnson et al., 2009). This raises a possibility that Rdi1 might be involved in Cdc42 fast recycling between the cytosol and polar cortex.

In this chapter we have explored cutting edge imaging and spectroscopic techniques to understand Cdc42 recycling hence maintenance mechanism at polar cortex. We found Rdi1 indeed plays a role in fast recycling while a slow pathway dependent on actin based endocytic recycling operates together with Rdi1 to give rise to a stable polar cortex. Disrupting actin and Rdi1 pathway simultaneously leads to rapid depolarization. A mathematical model predicts both the pathways must operate on overlapping window of similar size and the recycling rates can be fine-tuned to give rise distinct polarized morphogenesis (Slaughter et al., 2009). We find that the two recycling pathways are interlinked by their dependence on the Cdc42 GTPase cycle (Slaughter et al., 2009).

Result

Cdc42 at yeast polar cortex is recycled by two pathways

We investigated Cdc42 recycling mechanism at the yeast polar cortex in cells expressing GFP-Cdc42 (will be referred as Cdc42). To avoid heterogeneity in data acquisition we focused on cells with established polar cortex in a dividing population (Fig. 1a) (Wedlich-Soldner et al., 2004). To investigate the possible involvement of Rdi1 in Cdc42 recycling we performed FRAP in *Δrdi1* and found a drastic reduction of FRAP rate ($\tau = 1/t_{1/2}$) compared to Cdc42 in Wt cells (Fig. 1b, c). Disruption of actin structure using Latranculin A (LatA) reduced Cdc42 recovery rate (Fig. 1b, c) as previously observed (Roland JBC 2004). To investigate whether actin and Rdi1 function in parallel or dependent in Cdc42 recycling at polar cortex we performed FRAP in *Δrdi1* in presence of LatA which further reduced recovery rate compared to *Δrdi1*. However the FRAP study in this condition was difficult to compare to Wt or *Δrdi1* cells alone as in presence of LatA, *Δrdi1* cells depolarize rapidly (Fig 1d). The rapid dissipation of polar cap in presence of LatA in *Δrdi1* cells by contrast to Wt or *Δrdi1* alone (Fig. 1d) suggest Cdc42 at the polar cortex is maintained through the redundant but essential mechanism of Rdi1 and actin dependent recycling.

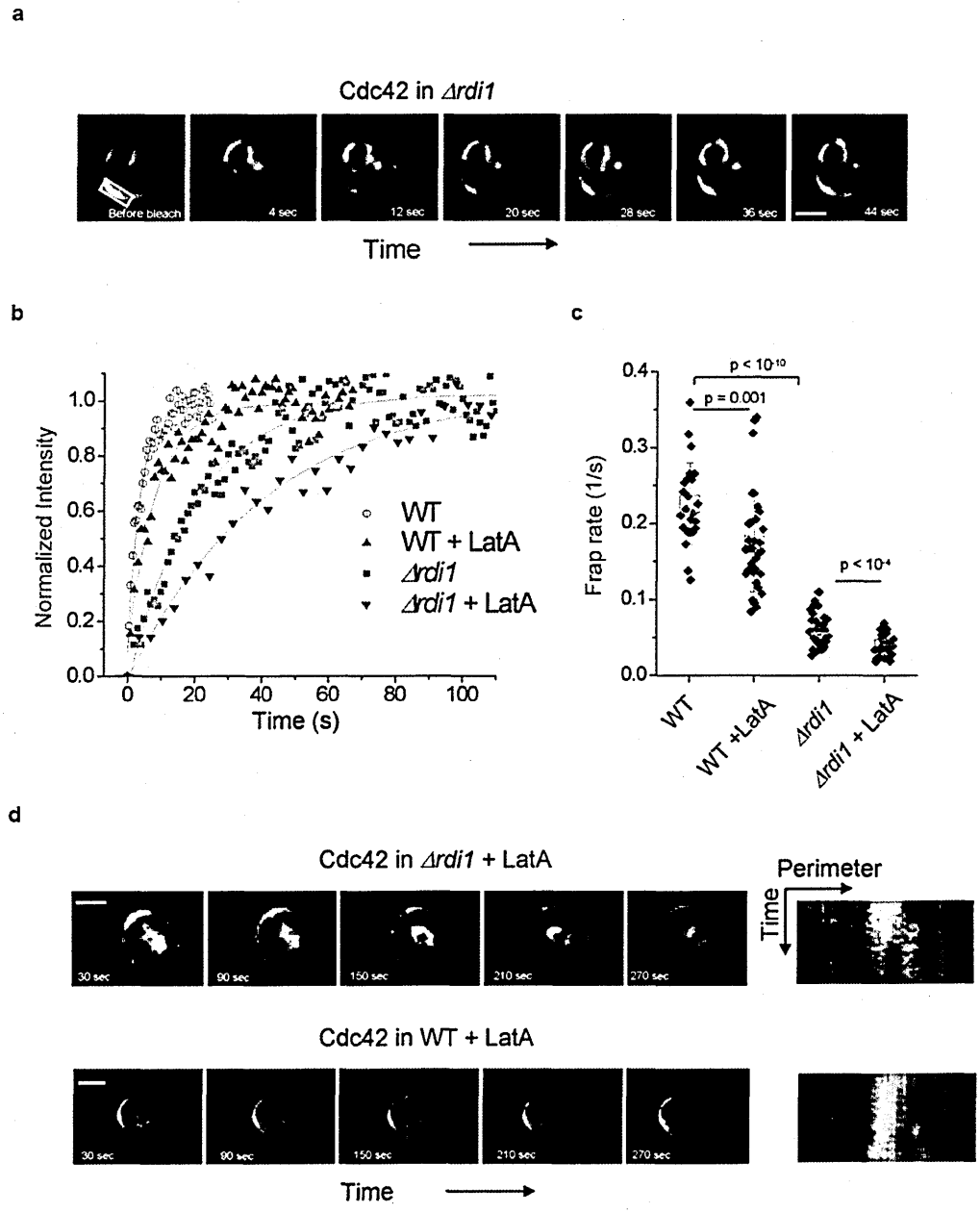

Figure 3-1. Cdc42 recycling dynamics measured with FRAP experiment.

(a) Example montage of a FRAP movie of a cell expressing GFP-Cdc42 in Δ*rdi1* strain. Red rectangle region marks the bleached are and "v" marks vacuole. Scale bar is 2.0 μm. (b) Normalized example FRAP curves for the indicated conditions. (c) Fluorescence intensity recovery rate (1/sec) measured from FRAP movies for the indicated conditions. Box represents standard error of mean (SEM) and whisker is standard deviation (SD). (d) Montage of a movie where Wt and Δ*rdi1* cell expressing GFP-Cdc42, treated with 100μM LatA. Kymographs around the cell perimeter for the corresponding movies are shown adjacent to each montage. Scale bar is 2.0 μm. These data were generated by Brian D.

Slaughter, using yeast strains constructed by Arupratan Das. This figure is taken from (Slaughter et al., 2009).

Mathematical model predicted Actin and Rdi1 pathways need to be overlapping in order to have distinct polarized Cdc42 distribution

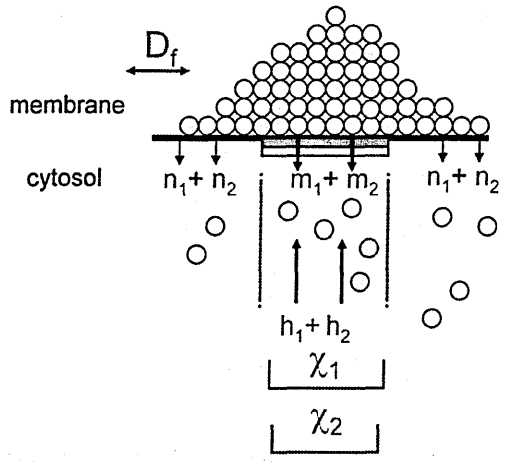

Figure 3-2. Cdc42 recycling parameters and validation of model predicted parameters using iFRAP experiment.

Outline of the mathematical model, D_f is the lateral diffusion of Cdc42 in the plasma membrane. m and n internalization rate inside and outside of the delivery window respectively. χ denotes delivery window size and h, delivery rate inside the window. Green and red symbols denotes the parameters corresponding to overlapping Rdi1 and actin delivery window of similar size. This figure was generated by Brian D. Slaughter and taken from (Slaughter et al., 2009).

One of the goals in this study was to understand quantitatively how two recycling pathways are coupled to give rise a stable polar cap and the other goal was to understand how these two pathways can fine tune the shape of polarized Cdc42 distribution. To achieve the second goal we used mathematical modeling mostly with similar assumptions as previous (Marco et al., 2007) with several modifications (Fig. 2) and shown by Equation 1. The detail of the mathematical model and how fine tuning model predicted parameters can give rise to distinct shape of the polar cap is explained in (Slaughter et al., 2009).

$$\frac{\partial f}{\partial t} = D_f \Delta f - m\chi f - n(1-\chi)f + h\chi F_C \qquad (1)$$ (Slaughter et al., 2009)

Mathematical model showed that, in order to explain the dynamics of Wt Cdc42 and the shape of the Cdc42 polarized distribution, the two recycling pathways must be spatially overlapping and of identical size. All other scenarios gave a non-physiological Cdc42 distribution (Slaughter et al., 2009). Furthermore model predicted parameters considering single pathway became statistically equivalent to the sum of parameters obtained from Δ*rdi1* (actin pathway is operating) and cells treated with LatA (Rdi1 pathway is operating) (Slaughter et al., 2009). This strongly suggests both actin and Rdi1 pathways are spatially overlapping with identical delivery window size and simultaneously raises a possibility of having a common regulator of both the pathways.

Cdc42 GTPase cycle regulates both actin and Rdi1 dependent recycling pathways

As explained above, the mathematical model (Slaughter et al., 2009) suggested that the two recycling pathways must be colocalized and consistent of delivery/ removal windows of similar size. Thus, some factor must link the two pathways. Therefore, we investigated whether any common mechanism operates both the pathways in the polar cortex. Cdc42 GTPase cycle appeared to be a potential mechanism since 1) Cdc42 mutant locked in GTP ($Cdc42^{Q61L}$) or GDP ($Cdc42^{D57Y}$) reduced FRAP rates in Wt (Wedlich-Soldner et al., 2004), and 2), in Δ*rdi1* no further reduction was observed (Fig. 3a) indicating in $Cdc42^{Q61L}$ mutant Rdi1 pathway is inhibited.

Mathematical model predicted in Δ*rdi1* cell $Cdc42^{Q61L}$ (Cdc42-GTP) internalization rate inside the delivery window is slower than Wt Cdc42 (Slaughter et al., 2009). One possibility for this slow internalization might be the defective endocytosis of $Cdc42^{Q61L}$ as it constitutively interacts with its effectors. To investigate this we introduced the mutation T35A to $Cdc42^{Q61L}$, which abolishes interaction with CRIB domain containing effectors (Gladfelter et al., 2001). Interestingly in the double $Cdc42^{Q61L\text{-}T35A}$ mutant, the recycling rate became more rapid than $Cdc42^{Q61L}$ alone whereas this effect was not observed for $Cdc42^{D57Y}$ mutant which does not bind to effectors (Fig. 3a). This suggests excess interaction with effectors inhibit Cdc42 to enter into the endocytic pathway.

We further studied whether removal of Cdc42 GAP Bem2 and Bem3, which are known to localize at the presumptive bud site (Knaus et al., 2007) has the similar effect of $Cdc42^{Q61L}$ mutant. Indeed we observed Cdc42 recycling rate was significantly reduced in *Δbem2Δbem3* (Fig. 3a). These results demonstrate that the Cdc42 GTPase cycle allows fast Cdc42 recycling at the polar cortex via unperturbed endocytic pathway

We next asked whether the Cdc42 GTPase cycle regulates the Cdc42-Rdi1 interaction in the cytosol and affects Cdc42 recycling at the polar cortex. To this end we performed FCCS experiment in cells expressing GFP-Cdc42 and Rdi1-mCherry (please see Chapter 2 for detail explanation). As a positive control we used linked GFP-mCherry (cross-correlation ~45%) and unlinked GFP and mCherry as negative control (Fig. 3b, c). Strong interaction with GFP-Cdc42 and Rdi1-mCherry was observed in the cytosol (cross-correlation 20%). Interestingly in the D57Y and $Cdc42^{Q61L}$ mutant the interaction was reduced drastically to an extend similar to $Cdc42^{R66E}$, mutant does not interact with Rdi1 (Gibson and Wilson-Delfosse, 2001) and $Cdc42^{C188S}$, a non-prenylated mutant (Masuda et al., 1994) which is expected to have no interaction with Rdi1 (Fig. 3b, c). These results suggest Cdc42-Rdi1 complex formation in the cytosol depends upon the Cdc42 GTPase cycle. Together these results suggest Cdc42 GTPase cycle acts as a common regulator of Rdi1 pathway through allowing complex formation between Cdc42 and Rdi1 and actin pathway through releasing effectors to allow proper endocytosis.

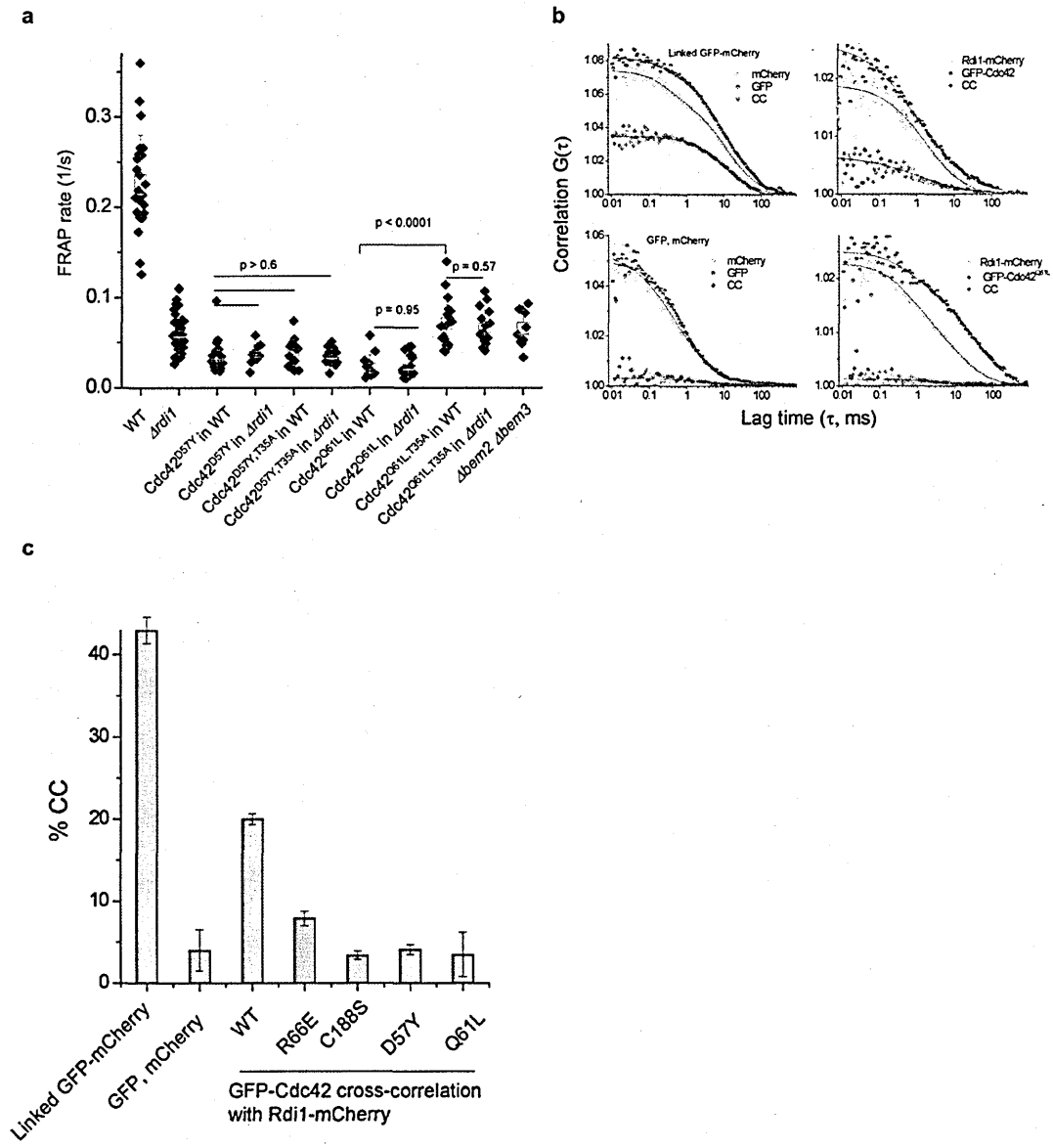

Figure 3-3. GTPase cycle regulation of Cdc42 recycling and Cdc42-Rdi1 complex formation in cytosol.

(a) FRAP rates (1/sec) for strains as indicated conditions. Box represents SEM and the whisker is SD. (b) Example curves obtained from fluorescence cross-correlation curves. Positive control is the linked GFP and mCherry at the COOH terminal of Bat2 protein (Slaughter et al., 2009) or expressed independently as a negative control. (c) Percentages of bound GFP-Cdc42 with Rdi1-mCherry were quantified under indicated conditions. Column represents average and the error bar is SEM. These data were generated by Brian D. Slaughter, using critical plasmids and yeast strains constructed by Arupratan Das. The figure is taken from (Slaughter et al., 2009).

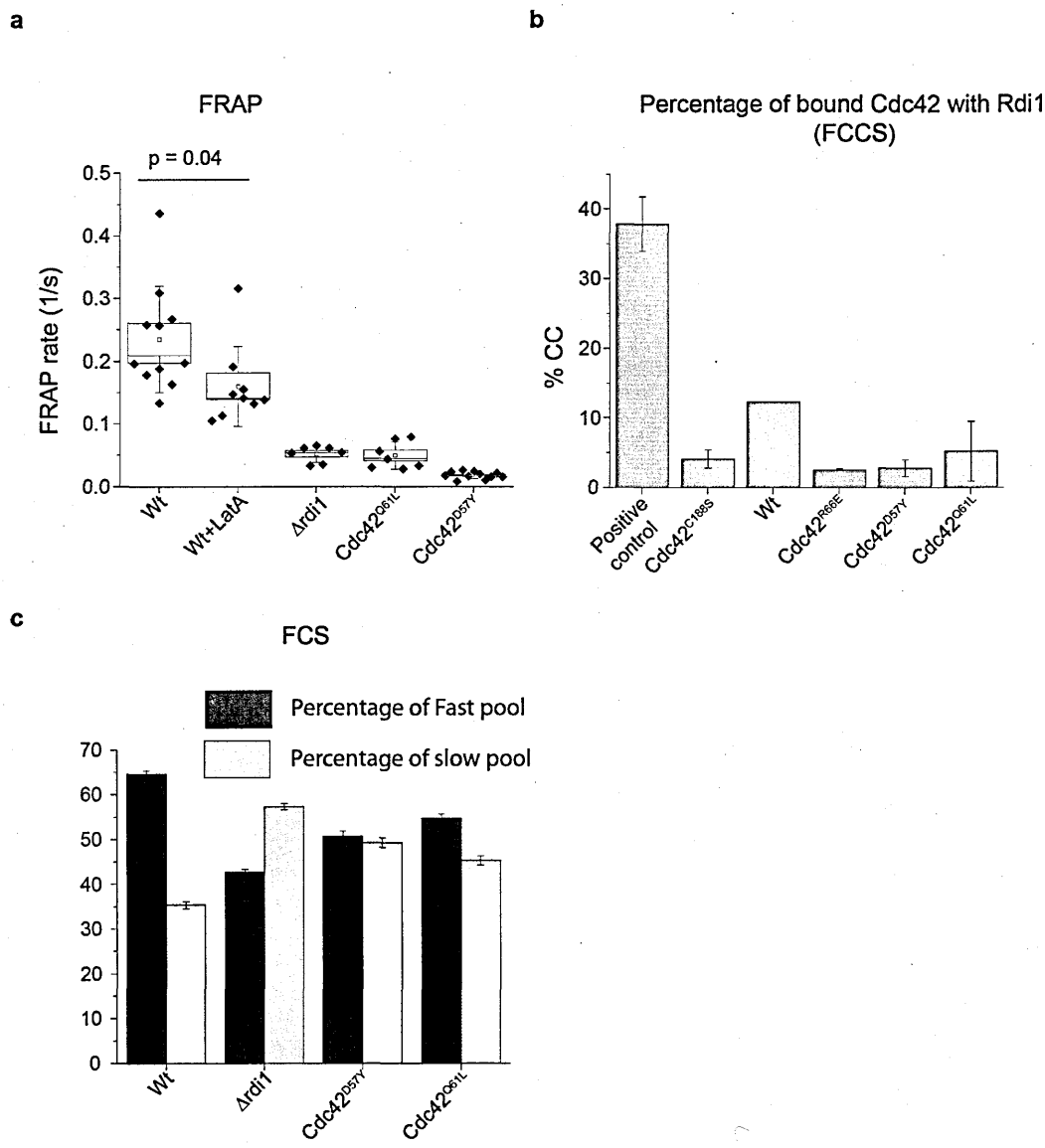

Figure 3-4. Cdc42 GTPase cycle mediated regulation of Cdc42 recycling and interaction with Rdi1 is conserved in external cue dependent (alpha factor) cell polarization.

(a) FRAP rates (1/sec) in shmooing cells under the indicated conditions. Box represents SEM and the whisker is SD. (b) Percentages of bound Cdc42 with Rdi1 quantified from FCCS experiment as indicated in (Fig3 b, c). Column represents average and the error bar is SEM. (c) Percentage of Cdc42 in cytosol distributed in slow and fast diffusing pool determined by fluorescence correlation spectroscopy (FCS) under the indicated conditions. Column represents average percentage of slow and fast diffusing pool. Error bar is SEM. Data presented here were generated independently by Arupratan Das.

Cdc42 GTPase cycle regulation of Rdi1 and actin pathways is conserved from budding to pheromone induced cell polarity

So far our study reflected that the actin and Rdi1 mediated recycling pathways are colocalized and regulated by Cdc42 GTPase cycle in maintenance of yeast cell polarity under dividing conditions. However cells can still polarize in presence of external stimuli. In yeast, cells polarize in response to mating pheromone (shmooing cell). We next focused whether the above mechanisms also operate in pheromone induced polarity. Cells were treated with 60μM mating pheromone for 150 min. Indeed we observed reduced recycling rate in the presence of LatA while in presence of *Δrdi1* alone the reduction was even more drastic (Fig. 4a). This suggests in presence of pheromone Cdc42 also recycles via two pathways one, actin mediated slow and Rdi1 mediated fast pathways. To understand whether Cdc42 GTPase cycle is also required for it's recycling at polar cortex in the presence of pheromone we studied FRAP on $Cdc42^{Q61L}$ and $Cdc42^{D57Y}$ mutants. Similar to polarized G1 cells in an asynchronous population, the above mutants reduced the recycling rate drastically in pheromone treated cells (Fig. 4a) suggesting a role for GTPase cycle in pheromone induced polarity maintenance.

In cycling cells we have observed that the GTPase cycle is required for Cdc42-Rdi1 complex formation in the cytosol. To investigate this phenomenon in shmooing cells we have performed FCCS experiment in cells expressing GFP-Cdc42 and Rdi1-mCherry in the presence of pheromone. Reduced cross-correlation was observed for $Cdc42^{Q61L}$ and $Cdc42^{D57Y}$ mutants to a level similar to $Cdc42^{R66E}$ and $Cdc42^{C188S}$ mutant further emphasizing the role of GTPase cycle in Cdc42-Rdi1 complex formation which is conserved from dividing to shmooing cells.

Rdi1 forms complex with Cdc42 through the interaction of protein surface and Cdc42 COOH terminal prenyl group. We next asked how this complex formation affects Cdc42 diffusion pattern in cytosol. To this end we have performed fluorescence correlation spectroscopy (FCS, also see chapter 2, 4 for experimental procedure and data analysis) in shmooing cells expressing GFP-Cdc42. We observed in Wt cells Cdc42 diffuses in two pools, majority of the protein (> 60%) with fast and the rest (<40%) with slow diffusion time (Fig. 4c). Interestingly in the absence of Rdi1, Cdc42 is enriched in the slow diffusing pool suggesting the fast diffusing pool is composed with Cdc42-Rdi1 complex (Fig. 4c). As the GTPase cycle regulates Cdc42-Rdi1 complex

formation, $Cdc42^{Q61L}$ and $Cdc42^{D57Y}$ mutants should be enriched in the slow diffusing pool. Indeed we observed both the mutants diffuse mostly in the slow pool (Fig. 4c). Together these results suggest Cdc42 GTPase cycle regulates Cdc42-Rdi1 complex formation in cytosol, responsible for Cdc42 fast diffusion and regulate both actin and Rdi1 mediated Cdc42 recycling to achieve robust cell polarity.

Discussion

Results presented in this chapter explore the underlying mechanisms behind how a dynamic but stable Cdc42 concentration is maintained at the polar cortex through two distinct pathways, one involving fast response GDI and the other through slow trafficking based pathway. GDI's are well known for their interaction with Cdc42 through the Cdc42 prenyl group and their ability to extract Cdc42 from the plasma membrane into the cytosol (Hoffman et al., 2000; Masuda et al., 1994; Richman et al., 2004). Here we have shown that apart from its ability to extract Cdc42 from the polar cortex, Rdi1 plays a pivotal role in fast Cdc42 recycling at the cortex. It's intriguing that Δ*rdi1* lacks any growth phenotype however not surprising as cell can still achieve the polarized morphology through trafficking based recycling.

We elucidate here the common regulator of both actin based and Rdi1 based Cdc42 recycling and found through FCCS measurements that the Cdc42 GTPase cycle regulates the Cdc42-Rdi1 interaction in the cytosol. Furthermore, inhibiting the cycle also blocks the endocytic pathway. Liposome based in vitro studies showed Rdi1 can extract Cdc42 from artificial membrane with equal rate independent of its nucleotide bound state and the affinity towards the GDP bound form is ~10 fold higher than the GTP bound form (Johnson et al., 2009). Our FCCS and FRAP based studies demonstrate that, in vivo, the Cdc42 GTPase cycle plays a more complex role than what we could infer from the in vitro study, as Cdc42 mutants with GTP (Q61L) or GDP (D57Y) locked form neither interacts with Rdi1 nor recycles as fast as the Wt protein.

We observed $Cdc42^{Q61L}$ mutant (GTP locked) can rescue the recycling rate significantly in presence of T35A mutant ($Cdc42^{Q61L, T35A}$) in Δ*rdi1*. The latter is defective in effector interaction suggesting Cdc42 recycling in constitutively active form is impaired through excess interaction with effectors probably blocking the mutant from entering into endocytic pathway, while introducing the effector loop mutant (T35A) rescued the phenotype by large. This can further be

supported as $Cdc42^{D57Y}$ mutant (GDP locked) is also slow in recycling but was not rescued by introducing T35A mutant, as GDP bound form does not interact with effectors. This supports the notion that active form of Cdc42 helps to enter or stimulates the formation of endocytic structures (Lechler et al., 2001; Li et al., 1995).

Another goal of this study was to understand how two recycling pathways based on actin and Rdi1 can give rise to different morphogenetic outcomes like pointed shmoo or round shaped bud. Mathematical modeling was able to successfully explain this phenomena based on the different recycling parameters (Slaughter et al., 2009). Mathematical model predicted reduction of *m* relative to *n* inside the delivery window (Fig. 2) resulted in pointed Cdc42 distribution. This was indeed observed in the $Cdc42^{Q61L}$ mutant in Δ*rdi1* and in shmooing cell where *m* reduced significantly compared to *n* which gave rise to pointed bud or pointed Cdc42 distribution in the polar cortex respectively (Slaughter et al., 2009).

Together these results suggest Cdc42 recycling parameters specially the internalization rate inside the polar cortex can help cell to adapt different polarized morphology in vegetative cell growth or in response to mating pheromone apart from having only maximum Cdc42 concentration at the polar cortex.

Methods

Please see chapter 2 for in detail description of the techniques: FRAP, iFRAP, FCS, FCCS and imaging used in this study.

Chapter 4. Flippase-mediated phospholipid asymmetry promotes fast Cdc42 recycling in dynamic maintenance of Cell Polarity

Arupratan Das[1], Brian D. Slaughter[1], Jay R. Unruh[1], Dan Bradford[1], Richard Alexander[1], Boris Rubinstein[1], and Rong Li[1,2,*]

[1] Stowers Institute for Medical Research, 1000 East 50th Street, Kansas City, MO 64110

[2] Department of Molecular and Integrative Physiology, University of Kansas Medical Center, 3901 Rainbow Boulevard, Kansas City, KS 66160

* Correspondence: rli@stowers.org

All the experiments in this chapter are performed by Arupratan Das.

The manuscript has been submitted.

Abstract

Lipid asymmetry between membrane leaflets at the plasma membrane is essential for such processes as cell polarity, cytokinesis and phagocytosis (Emoto and Umeda, 2000; Iwamoto et al., 2004; Yeung et al., 2008). Here we identify the lipid flippase complex, composed of Lem3, Dnf1 or Dnf2(Pomorski and Menon, 2006), to play a role in the dynamic recycling of the Cdc42 GTPase, a key regulator of cell polarity(Etienne-Manneville, 2004), in yeast. By using quantitative microscopy methods and modeling, we show that the flippase complex is required for fast dissociation of Cdc42 from the polar cortex by the guanine nucleotide dissociation inhibitor (GDI). A loss of flippase activity, or pharmacological blockage of the inward flipping of phosphatidylethanolamine (PE), a phospholipid with a positively charged head group, disrupts Cdc42 polarity maintained by the GDI-mediated recycling pathway. PE flipping is likely to reduce the charge interaction between a Cdc42 C-terminal cationic region with the inner leaflet of the polar cortex, enriched for the negatively charged lipid phosphatidylserine (PS), as demonstrated by analysis of Cdc42 mutants with altered charge properties. Using a reconstituted system with supported lipid bilayers, we show that the relative composition of PE versus PS directly modulates the rate of Cdc42 extraction from the membrane by GDI.

Introduction

Establishing stable cell polarity is crucial for cellular morphogenesis and differentiation. The Cdc42 small GTPase localizes to the site of polarized growth in yeast and orchestrates the structural and signaling events required for budding and formation of mating projections(Etienne-Manneville, 2004; Pruyne and Bretscher, 2000a; Slaughter and Li, 2006). Previous work showed that a polarized Cdc42 distribution is maintained dynamically through two colocalized pathways of recycling to counter Cdc42 diffusion in the membrane (Marco et al., 2007; Slaughter et al., 2009; Wedlich-Soldner et al., 2004). Whereas a slow pathway works through actin-based membrane trafficking, a fast Cdc42 recycling pathway is mediated through Rdi1, the yeast GDI for Rho family GTPases (Masuda et al., 1994). GDI is known to extract Rho GTPases from the membrane by forming a complex involving both protein-protein contacts and binding of GDI to the prenyl lipid anchor at the COOH terminus of the GTPases (DerMardirossian and Bokoch, 2005; Johnson

et al., 2009). When actin polymerization is inhibited, the Rdi1-mediated Cdc42 recycling is required for the polarization of Cdc42 at the presumptive bud site (Marco et al., 2007).

Results

***Δlem3* rescues Rdi1p overexpression growth defect**

In order to gain insights into the molecular mechanisms regulating the location and rate of Rdi1-mediated Cdc42 recycling, we performed a suppressor screen taking advantage of the fact that over-expression of Rdi1 under the Gal1 promoter represses yeast growth, likely due to the over-extraction of Cdc42 and other essential Rho family GTPases from membrane compartments (See Chapter 5 for detail description) (Richman et al., 2004) (also see Fig. 1d). We reasoned that deletion of a gene encoding a protein that facilitates Cdc42 extraction by Rdi1 could rescue the Gal-Rdi1 induced growth defect. As there are many possible mechanisms for the suppression of the growth defect, the candidates could be further narrowed down to those encoding proteins colocalizing with Cdc42 at the site of polarization. A centromeric plasmid expressing Rdi1 from a galactose inducible promoter was transformed into each strain of the yeast haploid non-essential deletion library. Growth of each deletion strain over-expressing Rdi1 was quantified and normalized relative to its growth without Rdi1 over-expression. This screen revealed ~ 277 initial candidates (this dataset will be reported elsewhere) that rescued the over-expression growth defect, among which 15 candidates were known to be localized to the plasma membrane (Supplementary Information, Fig. S1b). Among these 15 genes, LEM3 encodes a protein polarized at the presumptive bud site similarly to Cdc42 (Fig. 1a; Supplementary Information, Fig. S1a, S2a). Lem3 is a Cdc50 family protein forming a heterodimeric complex with P-type ATPases Dnf1 and Dnf2 and is involved in aminophospholipid flipping from the outer to inner plasma membrane leaflet(Iwamoto et al., 2004). Interestingly, we also found Dnf2 as a weak rescuer from the screen just missed by our initial cut-off for positives (Supplementary Information, Fig. S1a). Both Dnf1 and Dnf2 are also localized at the initial site of polarization, like Lem3 (Supplementary Information, Fig. S2a-c). Such localization pattern and their reported involvement in cell polarity (Saito et al., 2007) led us to perform an in-depth study on the possible role for aminophospholipid flipping in regulating Cdc42 recycling at the polar cortex. Characterization of another set of the

genes identified by the screen that form a pathway regulating Cdc42 recycling through internal membrane compartments will be reported elsewhere.

Lem3 is required for fast Cdc42 recycling

To test if *Δlem3* reduces the ability of Rdi1 to extract Cdc42, we first used fluorescence correlation spectroscopy (FCS) (Slaughter and Li, 2010) to investigate the mobile cytosolic concentration of GFP-Cdc42 expressed under the CDC42 promoter (Slaughter et al., 2009; Wedlich-Soldner et al., 2004) in wild-type (Wt) and *Δlem3* cells with or without Rdi1 over-expression. FCS records fluorescence intensity fluctuations using a confocal microscope equipped with a photon counter, and the data is usually subjected to an autocorrelation analysis. The autocorrelation curve can be fitted to extract the molar concentration of the diffusing specie from the amplitude of the curve (G_0) and the diffusion time (τ_D) from the shape of the curve (see (Slaughter and Li, 2010) for a recent review). To avoid heterogeneity in polarization stages and to allow comparison between experiments, all the in vivo single cell analyses in this work were performed with unbudded polarized cells with a Cdc42 polar cap at the incipient bud site in a cycling population. Autocorrelation curves of GFP-Cdc42 fitted poorly with a single species diffusion model but well with a two-species diffusion model (Fig. 1b) with a significant statistical preference towards the latter ($p<1 \times 10^{-10}$). This suggests the existence of at least two pools of mobile Cdc42 population, 64% displaying fast diffusion ($\tau_D = 2.9 \pm 0.3$ ms) and 36% displaying slow diffusion ($\tau_D = 70 \pm 8$ ms) (Fig. 1b; Supplementary Information, Fig. S3a, b). The fast pool was significantly reduced in the Δrdi1 background and for the $Cdc42^{R66E}$ mutant, which disrupts Rdi1 interactions (Gibson and Wilson-Delfosse, 2001) (Supplementary Information, Fig. S3a). The vast majority (> 95%) of Rdi1 exists in a fast diffusing population ($\tau_D = 2.2 \pm 0.1$ ms) (Supplementary Information, Fig. S3c, d). The slow pool of Cdc42, on the other hand, was diminished by the $Cdc42^{C188S}$ mutation (Supplementary Information, Fig. S3a, b), which prevents prenylation. This analysis, along with the observed in vivo cross-correlation of Cdc42 and Rdi1 (Slaughter et al., 2009), suggests that the fast pool of Cdc42 consists largely of a Cdc42-Rdi1

complex, while the slow pool is dependent on prenylation and therefore is likely to be membrane vesicle-associated.

Induction of Rdi1 over-expression in cells bearing pGAL1-RDI1 with galactose resulted in a time-dependent increase in total mobile Cdc42 concentration in the cytosol (Fig. 1c). This increase is accompanied by a similar increase in Cdc42 concentration in the fast but not slow pool, consistent with extraction of Cdc42 by Rdi1 from the plasma membrane into the soluble pool (Fig. 1c). Consistently, depletion of Cdc42 from the plasma membrane, especially from the polar cortex, can be observed (Fig. 1d, e). In *Δlem3* cells, the Cdc42 polar cap was more prominent than in Wt cells prior to Gal-Rdi1 induction (Fig. 1d, e), accompanied by a smaller mobile Cdc42 pool (Fig. 1f). While Rdi1 overexpression reduced the concentration of Cdc42 in the polar cap of Wt cells, in *Δlem3* cells a nearly Wt pre-extraction level remained (Fig. 1d, e) even after 150 minutes of Rdi1 induction. Consistently, mobile Cdc42 particle number in the cytosol remained similar to the pre-induction level even after 150 min of Gal induction (Fig. 1f). As the mean fluorescence intensity of GFP-Cdc42 over the entire cell was slightly reduced in Δ*lem3* (by ~15%) (Supplementary Information, Fig. S4) compared to that in Wt, the reduced Cdc42 soluble pool after 150 min Gal induction in Δ*lem3* (reduced by ~40%, Fig, 1c, f) can be explained as a combined effect of a slightly reduced expression and the reduced extraction from the polar cortex.

The above result suggests that *Δlem3* increases the steady-state pool of Cdc42 at the polar cortex. This effect may be due to either slowing down Cdc42 dissociation from the polar cortex or promoting fast re-association of Cdc42 with the polar cortex. To distinguish between these possibilities, we performed fluorescence recovery after photobleaching (FRAP) experiments of GFP-Cdc42 at the polar cortex. FRAP reflects the recycling process whereby, following photobleaching at the cortex, the bleached molecules at the polar cortex dissociate while the fluorescent molecules from the cytosol associate. We previously established a mathematical model for Cdc42 recycling that allows extrapolation of the rates for Cdc42 dissociation and association from FRAP data (Slaughter et al., 2009) (Fig. 2a, b). To apply this model to *Δlem3* cells, the window of polarized delivery was determined in the mutant strain (Fig. S5). Model computation found that Δlem3 most significantly reduces m, the rate of Cdc42 dissociation from the polar cap

region, but the effect is less significant on n, the dissociation rate outside the polar cap region (Fig. 2c, d). h, the rate at which Cdc42 is targeted to the polar cap, was also slightly reduced, not enhanced, in Δlem3 compared to Wt (Fig. 2e). The mathematical model also predicts that a reduced m relative to n leads to a slightly more pointed polar cap (Slaughter et al., 2009), which could be observed in Δlem3 cells (Supplementary Information, Fig. S6). As an experimental validation of the model computed m, we performed inverse FRAP (iFRAP) (Slaughter et al., 2009) to measure the rate of internalization of GFP-Cdc42 at the polar cap. Here the fluorescence intensity at the plasma membrane and cytosol, but not the polar cortex, is bleached. Dissociation of the bright molecules from the polar cortex is measured as the intensity decays at this region. Indeed, iFRAP showed a reduced rate of internalization of GFP-Cdc42 at the polar cap in *Δlem3* cells (Fig. 2f, g).

Cdc42 recycling from the polar cortex is governed by two functionally redundant pathways, one involving Rdi1 and the other involving actin-mediated endocytosis (Slaughter et al., 2009). To determine which of these pathways is inhibited in *Δlem3*, iFRAP was performed on *Δlem3* cells in the presence of latrunculin-A (LatA), an actin polymerization inhibitor. Disrupting actin polymerization in *Δlem3* further slowed down Cdc42 dissociation to an extent comparable to the effect of LatA on Wt cells (Fig. 2f, g), suggesting that in the *Δlem3* mutant the actin pathway is operative to a similar extent as in the Wt. By contrast, the combined effect of Δrdi1 and *Δlem3* on the dissociation of Cdc42 from polar-cap is negligible compared to Δrdi1 alone (Fig. 2g). These results suggest that Lem3 selectively promotes Rdi1-mediated Cdc42 dissociation from the polar cortex. Furthermore, as shown in previous work where simultaneous disruption of both actin and the Rdi1 pathway led to rapid cell depolarization(Slaughter et al., 2009), LatA treatment also led to drastic reduction of polarity in *Δlem3* cells compared to the DMSO control (Fig. 2h), consistent with a role for Lem3 as an important regulator of Rdi1-mediated Cdc42 recycling in the establishment of a stable polarity for budding.

PE mobilization by the Lem3 flippase complex enhances Cdc42 dissociation by Rdi1

Lem3 is a non-catalytic subunit of the lipid flippase complex with the P4-ATPases Dnf1 and Dnf2, which selectively translocates aminophospholipids, such as PE and phosphatidylcholine (PC), from the outer to inner plasma membrane leaflet(Hanson et al., 2003; Kato et al., 2002; Pomorski et al., 2003; Pomorski and Menon, 2006). To test whether this flippase complex is involved in fast Cdc42 dissociation from the polar cortex, we performed iFRAP on *Δdnf1* and *Δdnf2* single or double mutant cells. Cdc42 dissociation was significantly slowed in these mutant cells and interestingly even the single mutants exhibited significant reductions (Fig. 3a), consistent with the previous report that even the single *Δdnf1 or Δdnf2* mutant showed significant exposure of PE at the outer membrane leaflet at the bud tip(Iwamoto et al., 2004). To further demonstrate that the reduced rate of Cdc42 recycling was a direct consequence of the loss of flippase activity, we tested if acute inhibition of lipid flipping had the same effect by using the tetracyclic peptide Ro09-0198 (Ro, also called cinnamycin), which specifically binds to PE exposed on the outer plasma membrane leaflet when added to the culture media(Aoki et al., 1994; Iwamoto et al., 2004). Inhibiting PE flipping by the Ro peptide at 50 μM slowed down Cdc42 dissociation from polar cortex in Wt cells but not in *Δlem3* cells (Fig. 3b). We note that the Ro peptide concentration used in our experiment did not cause a high level of cell death (only ~ 5% and comparable to the level with solvent control) as determined by propidium iodide and flow cytometry analysis (Supplementary Information, Fig. S7). Together the above experiments show that PE flipping is required for fast Cdc42 dissociation from the polar cortex.

A previous study observed an enhanced PS internalization while PE and PC flipping is inhibited in the *Δdnf1Δdnf2* double mutant (Stevens et al., 2008), possibly reflecting a mechanism of maintaining membrane phospholipid homeostasis. However, as a consequence, this could lead to an increase in negatively charge phospholipids at the inner membrane leaflet of the polar cortex. As Cdc42 contains a highly conserved cationic tail immediately adjacent to the prenylation site, the slowed Cdc42 dissociation in *Δlem3* may be due to an enhanced charge interaction between Cdc42 and membrane lipids. To test this possibility, we first used the PS biosensor GFP-Lact-C2 (Yeung et al., 2008) to monitor whether *Δlem3* altered the distribution of PS on the inner plasma membrane

leaflet. Consistent with the reported observation(Yeung et al., 2008), PS is concentrated at the site of polarization in Wt cells (Fig. 3c; Supplementary Information, Fig. S8a). Interestingly, intensity quantification for half of the cortex containing the polar cap region vs. the opposite half found that the GFP-Lact-C2 signal is more strongly polarized in the *Δlem3* mutant compared to that in Wt, and the enhance PS polarization is also observable after bud emergence (Fig. 3c-e and Supplementary Information, Fig. S8b). By contrast, the distribution of GFP-2xPH-PLCδ(Stefan et al., 2002), a biosensor for $PI(4,5)P_2$ (PIP2), was not significantly different between Wt and *Δlem3* cells (Supplementary Information, Fig. S9a-c). This result suggests that in the *Δlem3* mutant a defect in PE flipping is associated with enrichment for the anionic lipid PS in the inner membrane leaflet at the polar cortex.

To test if charge interactions between phospholipids at the polar cortex and the Cdc42 cationic tail (aa183-187, KKSKK) play any role in Cdc42 recycling, we increased the Cdc42 polycationic charge by mutating S185 to lysine (KKSKK to KKKKK) and performed iFRAP on Wt and *Δlem3* cells expressing $Cdc42^{S185K}$. In Wt cells, the $Cdc42^{S185K}$ dissociation rate from the polar cortex was significantly slower than that of Cdc42, approaching the same slow rate of Cdc42 dissociation in *Δlem3* (Fig. 3f). In *Δlem3*, $Cdc42^{S185K}$ also exhibited a moderate but significant decrease in dissociation rate compared to that of Cdc42 (Fig. 3f). As it is possible that serine185 might act as an electrostatic switch through phosphorylation(Forget et al., 2002), we also mutated this residue to alanine. However, the $Cdc42^{S185A}$ did not exhibit a reduced iFRAP rate compared to Cdc42 in Wt cells and displayed even a slightly increased iFRAP rate compare to Cdc42 in *Δlem3* (Fig. 3f), suggesting that it is unlikely phosphorylation of serine185 regulates Cdc42 dissociation. We also mutated the S185 residue to the negatively charged aspartic acid, and the resulting mutant protein ($Cdc42^{S185D}$), unlike $Cdc42^{S185K}$, was poorly localized to the polar cap in both Wt and *Δlem3* cells (Fig. 3g, h). These observations support the notion that charge interactions between the Cdc42 polycationic tail and the phospholipids at the polar cortex strongly influence Cdc42 recycling and plasma membrane association.

Phospholipid composition affects Cdc42 recycling through modulating the charge interaction between Cdc42 and the membrane

To further determine if lipid composition can directly influence Rdi1-mediated Cdc42 dissociation from the membrane, we employed an in vitro system involving supported lipid bilayers (SLB) to eliminate the confounding effects of many other factors, such as the Cdc42 GTPase cycle and effector interactions, on Cdc42 dynamics in the cell. SLBs were assembled from liposomes with two different lipid compositions, including one enriched for PS (see Methods; referred to as 40% PS, 15% PE), and the other enriched for PE (referred to as 40% PE, 15% PS). We took advantage of the biarsenical dye FlAsH which fluoresces upon binding to a tetra cysteine motif (TC). Prenylated Cdc42 with an N-terminal TC motif (TC-Cdc42) was expressed and purified from a yeast plasma membrane fraction and C-terminal (His)6-tagged Rdi1 from bacteria (Supplementary Information, Fig. S10a,b) (see Methods). After labeling with FlAsH, TC-Cdc42 was added to the SLB and appeared as a fluorescent layer with some bright foci when observed with total internal reflection fluorescence microscopy (TIRF) (Supplementary Information, Fig. S11a). The binding to the SLB was dependent on the prenyl group of Cdc42 as non-prenylated TC-Cdc42 purified from bacteria did not associate with the SLB (Supplementary Information, Fig. S11b, c). In the SLB with 40% PS, 15%PE, the fluorescence intensity of the SLB-bound TC-Cdc42, observed with TIRF, decreased spontaneously and slowly in the presence of BSA control, and this decay was not enhanced by the presence of different Rdi1 concentrations (Fig. 4a, c). Importantly, in the case of the SLB with 40% PE, 15% PS, addition of Rdi1 stimulated the dissociation of Cdc42 from the membrane in a dose-dependent manner (Fig. 4b, c). This result confirms that enrichment of PE in the phospholipid directly enhances Rdi1-mediated Cdc42 dissociation from the membrane.

Based on the data presented above we propose a model whereby the localized Lem3-Dnf1/2 flippase complex acts as an electrostatic switch to promote fast Cdc42 dissociation from the plasma membrane by Rdi1 (Fig. 4e). At the steady state, the polar cortex region is enriched for PE in the outer leaflet and PS in the inner leaflet (Saito et al., 2007; Yeung et al., 2008). Such lipid asymmetry facilitates the localization of Cdc42 to the polar cortex by enhancing the charge

interaction between the polycationic tail of Cdc42 and the negatively charged membrane surface. A local and perhaps transient increase in lipids with positively charged head groups (such as PE) as a result of localized flippase activity destabilizes the charge interaction of Cdc42 with the inner membrane leaflet, increasing the chance of exposure of the prenyl moiety on Cdc42, thus promoting its capture by the cytosolic Rdi1 protein.

Discussion

A previous study implicated the Lem3 flippase activity in regulating the activity of the GTPase activating proteins (GAP) for Cdc42 and proposed that this regulation is important for the apical to isotropical switch of cell growth at G2/M (Saito et al., 2007). Two lines of considerations suggest that the regulation of Cdc42 dynamics observed in our study by the flippase complex is not a result of GAP regulation. First, the conclusion that PE flipping regulates GAP activity in the previous work was based on the in vitro demonstration that PE and PS stimulated the GAP activity of Rga1 toward Cdc42, contrasting the inhibitory effect of PIP_2. However, as shown in this work, and also as supported by an earlier study (Stevens et al., 2008), the PE flipping defect in the flippase mutants is accompanied by a further enrichment of PS, not PIP_2, at the inner membrane leaflet of the polar cortex. As PS and PE are equally effective in stimulating Cdc42 GAP in vitro (Saito et al., 2007), the reciprocal enrichment of PS and PE at the inner and outer membrane leaflet in the mutant, respectively, would predict little net effect on the GAP activity. By contrast, our model is fully consistent with the change in the charge property of the inner membrane leaflet in the flippase mutants, and our in vitro data supports a direct effect of the lipid composition on Cdc42 dissociation by Rdi1. Second, in the previous study the key in vivo result supporting the authors' conclusion was that over-expression of the GAP Rga1 rescued the elongated bud morphology in *Δlem3*, leading to the idea that lipid flipping regulates GAP activity in vivo. However, in budded cells beyond the nascent-bud stage, Rga1 is localized at the bud neck (Caviston et al., 2003), while Lem3 is at the bud tip (Kato et al., 2002). Thus, it is unlikely that a direct regulation of the GAP by localized flippase activity underlies the observed genetic interaction. Consistently, Rga1 over-expression does not rescue the defect in Cdc42 dynamics in *Δlem3* (Supplementary Information, Fig. S12). Taken together, our study reveals a new

mechanism by which dynamic lipid asymmetry regulates a highly conserved signaling process in cellular morphogenesis. This mechanism works in parallel with the GTPase cycles and effector interactions in the control of Cdc42 dynamics and function.

ACKNOWLEDGEMENTS

The authors thank W. Wiegraebe (Stowers Institute for Medical Research) for advice on imaging and K. Lee (Harvard Medical School) for advice on supported lipid bilayer preparation. This study was done to fulfill, in part, requirements for A.D.'s PhD thesis as a student registered with the Open University. This work was supported by NIH grant RO1-GM057063 to R.L.

AUTHOR CONTRIBUTIONS

A.D. and R.L. designed the experiments; A.D. performed all experiments and prepared the manuscript, with help from B.D.S. and J.R.U.; R.A. and D.B. assisted in the whole genome screening; B.R. assisted in data analysis; R.L. conceived and supervised the project and revised the manuscript.

METHODS

Genome-wide screening for suppressors of Gal-Rdi1. (Please see Chapter 5 method section, page 80-81) Based on the distribution shown in Figure S1a, we used a growth ratio cutoff of 0.56, such that strains with a growth-ratio equal to or above 0.56 were considered as rescuer candidates. Based on gene annotation in the Saccharomyces genome database (SGD), genes encoding proteins involved in galactose-regulated transcription pathway and gene expression were excluded. For the purpose of this study, we focused on a sub-group of the rescuer candidates that are localized to the plasma membrane (Fig.S1b).

Yeast growth and treatments. A detailed list of yeast strains used in this study is provided in (Supplementary information, Table 1). For Rdi1 over-expression, strains were grown in synthetic media with raffinose until mid-log phase, at which time they were induced with 2% galactose. In most experiments GFP-Cdc42 was expressed under the Cdc42 promoter; for experiments where certain Cdc42 mutants were examined, expression was induced under the Gal1 promoter for 90-120 min, at which point the level resembles the endogenous level of Cdc42(Slaughter et al., 2009). Ro peptide (Sigma) was added at 50 μM concentration for 30min at room temperature to an exponential growing culture. To disrupt actin filaments, Lat-A (BioMol) at 100μM was incubated with cells for 15min at room temperature.

Quantification of cell death and viability in the presence of Ro peptide. Cell death was measured as follows. Exponentially growing Wt (RLY2530) cells were treated with Ro peptide as mentioned above in parallel with the solvent control treatment of an equivalent amount of solvent (water-acetonitrile; 1:1). Treated cells were washed with Sodium citrate (0.05M) and resuspended in 1ml of sodium citrate buffer. Dual staining for live/dead cells were performed using propidium iodide (stains permeabilized dead cells) and SYTO9 (stains live cells) following Molecular Probes protocol (Live/Dead Fungal Light Yeast Viability Kit, Molecular Probes). Live/ dead cells were counted using flow cytometry (MACSQuant Analyzer). Control for dead cells was prepared by incubating Wt cells at 75^0C for 15 min and for live cells at 23^0C for 15 min.

Live cell imaging and data analysis. FRAP and iFRAP experiments and data analysis were performed as described (Slaughter et al., 2009). Confocal images were taken with an inverted Zeiss 200 microscope equipped with a spinning-disc confocal system (Yokagawa) and a 100X, 1.45NA Plan-Fluor oil objective. GFP emission was collected through a BP505-540 nm filter onto an EM-CCD (Hamamatsu C9100). High signal to noise for the still images in Figure 3c, 3g, 3h, S2, S5, S6, S8a-b and S9a were obtained by summing 20 middle confocal slices of short movie of 20 frames. Confocal images for cells with Rdi1 over-expression (Fig. 1d) were acquired using the avalanche photodiode (APD) imaging module of a Zeiss Confocor 3, using a 40X, 1.2-NA C-Apochromat water objective. Images were presented with identical contrast between Wt and Δ*lem3* in Figure 1d, 3c, 3g, 3h, S6, S8b, S9a, S11a, b. Image analysis and data extraction were performed using imageJ software, statistical analysis and data plotting were performed using OriginLab Pro software.

Fluorescence correlation spectroscopy. Please see chapter 2 for detail explanation of FCS study, data analysis and the focal volume calculation using FCS.

Comparison between one-component vs. two-component model for FCS data fitting

An F-test was performed to compare the one component and two component diffusion model (Bevington, 2003). FCS obtained from GFP-Cdc42, two component model represented a strong improvement in the quality of the fit as judged by the F-test ($p<1 \times 10^{-10}$) and the visual inspection of quality of the fit and residuals (Fig.1b). The FCS data obtained from Rdi1-mCherry was also fitted with one and two-component models. In either case, the autocorrelation curve for Rdi1 is dominated by a rapidly diffusing component (more than 95% of population) (Supplementary Information, Fig. S3c, d). An F-test between the models preferred the two-component fit with a p-value of less than 1×10^{-10}. However, given the small amplitude of the slow component, we conclude that it represents a relatively insignificant portion of the Rdi1 population.

For measurements of fast and slow pool concentrations of GFP-Cdc42 in the presence of Gal-Rdi1 (see Fig 1c, f), it is reasonable to assume that fast and slow diffusion times will remain unchanged. Therefore the diffusion times were fixed to the values obtained for the Wt strain at the 0 min time point for Gal induction. Indeed, the curves were reasonably well fit by this model in

every case. This allows for unbiased estimation of fast and slow pool concentrations as a function of Gal induction time.

Modeling. For each cell, the mathematical model was applied for the analysis of the FRAP movie. Model parameters and assumptions are as described previously (Slaughter et al., 2009). In brief, the model shown by Equation 4 explains the dynamics of surface density f(r, Φ, t) of Cdc42 which depends on d_f, the diffusion coefficient along the plasma membrane, m, the Cdc42 internalization rate inside the delivery window. n is the internalization rate outside the window and h represents the rate of delivery inside the window. F_c is the total amount of cytosolic Cdc42, while χ=1 in the delivery window, which was found to be similar and overlapping both for Rdi1 and the actin-based recycling pathways (Slaughter et al., 2009), and χ=0 outside it . Considering the overlapping window size between the actin and Rdi1 based recycling mechanisms, we measured the window size from the formin Bni1 distribution in *Δlem3* cells (Supplementary Information, Fig. S5a-c) and found it similar to the distribution of Bni1 in Wt cells (Slaughter et al., 2009). The parameters of Cdc42 dynamics were extracted by the model based on FRAP movies.

$$\frac{\partial f}{\partial t} = d_f \Delta f - m\chi f - n(1-\chi)f + h\chi F_C \qquad (4) \text{ (Slaughter et al., 2009)}$$

Recombinant protein purifications. To purify TC-Cdc42 from the yeast plasma membrane, we constructed a plasmid with a "pGAL1-GST-HA-TC-Cdc42" sequence (GST-HA-TC sequence will be referred to as FlAsH cassette and Cdc42 protein with N-terminally tagged FlAsH cassette as TC-Cdc42) by subcloning the FlAsH cassette into a pRS316-based yeast vector, formerly used to expressed pGal-Myc-GFP-Cdc42, by the Gap-repair technique(Ma et al., 1987). We used a genetically encoded tetracysteine motif (HRWCCPGCCKTF) (TC) (Martin et al., 2005) that binds efficiently to the biarsenical dye FlAsH and absorbs at 488nm and emits at 525 nm. The FlAsH cassette was amplified from a pGEX vector containing a GST sequence using the following primers with the mentioned order of sequences: forward primer - 40bp-homologous to the 3' end of pGAL, BamH1, 20bp 5' GST sequence; reverse primer - 20bp 3' end of GST sequence, HA, TC, linker, XhoI, 40bp-homologous to the Cdc42 ORF 5' sequence. The circular recombinant plasmid

was generated by transforming yeast with the gapped vector (with Myc-GFP excised) and the FlAsH cassette PCR product, both having appropriate homology at their free ends.

For purification of yeast-expressed prenylated Cdc42, the above vector with the GST-HA-TC-Cdc42 was transformed into a Δrdi1 strain. The tagged Cdc42 was over-expressed to maximize the amount of protein at the plasma membrane and purified from a plasma membrane fraction. Cell fractionation to prepare plasma membrane and protein purification was carried out as previous described (Goud et al., 1988; Johnson et al., 2009) with modifications. Cells were grown overnight at 30^0C and induced with 2% galactose at 30^0C for 3hr and pelleted at 6238 x g for 10 minutes. The cell pellet was resuspended in 10mM sodium-azide solution, pelleted, and subsequently resuspended with spheroplast buffer (1.4M sorbitol, 50mM KPi [pH7.5], 10mM azide, 40mM β-mercaptoethanol and 3mg zymolase-100T[US Biological (Z1005)]) and incubated for 45 min with gentle shaking at 37^0C. The spheroplasts were resuspended in lysis buffer (0.8M sorbitol, 10mM triethanolamine, 1mM EDTA [pH7.2] and 5mM $MgCl_2$) supplemented with 1mM DTT, 1mM PMSF and 1X protease inhibitor cocktail (PI) (Sigma-Aldrich, P2714) and homogenized 20 times with a 10ml Wheaton tissue grinder. Unlysed cells were pelleted at 400 x g for 10 min. The pellet (P1) obtained at this step was rewashed with 5mL lysis buffer and the supernatants were pooled (S1). The plasma membrane-containing S1 pool was centrifuged twice at 158,420 x g for 45 min to pellet plasma membrane fractions (P2). The plasma membrane-rich pellet P2 was resuspended in solubilization buffer (50mM Tris [pH7.5], 300mM NaCl, 5mM $MgCl_2$, 1% Triton X-100 and 0.8M sorbitol), briefly homogenized 15 times on ice and the resultant solution was incubated under shaking for 45 min at 4^0C. The solution was further centrifuged at 9000 X g for 20min and the supernatant (S3) was loaded on glutathione-agarose beads (Sigma, G4510) pre-equilibrated with solubilization buffer. The beads were washed with several column volumes of wash buffer (50mM Tris [pH7.5], 300mM Nacl, 5mM $Mgcl_2$, and 0.1% CHAPS) supplemented with PI, PMSF and DTT. Before elution, beads were rinsed with elution buffer (Tris-HCl [pH8.0] and 0.1% CHAPS]. Finally, TC-Cdc42 was eluted with 10mM reduced glutathione (Sigma-Aldrich, G4251).

For Rdi1 purification, yeast Rdi1 was subcloned into the pET-28a vector with a C-terminal hexahistidine tag. Protein purification was done as previously described(Johnson et al., 2009) with minor modifications. Briefly BL21 E.coli cells containing the pET-28a vector with Rdi1-6XHis were grown at 37^0C until optical density reached 1.0, at which point cells were induced with isopropyl β-D-1-thiogalactopyranoside (IPTG, 1mM) for another 3hr at 37^0C. Cells were pelleted at 6238 x g for 10 min and resuspended in TBSM buffer (50mM Tris [pH7.5], 150mM NaCl and 5mM $MgCl_2$). Cells were lysed by sonication in the presence of protease inhibitor cocktail (Thermo Scientific, product # 78430), 1mM PMSF and 1mM DTT on ice and the supernatant was collected at 30996 x g for 20 min. Prior to loading on Ni^{2+} resin (Catalog # 156-0133) the supernatant was filtered through a 0.22μm steri-cup. Before protein elution the column was washed with several column volumes of TBSM containing 20mM imidazole. Finally the protein was eluted with TBSM containing 500mM imidazole.

For non-prenylated Cdc42, the HA-TC-Cdc42 sequence was amplified by PCR and subcloned into a pGEX vector to generate the resulting GST-HA-TC-Cdc42 sequence. After induction with IPTG, cell extracts containing were prepared in TBSM buffer as explained above. The protein was loaded on TBSM-equilibrated glutathione-agarose beads. After washing with several column volumes of TBSM, the protein was eluted with 10mM reduced glutathione in TBSM.

Liposome Preparation. To prepare liposomes we purchased chloroform solutions of porcine brain PE (catalog # 840022C), porcine brain PS (catalog # 840032C), and porcine brain PC (catalog # 840053C) from Avanti Polar lipids, Inc. Cholesterol was purchased from Nu-Chek prep, and dissolved in chloroform. Lipids were mixed in a clean glass tube and dried under a gentle stream of nitrogen gas and further dried under vacuum for 1hr. The dried lipid mixture was hydrated and resuspended with the TBSM buffer to a final concentration of 2mM (Lee et al., 2010) and bath sonicated for 30 min at 45^0C to produce the final liposome solution(Poste, 1976).

Cdc42 extraction assay using TIRF microscopy. Supported lipid bilayers were prepared on No. 1.5 glass coverslips. Coverslips were made hydrophilic with a rinse with a concentrated H_2SO_4 and H_2O_2 (3:1) mixture and thoroughly washed with ultrapure water and dried with a stream of nitrogen

gas. Liposomes with the composition 40% PS, 15% PE, 5% PC and 40% cholesterol, or 40% PE, 15% PS, 5% PC and 40% cholesterol, were added to this coverslip and incubated for 20 min and washed thoroughly with TBSM buffer. Prenylated Cdc42 with the TC FlAsH binding motif was labeled with 166.6μM FlAsH dye (Invitrogen, Carlsbad, CA catalog # T34561) for 1hr at room temperature and added to the lipid bilayer at 63-126 nM final concentration, followed by 10 min incubation. Unbound and loosely bound protein was thoroughly washed out from the lipid bilayer with TBSM buffer. Separate coverslips with the above reaction mixtures were used for observation of fluorescence intensity decay in the presence of TBSM buffer with 1250nM BSA or TBSM buffer supplemented with 250nM, 750nM or 1250nM Rdi1 at room temperature. TIRF measurements were performed using a Carl Zeiss (Jena, Germany) Axiovert 200 M inverted microscope equipped with the Laser TIRF accessory and a Plan-Apochromat 100X, 1.46 NA objective. FlAsH-Cdc42 was excited with a 488 nm laser line, and emission was separated through a Z488RDC dichroic mirror, and collected through a HQ525/50m emission filter (Chroma Technology Corp., Bellows Falls, VT) onto a C9100-13 EM-CCD digital camera from Hamamatsu Photonics (Japan) at maximum gain. Movies were acquired 20 ms exposure time using 1% laser power at an interval of 20sec using Carl Zeiss Axiovision software.

TIRF images were acquired with or without laser excitation at every 20 s for 800-1200 s and the series without laser excitation were subtracted as background. Image processing and data extraction were done using ImageJ software to measure the average of selected image regions as a function of time. We note that in the presence of 40% cholesterol, the bright foci of Cdc42 do not decay in intensity under all conditions. Thus, to quantify Cdc42 extraction from the SLB, 3 to 10 rectangular SLB areas excluding the bright foci were sampled from each experiment and 1 to 4 experiments were done for each reaction condition. The fluorescence intensity (I) decay for each area was fitted for to an exponential decay model, $I = A_0 + A_1\exp(-\alpha t)$, where α is the exponential decay rate. Statistical analysis and presentation of the decay rates obtained from above analysis was performed in OriginLabPro software.

Statistical analysis Statistical differences between two sets of data other than FCS data (see above) were analyzed with a two-tailed unpaired Student t-test.

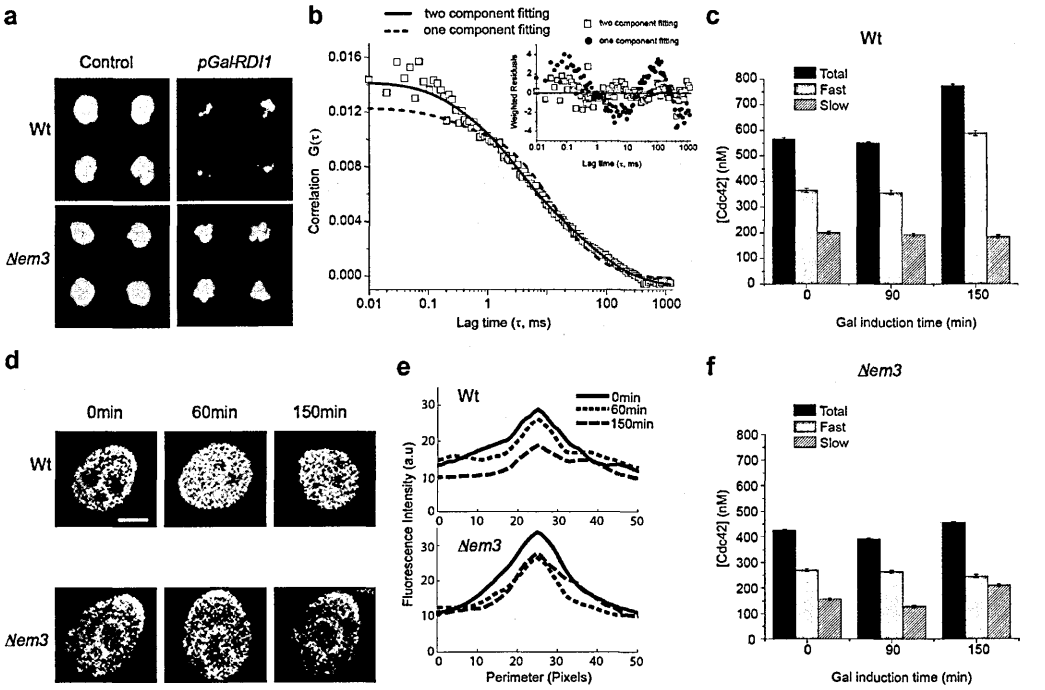

Figure 4-1. *Δlem3* suppresses the effect of RDI1 over-expression on growth and Cdc42 distribution.

(**a**) Images of Wt and the *Δlem3* mutant grown on solid media with or without Rdi1 over-expression (pGal-RDI1) from the genome-wide screen. Four replicate spots were observed for each strain. (**b**) Example auto-correlation curve of GFP-Cdc42 in Wt cells under its endogenous promoter. FCS data was averaged over 13 cells and fitted with a one-component or two-component diffusion model. Weighted residuals obtained from each fitting are shown in the inset. (**c**) Mobile Cdc42 concentration (nM) of the fast and slow diffusing pools (as indicated) determined at different times of pGal1-Rdi1 induction in Wt cells. Shown are means and estimated standard errors (see Supporting Methods) from the analysis of average autocorrelation curves obtained from 14-27 cells for each time point. (**d**) Representative images of GFP-Cdc42 at the polar cap in unbudded Wt and *Δlem3* cells at different times of Rdi1 induction (as indicated above each column). Scale bar: 2 μm. (**e**) Fluorescence intensity profiles of GFP-Cdc42 along the perimeter of Wt or *Δlem3* cells at different time points of Gal-RDI1 induction. Fluorescence traces from 10-12 cells were first aligned by their peak positions to the same position and then averaged to yield each of the profiles shown. (**f**) Same analysis and display as in (**c**) for *Δlem3* cells.

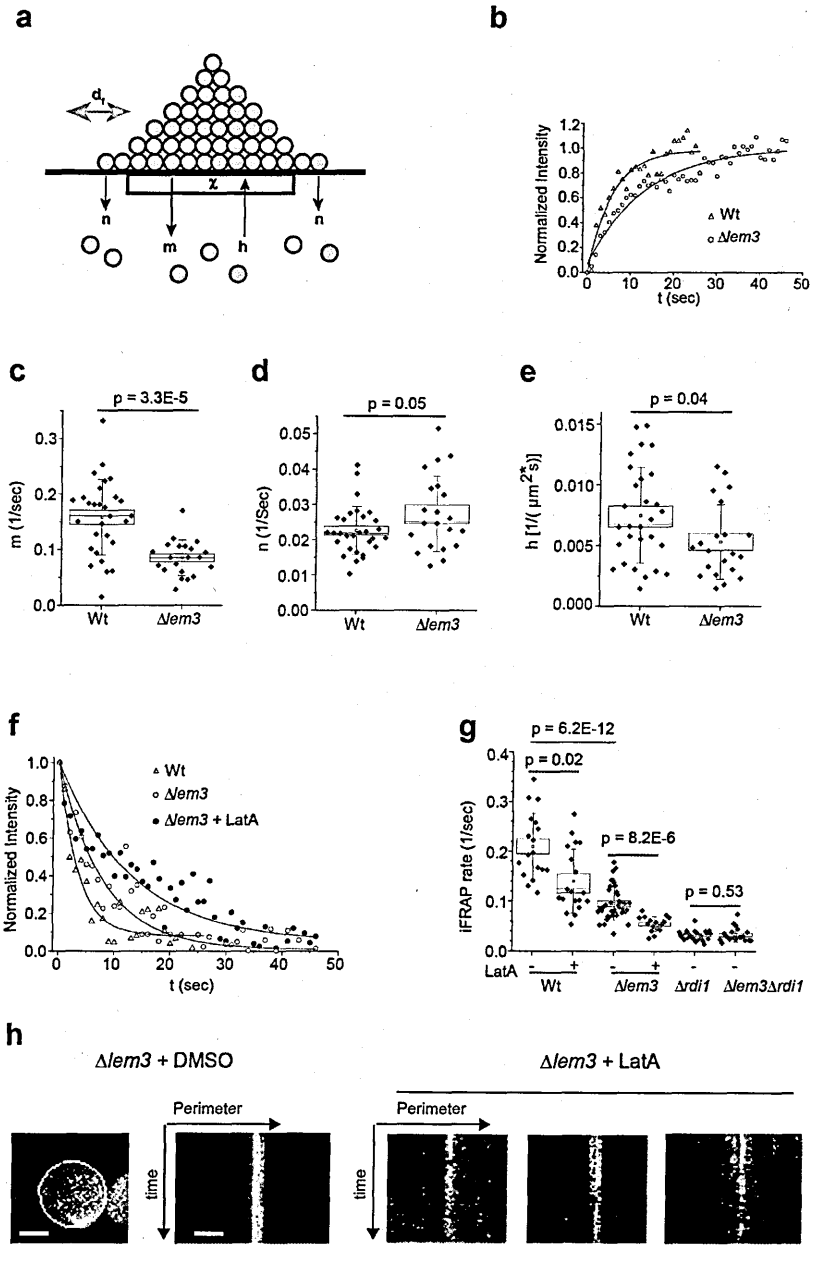

Figure 4-2. Lem3 regulates Rdi1-mediated Cdc42 extraction and polar cap morphology. (**a**) Schematic representation of the mathematical model as previously described (Slaughter et al., 2009). Gray horizontal bar represents the overlapping Rdi1 and actin-based delivery window (χ) which is approximately 25% of the perimeter as quantified from the Bni1 distribution (Supplementary information, Fig. S5) (Slaughter et al., 2009); d_f, lateral diffusion rate of Cdc42 in the membrane; m and n, internalization rates inside and outside the delivery window, respectively; h: delivery rate inside the window. (**b**) Example

normalized FRAP curves of GFP-Cdc42 from Wt and Δ*lem3* cells. Solid lines represent the exponential fit of the FRAP data. (**c-e**) Extracted model parameters from FRAP data. Each point represents a value from a single cell. The small square is the mean; the box range is SEM; whiskers represent standard deviation (SD); line is median. (**f**) Examples of normalized iFRAP curves from cells expressing GFP-Cdc42. (**g**) iFRAP rates (1/s) from cells expressing GFP-Cdc42. Box plots are as described in (c-e). (**h**) Example kymographs obtained from bleach corrected movies (300s-385s long) along the perimeter of *Δlem3* cells expressing GFP-Cdc42 in the presence of solvent control (DMSO) or 100 μM LatA (3 examples are shown). Data shown panel (h) has the contribution from Brian D. Slaughter.

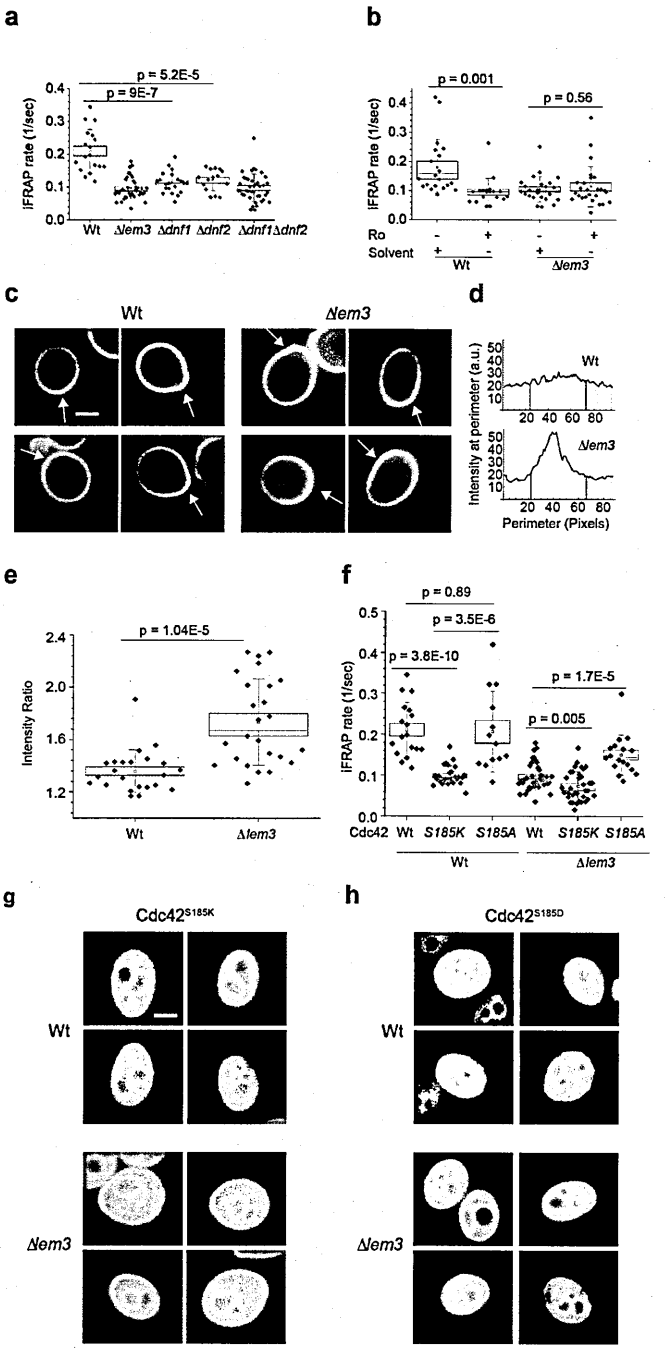

Figure 4-3 Flippase activity and charge interactions regulate Cdc42 dynamics.

(a) iFRAP rates of GFP-Cdc42 in polarized unbudded cells with single or double deletion of DNF1 and DNF2 in box plots as described in Figure 2 legend. (**b**) iFRAP rates displayed as in (**a**) for GFP-Cdc42 in Wt and Δ*lem3* cells after treatment with 50 μM Ro-peptide for 30 min at room temperature. Solvent control was with the same volume of water-acetonitrile (1:1). (**c**) Representative confocal images of Wt and Δlem3 cells expressing GFP-Lact-C2. White arrows point to polar cap. Scale bar: 2μm. **(d)**

Representative fluorescence intensity traces along the cell perimeter. White area represents total fluorescent intensity in the half of the plasma membrane containing the polar cortex, whereas the opposite half is represented as a gray area. (**e**) Ratios of fluorescence intensity in the half of the plasma membrane containing the polar cap (white area) over that in the rest of the plasma membrane (grey area). Box plots are as described in (a). **(f)** Internalization rate of $Cdc42^{S185K}$ and $Cdc42^{S185A}$ at the polar cap measured with iFRAP in Wt and Δ*lem3* cells, displayed as in (**a**). (**g-h**) Representative confocal images of Wt and Δ*lem3* cells expressing GFP-tagged $Cdc42^{S185K}$ (**g**) or $Cdc42^{S185D}$ (**h**). Scale bar: 2μm.

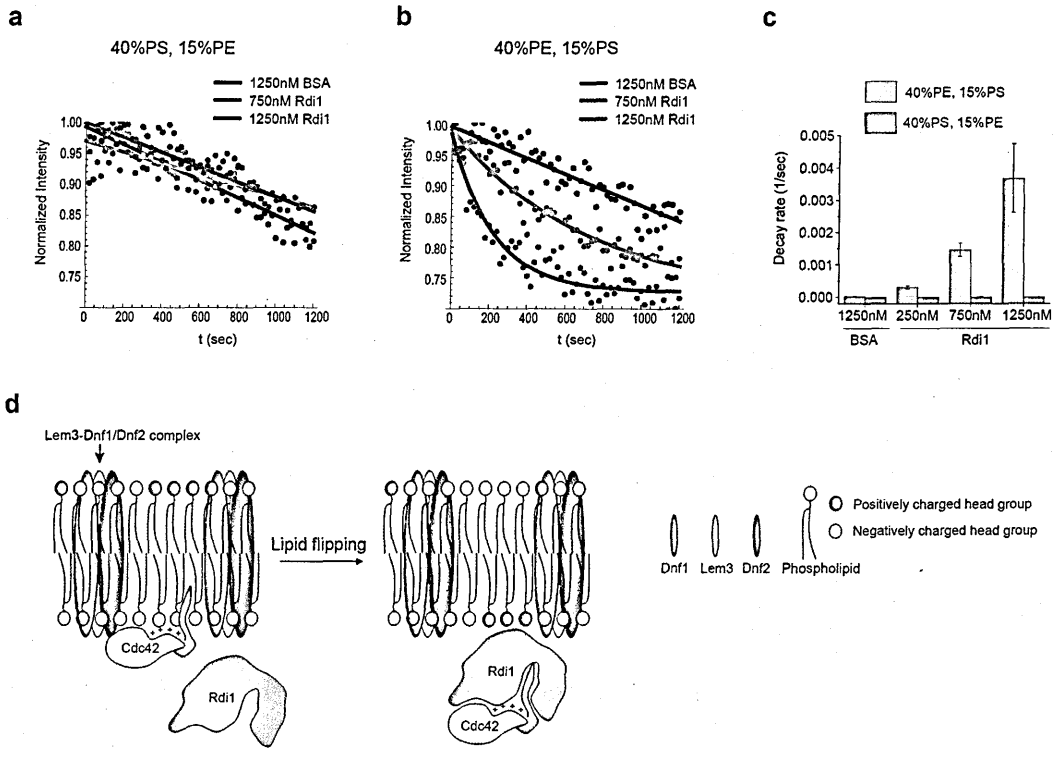

Figure 4-4. Rdi1-mediated Cdc42 dissociation from supported lipid bilayers (SLB). **(a)** Example traces of fluorescence intensity decay due to dissociation of FlAsH labeled TC-Cdc42 from the SLB containing 40% PS and 15% PE as measured by TIRF microscopy. Fluorescence intensity values were normalized to the maximum intensity of each trace (dots) and fitted to an exponential decay model (lines). **(b)** Same experiment and data presentation as in (**a**) but in the presence of higher concentration of PE (40%) relative to PS (15%). (**c**) Rates of TC-Cdc42 dissociation from the SLB determined from the TIRF movies, for 40% PE, 15% PS (n = 10, 10, 18, 18 from left to right) and for 40% PS, 15% PE (n = 10, 10, 15, 10 from left to right). Bar graphs show mean and SEM. **(d)** A schematic model depicting that, by changing the charge property of the inner membrane

leaflet, the flippase complex regulates Rdi1-mediated dissociation of Cdc42 from the plasma membrane. On the left, the Cdc42 prenyl group (red) is inserted in the inner leaflet of the plasma membrane at the polar cortex with electrostatic interaction between Cdc42 cationic C-terminal region (+) and the negatively charged phospholipid head groups (blue circles) providing stability for this association. The flippase complex mobilizes phospholipids with positively charged head groups such as PE from the outer to inner leaflet, reducing the electrostatic interaction between Cdc42 and the membrane and enhancing the access of Rdi1 to the Cdc42 prenyl group, and thus facilitating the formation of the cytosolic Cdc42-Rdi1 complex.

Supplemental Information

a

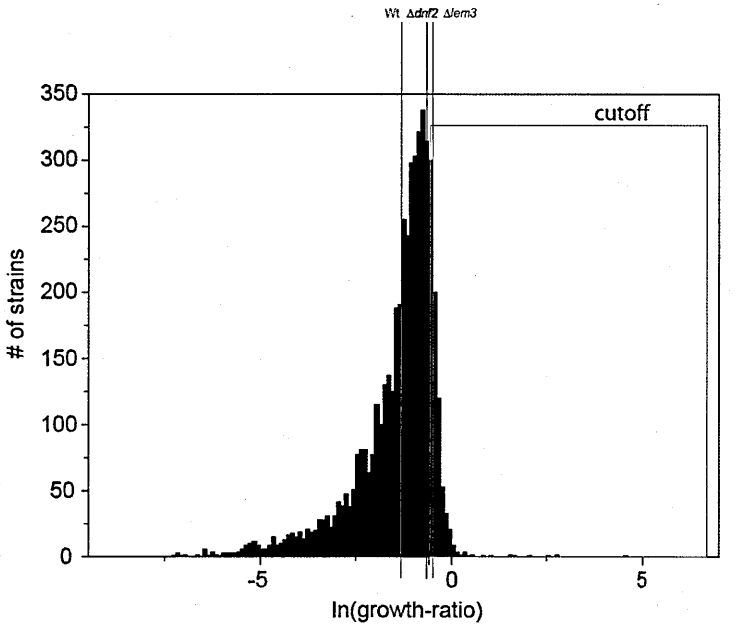

b Rescuer candidates that localize to the plasma membrane.

LEM3	Membrane protein of the plasma membrane and ER, interacts specifically in vivo with the phospholipid translocase (flippase) Dnf1p; involved in translocation of phospholipids and alkylphosphocholine drugs across the plasma membrane.
THI73	Putative plasma membrane permease proposed to be involved in carboxylic acid uptake and repressed by thiamine; substrate of Dbf2p/Mob1p kinase; transcription is altered if mitochondrial dysfunction occurs
PUN1	Plasma membrane protein with a role in cell wall integrity; co-localizes with Sur7p in punctate membrane patches; null mutant displays decreased thermotolerance; transcription induced upon cell wall damage and metal ion stress
FUS1	Membrane protein localized to the shmoo tip, required for cell fusion; expression regulated by mating pheromone; proposed to coordinate signaling, fusion, and polarization events required for fusion; potential Cdc28p substrate
ROD1	Membrane protein that binds the ubiquitin ligase Rsp5p via its 2 PY motifs; overexpression confers resistance to the GST substrate o-dinitrobenzene,zinc, and calcium; proposed to regulate the endocytosis of plasma membrane proteins
SSO1	Plasma membrane t-SNARE involved in fusion of secretory vesicles at the plasma membrane and in vesicle fusion during sporulation; forms a complex with Sec9p that binds v-SNARE Snc2p; syntaxin homolog; functionally redundant with Sso2p
SSO2	Plasma membrane t-SNARE involved in fusion of secretory vesicles at the plasma membrane; syntaxin homolog that is functionally redundant with Sso1p
YPS1	Aspartic protease, member of the yapsin family of proteases involved in cell wall growth and maintenance; attached to the plasma membrane via a glycosylphosphatidylinositol (GPI) anchor
PSR2	Functionally redundant Psr1p homolog, a plasma membrane phosphatase involved in the general stress response; required with Psr1p and Whi2p for full activation of STRE-mediated gene expression, possibly through dephosphorylation of Msn2p
PMP3	Small plasma membrane protein related to a family of plant polypeptides that are overexpressed under high salt concentration or low temperature, not essential for viability, deletion causes hyperpolarization of the plasma membrane potential
YPS3	Aspartic protease, member of the yapsin family of proteases involved in cell wall growth and maintenance; attached to the plasma membrane via a glycosylphosphatidylinositol (GPI) anchor
SNC2	Vesicle membrane receptor protein (v-SNARE) involved in the fusion between Golgi-derived secretory vesicles with the plasma membrane; member of the synaptobrevin/VAMP family of R-type v-SNARE proteins
LDB19	Protein involved in regulating the endocytosis of plasma membrane proteins by recruiting the ubiquitin ligase Rsp5p to its target; localization changes in response to nutrient levels; null mutant has reduced affinity for alcian blue dye
SUR7	Plasma membrane protein that localizes to furrow-like invaginations (MCC patches); component of eisosomes; associated with endocytosis, along with Pil1p and Lsp1p; sporulation and plasma membrane sphingolipid content are altered in mutants
TPN1	Plasma membrane pyridoxine (vitamin B6) transporter; member of the purine-cytosine permease subfamily within the major facilitator superfamily; proton symporter with similarity to Fcy21p, Fcy2p, and Fcy22p

Figure 4-S 1. Genome-wide screen for rescuers of Rdi1 over-expression growth defect. (**a**) Distribution of ln(growth-ratio) over the entire yeast haploid non-essential deletion library after 98 hrs of growth at 23°C (see Methods). Growth ratio is defined as the ratio of growth of a given strain with two without Rdi1 overexpression. Green line represents

the Wt value and the cyan box represents the cutoff range of the in(growth-ratio) for rescuer candidates, including Δ*lem3* (the pink line). Δ*dnf2* (blue line) had a slightly lower in(growth-ratio) than the cutoff and was therefore not in the initial rescuer list. (**b**) A list of the rescuer candidates that localize to the plasma membrane, with SGD description (www.yeastgenome.org).

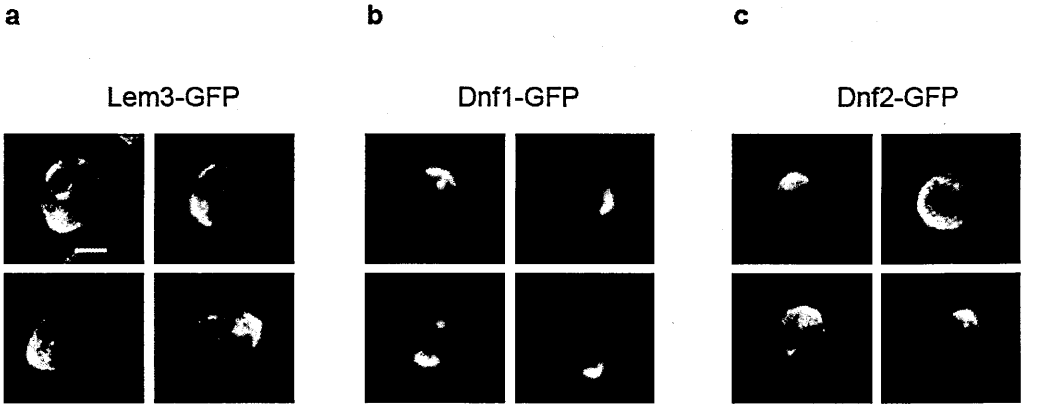

Figure 4-S 2. Lem3p, Dnf1p, Dnf2p localize to the polar cortex at the incipient bud site. Confocal images of unbudded polarized cells expressing Lem3-GFP (**a**), Dnf1-GFP (**b**) and Dnf2-GFP (**c**). Scale bar: 2 μm

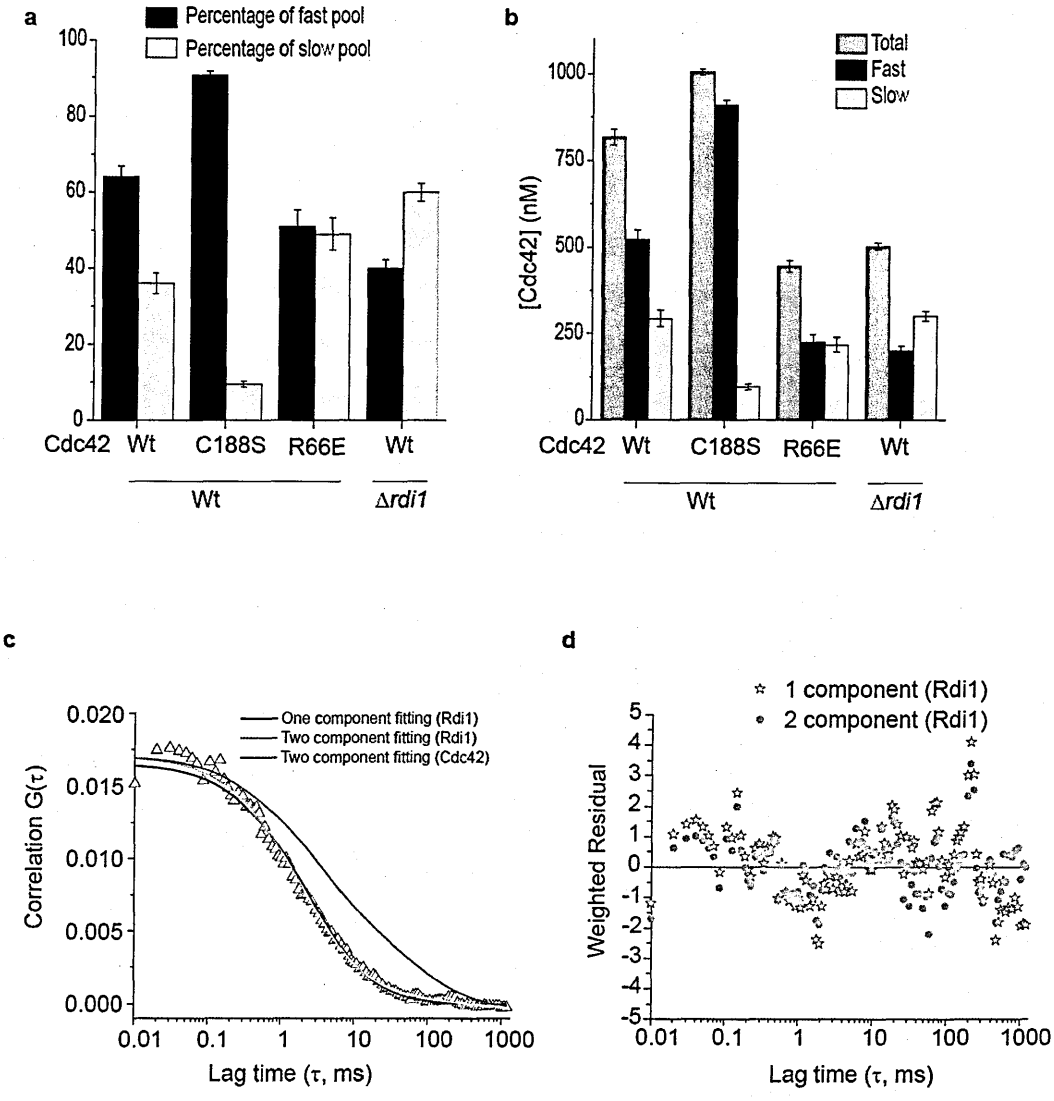

Figure 4-S 3. Cdc42 fast diffusion in the cytosol depends on Rdi1 and its prenyl group.
(a) FCS experiments were performed in live yeast cells (wild type or Δrdi1) expressing GFP tagged Cdc42, $Cdc42^{R66E}$, or $Cdc42^{C188S}$. Autocorrelation curves were fitted to a two-component model to extract percentages of slow and fast diffusing molecules. Error bars represent the estimated standard errors in the parameters determined from fitting an average autocorrelation curves obtained from 10-24 cells (see Methods). **(b)** Molar concentration (nM) of soluble Cdc42 in the cytosol calculated from the FCS data as described in (a). **(c)** The average autocorrelation curve obtained from FCS experiments in live cells (n=12) expressing Rdi1-mCherry was also fitted with one and two-component models. An F-test between the models showed a significant difference at 95% confidence level ($p<1 \times 10^{-10}$). However, the slow component represents a relatively insignificant portion of the Rdi1 population (< 5%). The two component-fitted curve for Cdc42

autocorrelation data (Fig. 1b) normalized to the initial amplitude of Rdi1 two-component fitted curve is overlaid to compare the decay pattern. Notice that the Cdc42 curve possesses a much more prominent slow component. (**d**) Distribution of weighted residuals obtained from one and two component model fitting of Rdi1 FCS data shown in (c).

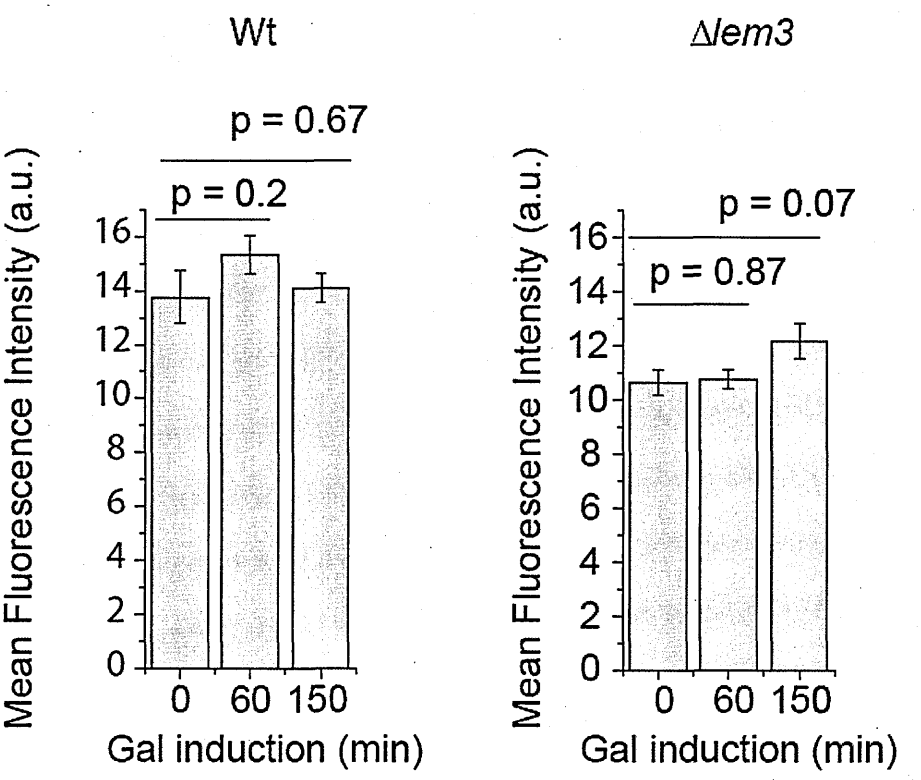

Figure 4-S 4. Mean fluorescence intensity measurement.

Quantification of the mean fluorescence intensity over the entire cell for Wt and Δ*lem3* cells at different Rdi1 induction time points as shown in (Fig. 1d).

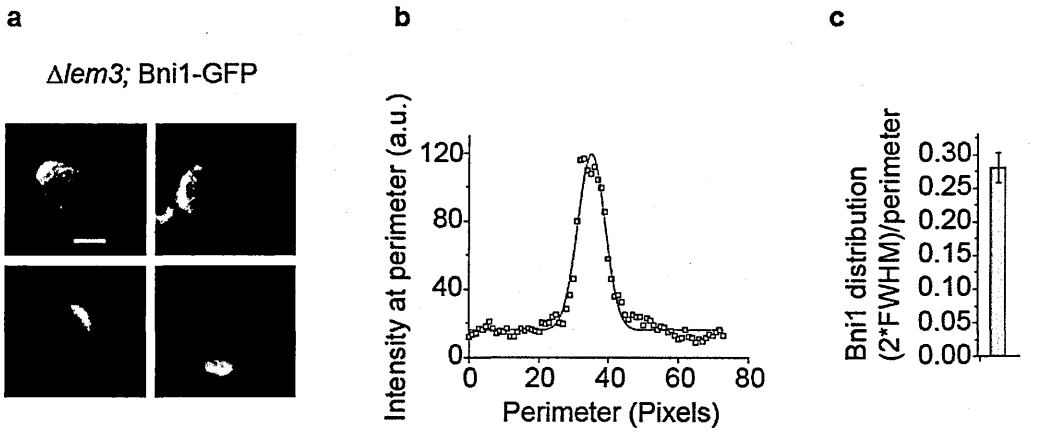

Figure 4-S 5. Delivery window size determination in *Δlem3* mutant.

The delivery window size in *Δlem3* was measured by the distribution of GFP tagged formin Bni1 as described previously(Slaughter et al., 2009). (**a**) Confocal images represent unbudded polarized cells expressing Bni1-GFP. Scale bar: 2 μm. (**b**) The fluorescence distribution along the perimeter was fitted to a Gaussian model. (**c**) The window width is approximated as 2 times the full width half max (FWHM) of the Gaussian distribution. Shown is the mean and SEM (n=16).

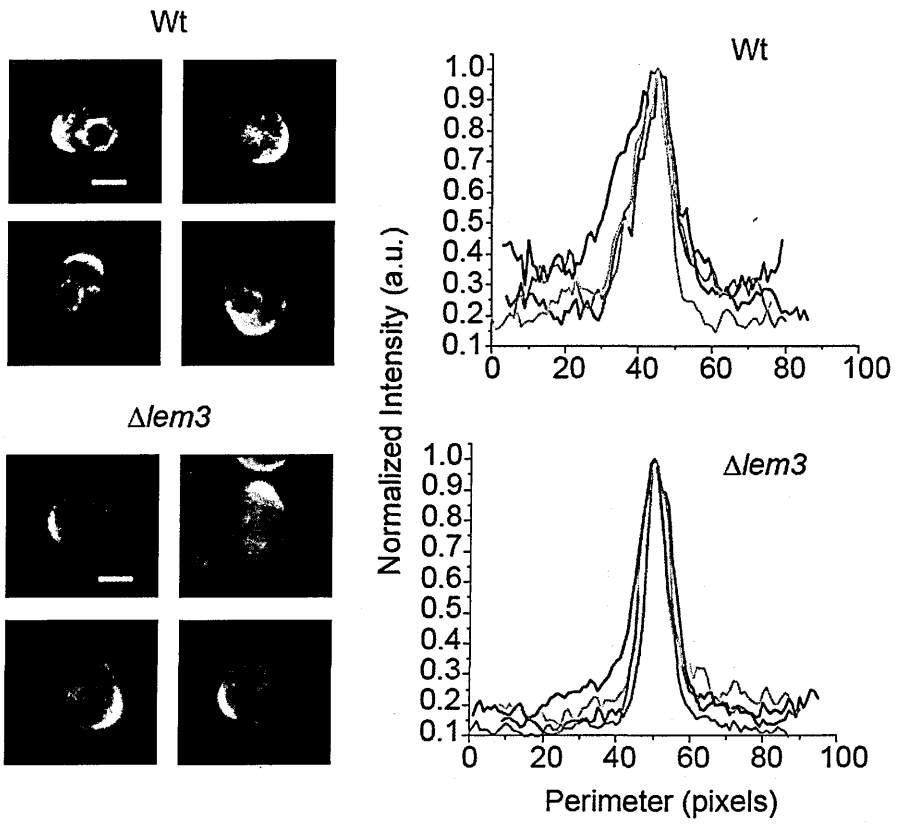

Figure 4-S 6. Cap shape comparison between Wt and *Δlem3*.

Representative images of GFP-Cdc42 at the polar cap in unbudded Wt and *Δlem3* cells. Fluorescence intensity traces along the perimeter are normalized and aligned with respect to peak intensity and shown adjacent to each cell type. Scale bar: 2 μm.

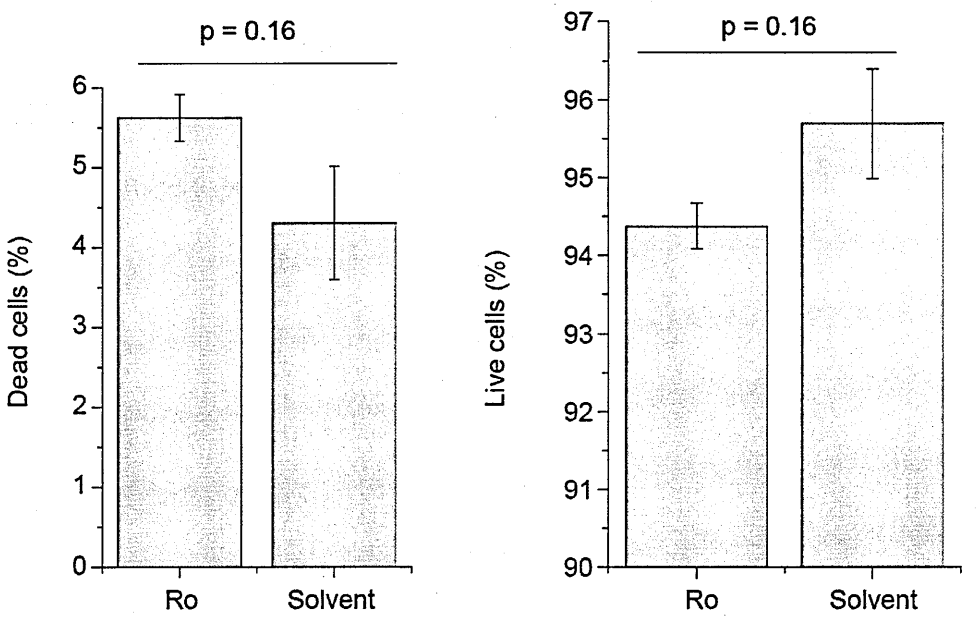

Figure 4-S 7. Cell death and viability analysis of Ro peptide-treated cells using flow cytometry.

Ro peptide was added to Wt cells at a final concentration of 50μM as in (Fig. 3b). Permeabilized dead cells were detected by propidium iodide staining, whereas live cells were detected using SYTO9. Shown are percentages of dead or alive cells (mean ± SEM) out of ~80,000 cells from three independent experiments.

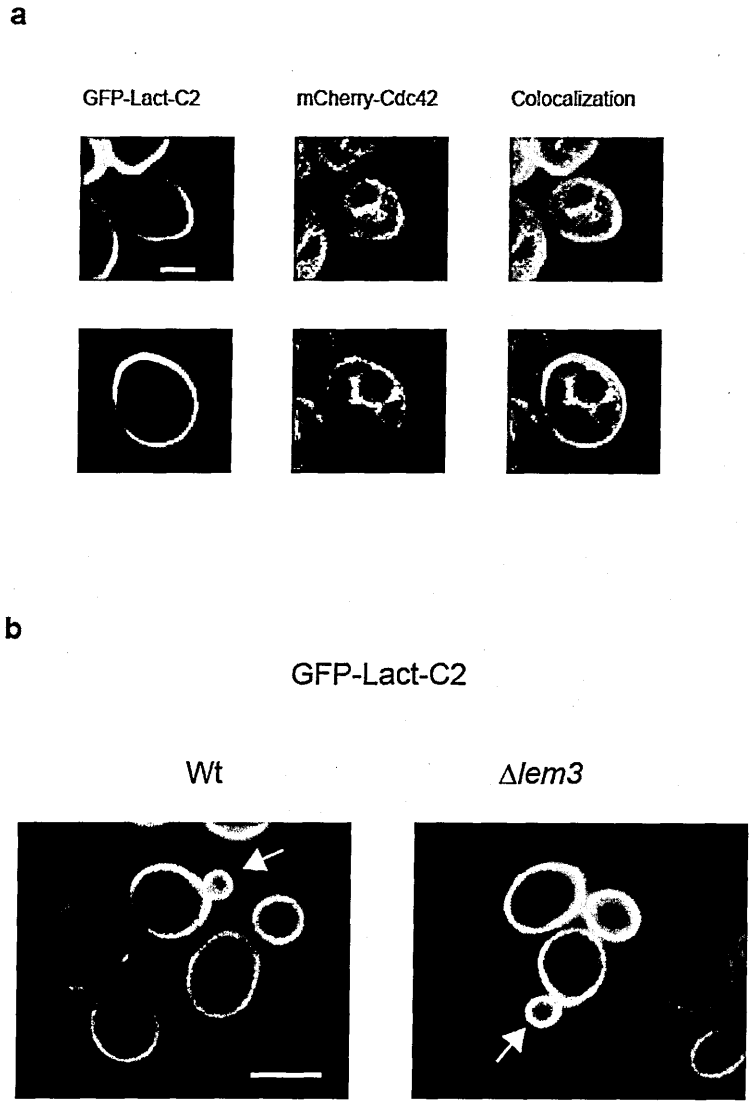

Figure 4-S 8. PS polarization overlaps with Cdc42 polar cap.

(**a**) Confocal images of unbudded polarized cells in a cycling population expressing Cdc42 tagged with mCherry at the N-terminus and GFP-Lact-C2. Scale bar: 2 μm. (**b**) Images of budded Wt or Δ*lem3* cells expressing GFP-Lact-C2. Arrow points to enriched GFP signal in the small buds of Δ*lem3* cells compared to Wt cells. Scale bar: 4 μm.

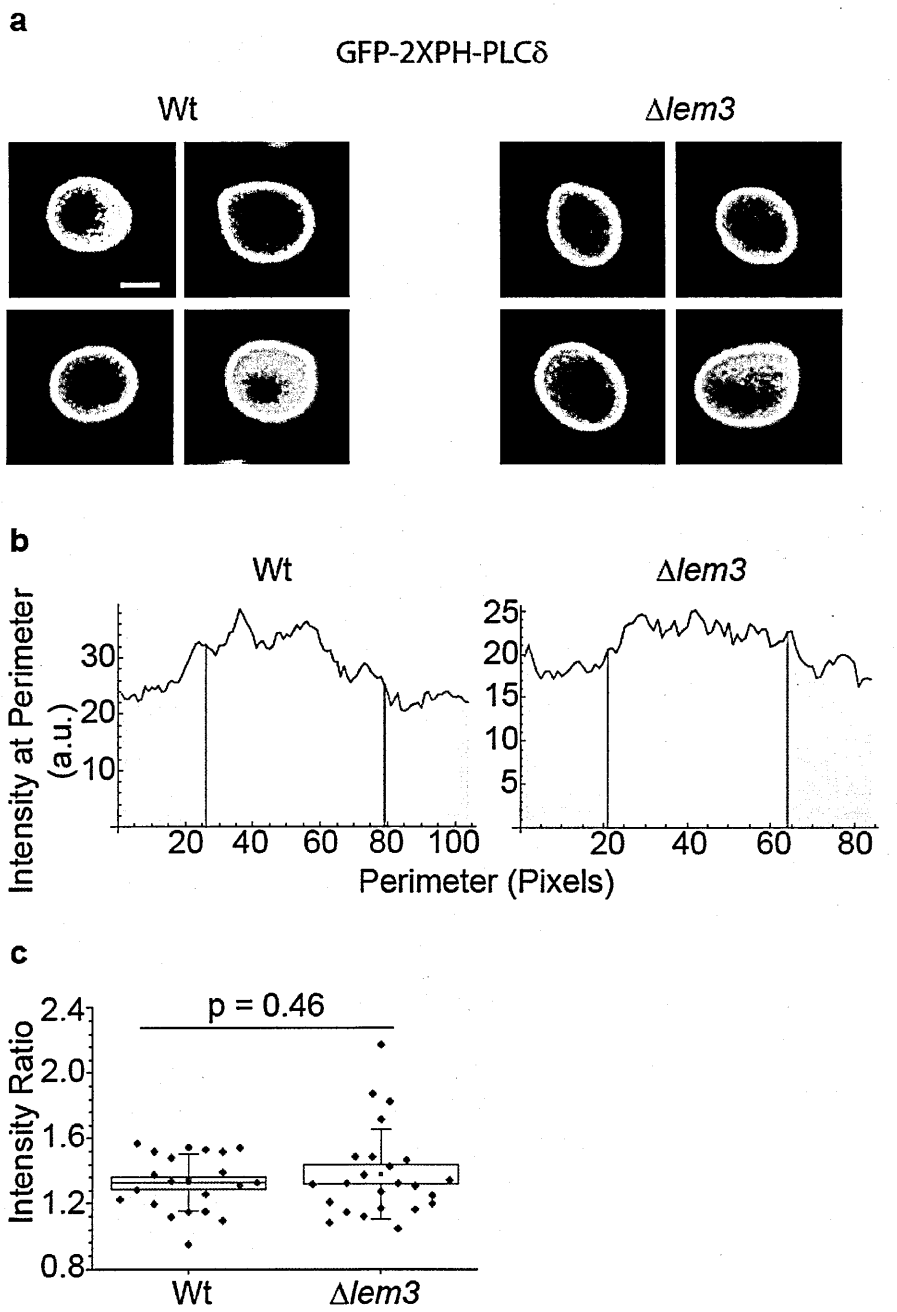

Figure 4-S 9. PIP2 localization is similar between wild-type and *Δlem3* cells.

(a) Confocal images of unbudded polarized wild-type or Δlem3 cells expressing GFP-2xPH-PLCδ, a biosensor for PIP_2. **(b) Representative** fluorescence intensity traces along the cell perimeter as shown in (Fig. 3d). **(c)** Intensity ratios of the half of the plasma membrane containing the polar cap (white area) over the opposite half (grey area). Small square is the mean; box range shows SEM; whiskers are standard deviation (SD); line is median.

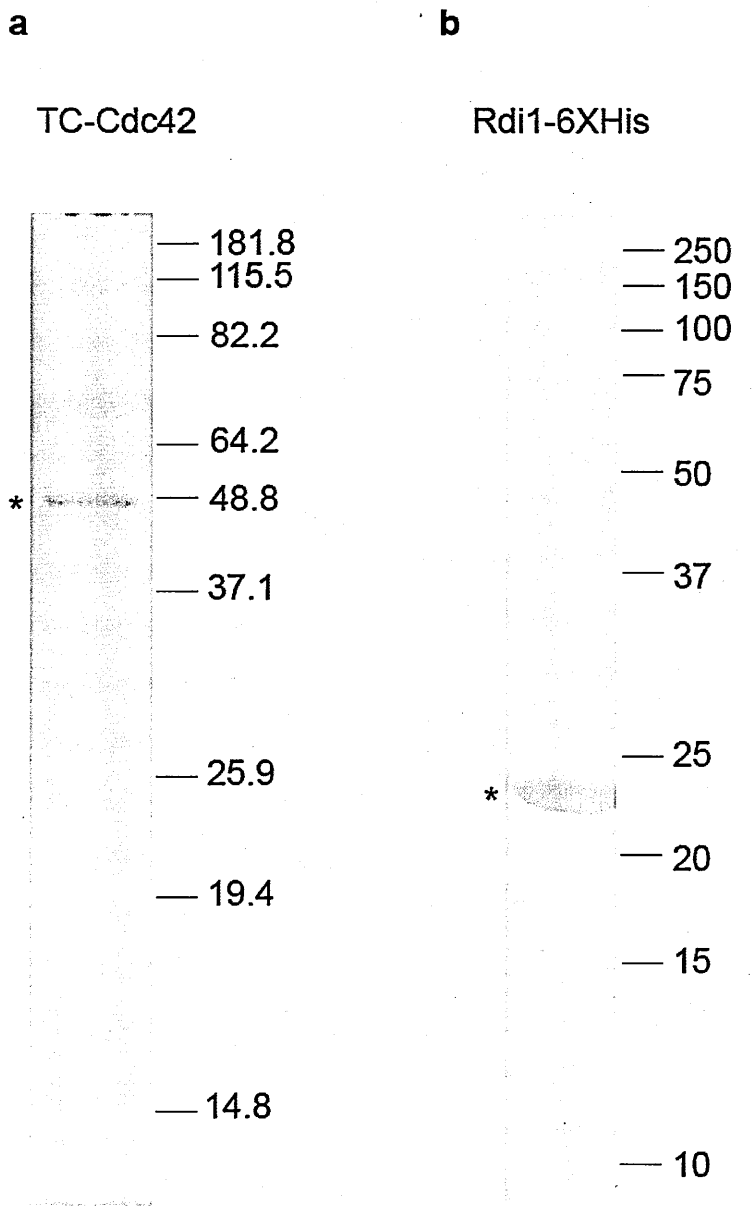

Figure 4-S 10. SDS-PAGE followed by Coomassie staining of the purified proteins.
(a) Prenylated TC-Cdc42 (GST-HA-TC-Cdc42) protein was expressed and purified from the yeast plasma membrane. **(b)** C-terminally hexahistadine-tagged Rdi1 protein was expressed and purified from bacteria cell lysate. Asterisks mark the respective protein band of interest.

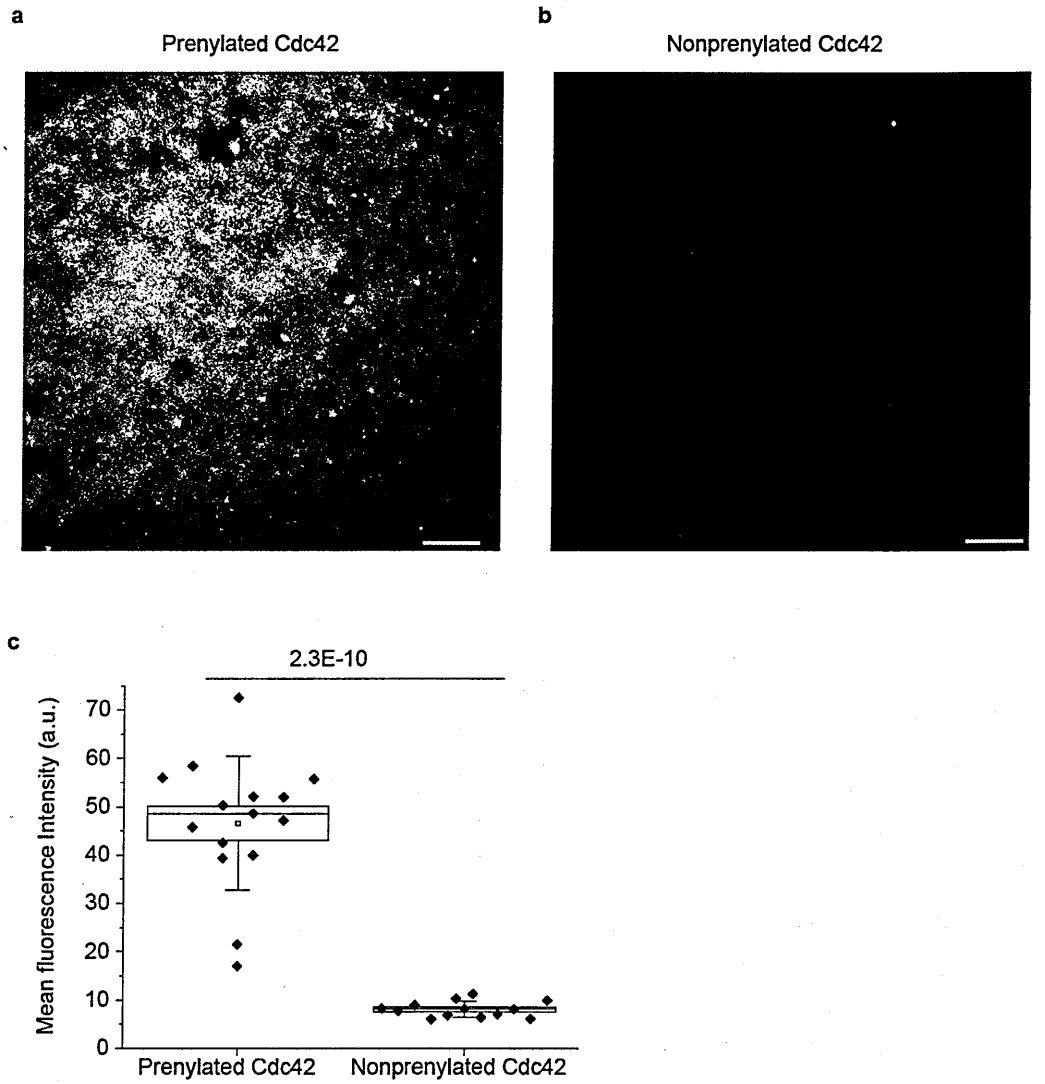

Figure 4-S 11. Prenyl group is required for TC-Cdc42 association with the SLB.
(a) TIRF image of the SLB with 40% PS, 15% PE loaded with 126 nM FlAsH labeled prenylated Cdc42 (purified from yeast plasma membrane). **(b)** SLB with 40% PS, 15% PE similarly labeled as above with 126 nM FlAsH labeled non-prenylated Cdc42 (purified from bacteria), with the rest of the conditions and image acquisition identical to (**a**). Images were presented with identical contrast. Scale bar: 10 μm. **(c)** Mean fluorescence intensity sampled over 13-15 different optical fields on SLBs loaded with FlAsH-labeled prenylated or nonprenylated Cdc42 as explained above. Box plots are shown as described for Figure S9c.

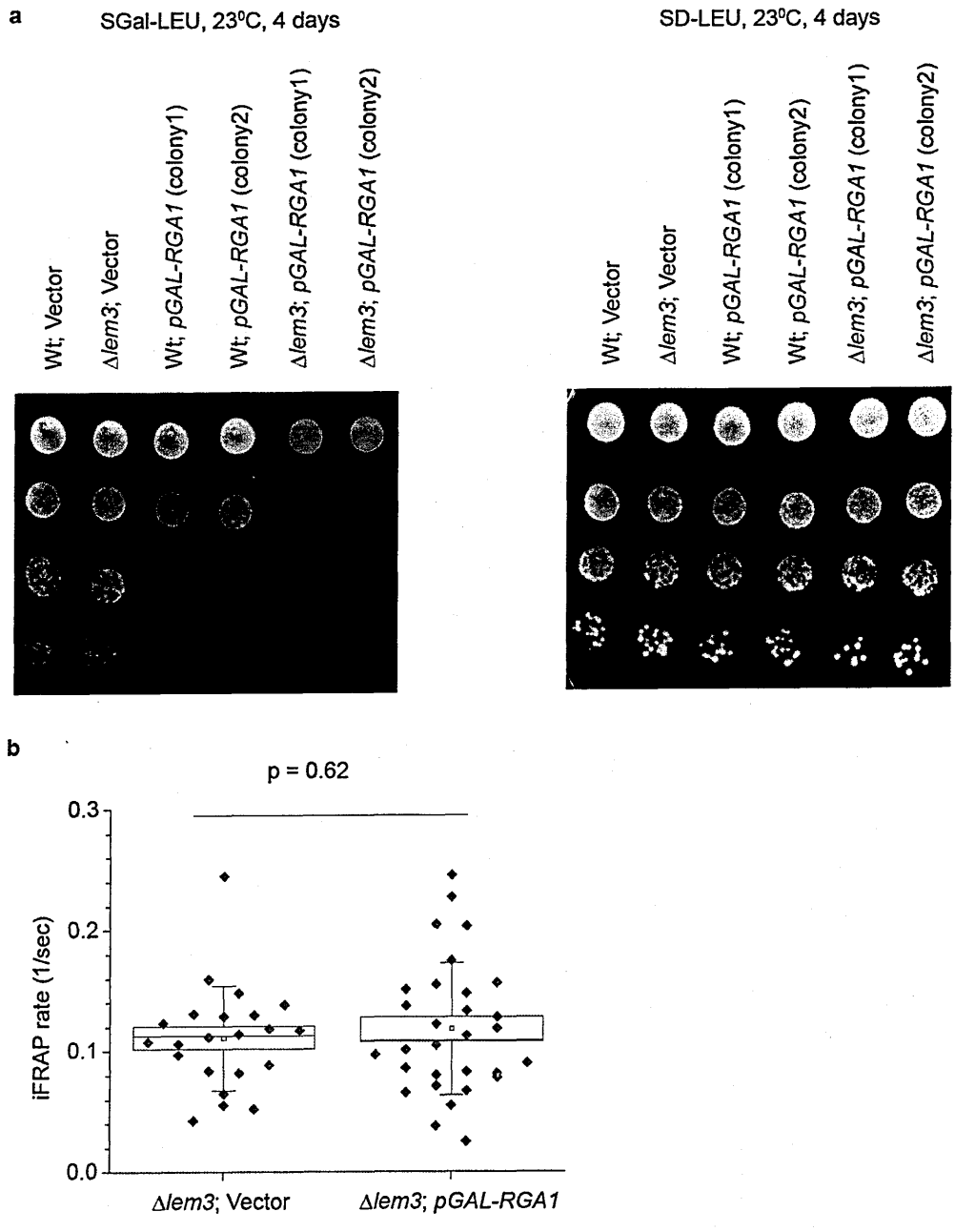

Figure 4-S 12. Over-expression of Rga1 (Cdc42 GAP) does not rescue Cdc42 dissociation rate at *Δlem3* polar cortex.

(a) Serial tenfold dilutions of cultures for the indicated strains were spotted on SGal-Leu and SD-Leu plates. Plates were scanned after 4 days incubation at 23°C. Notice that Rga1 overexpression causes a growth defect, which is exacerbated by *Δlem3*. **(b)** iFRAP rates (1/s) of GFP-Cdc42 in *Δlem3* cells bearing vector control or pGAL1-RGA1. Box plots are shown as described for Figure S9c.

Supplementary Table 1. Yeast strains used in this study (Chapter 4)

Strains	*Genotype**
RLY 2530	his3Δ1;leu2Δ0;met15Δ0;ura3Δ0
RLY3458	*RDI1-mCHERRY::HIS*
RLY3556	*pGAl1-GFP-myc6-CDC42^{R66E} CEN URA3 RDI1-mCHERRY::HIS5*
RLY3557	*pGAl1-GFP-myc6-CDC42^{C188S} CEN URA3 RDI1-mCHERRY::HIS5*
RLY3811	*pGAL1-RDI1 CEN HIS5*
RLY3856	*LEM3-GFP::HIS5*
RLY3857	*DNF1-GFP::HIS5*
RLY3858	*DNF2-GFP::HIS5*
RLY4153	*lem3Δ :: KAN pRL369(pCDC42-GFP-myc6-CDC42/ pRS306 URA3)*
RLY4154	*dnf1Δ :: KAN pRL369(pCDC42-GFP-myc6-CDC42/ pRS306 URA3)*
RLY4155	*dnf2Δ :: KAN pRL369(pCDC42-GFP-myc6-CDC42/ pRS306 URA3)*
RLY4273	*lem3Δ :: KAN pRL369(pCDC42-GFP-myc6-CDC42/ pRS306 URA3) pGAL1-RDI1 CEN HIS5*
RLY4277	*pRL369(pCDC42-GFP-myc6-CDC42/ pRS306 URA3)*
RLY4300	*pRL369(pCDC42-GFP-myc6-CDC42/ pRS306 URA3 pGAL1-RDI1 CEN HIS5*
RLY4796	*pGAl1-GFP-myc6-CDC42^{S185A} CEN URA3*
RLY4797	*pGAl1-GFP-myc6-CDC42^{S185K} CEN URA3*
RLY4826	*rdi1Δ :: LEU2 pGAL1-GST-HA-FlASH-CDC42/ pRS316 URA3)*
RLY4839	*pGAl1-GFP-myc6-CDC42^{S185D} CEN URA3*
RLY4875	*CEN LEU2*
RLY4921	*lem3Δ :: KAN pGAl1-GFP-myc6-CDC42^{S185K} CEN URA3*
RLY4922	*lem3Δ :: KAN pGAl1-GFP-myc6-CDC42^{S185D} CEN URA3*
RLY4923	*lem3Δ :: KAN pGAl1-GFP-myc6-CDC42^{S185A} CEN URA3*
RLY6593	*dnf1Δ :: KAN dnf2Δ :: KAN pRL369(pCDC42-GFP-myc6-CDC42/ pRS306 URA3)*
RLY6617	*lem3Δ :: KAN ; rdi1Δ :: LEU2 pRL369(pCDC42-GFP-myc6-CDC42/ pRS306 URA3)*
RLY6766	*GFP-LACT-C2 CEN URA3*
RLY6768	*lem3Δ :: KAN GFP-LACT-C2 CEN URA3*
RLY6875	*pCDC42-mCHERRY--CDC42/ pRS305 LEU2 GFP-LACT-C2 CEN URA3*
RLY6907	*GFP-PHx2-PLCδ CEN URA*
RLY6908	*lem3Δ :: KAN GFP-PHx2-PLCδ CEN URA*
RLY6909	*lem3Δ :: KAN BNI1-GFP::HIS5*
RLY7104	*rdi1Δ :: LEU2 pRL369(pCDC42-GFP-myc6-CDC42/ pRS306 URA3)*
RLY7544	*lem3Δ :: KAN CEN LEU2*
RLY7550	*pGAL1-RGA1 CEN LEU2 (colony1)*
RLY7551	*pGAL1-RGA1 CEN LEU2 (colony2)*

RLY7552	*lem3Δ :: KAN pGAL1-RGA1 CEN LEU2 (colony1)*
RLY7553	*lem3Δ :: KAN pGAL1-RGA1 CEN LEU2 (colony2)*

All the strains are prepared and used in this study except RLY3557(Slaughter et al., 2009) and RLY3856-RLY3858(Huh et al., 2003) .

* All strains used in this study are derivatives of S288c background with the following genotype: MATa his3Δ1;leu2Δ0;met15Δ0;ura3Δ0

Chapter 5. Genome wide screening and further studies related to previous chapters and candidates obtained from screening

All the experiments shown in this chapter are performed by Arupratan Das under the guidance of Rong Li.

Acknowledgement: I thank Juntao Tony Gao for the module analysis and the explanation in the method and Norman Pavelka for the statistical analysis on candidates obtained from genome wide screening. I also thank Brian D. Slaughter, Richard Alexander and Dan Bradford (Molecular Biology) for helping me to perform the screening.

5.1. Genome wide screening to find molecular players of Rdi1 mediated Cdc42 recycling at polar cortex

Abstract

In budding yeast the presumptive bud site undergoes complex modifications during the polarization process, both due to polarized accumulation of certain proteins and with compositional change of the plasma membrane relative to the rest of the cell surface. Cdc42 accumulation and maintenance through different positive feedback loops are likely to involve many other proteins apart from actin and Bem1, considering the complex environment of polar cortex. Over expression of Rdi1 suppressed yeast growth with diminished Cdc42 levels at the polar cortex. Using this as an experimental tool Rdi1 was over-expressed in the yeast nonessential gene knockout library to find ORF deletions that suppress (rescuers) or exacerbate (worse growers) the Rdi1 over-expression growth defect. List of candidates emerged in both groups. Candidates obtained from the screening are still at the preliminary level, a detail investigation is yet to be performed. However, as a first step to understand the cellular events these genes participate, a network of physical interactions among rescuer and worse grower candidates was performed to visualize modules in the network correspond to specific cellular events. Candidates grouped based on their physical interactions began to reveal several mechanistic modules for example, among rescuers candidates, lipid flippase complexes with other proteins involve in vesicle trafficking (Lem3, Cdc50, Drs2, etc) shared one module. Likewise among worse growers, p21-activated kinases (PAKs) (Ste20, Cla4) shared one of the worse grower modules.

Introduction

Understanding cell polarity in depth is key to understand several biological processes such as cell motility, active absorption in epithelial cells and neuronal growth. Cdc42, the central regulator of cell polarity (Etienne-Manneville, 2004) was found to be dynamic at polar cortex from FRAP based study (Wedlich-Soldner et al., 2004). This indicates existence of one or more

pathways through which Cdc42 is maintained at the polar cortex and understanding of these pathways will enlighten the knowledge of polarity maintenance mechanism.

A stable polar cortex can be maintained through the balance between two-dimensional membrane diffusion, internalization from plasma membrane to the cytoplasm and directed transport back to the polar cortex (Marco et al., 2007). This balance can be achieved by actin dependent endocytosis-exocytosis and Guanine dissociation inhibitor protein (GDI) (for yeast known as Rdi1). Cell can maintain its polarity even in the absence of either actin cables or Rdi1, however in the absence of both, cells lose polarity completely (Slaughter et al., 2009).

We and others have observed that Rdi1 extracts Cdc42 from plasma membrane (Richman et al., 2004) and over-expression of Rdi1 leads to growth defect (Masuda et al., 1994) (Fig. 1a). Rdi1 mediated Cdc42 recycling at polar cortex relies upon three successful steps. First, dissociation of Cdc42 from polar cortex by Rdi1, this we will be referring to as "extraction", second, dissociation of Cdc42-Rdi1 complex and third, retargeting of Cdc42 to the polar cortex (Fig. 1b).

Although cell polarity is an essential process it relies on many functionally redundant mechanisms, and the complex environment of the polar cortex makes it difficult to dissect out the molecular mechanism. To investigate the factors that can tune and localize Rdi1 mediated recycling, we hypothesize that if excess Cdc42 extraction from plasma membrane causes growth defect (also see chapter 4, Fig. 1) then deletion of genes that involve in extraction process should rescue the growth defect, this we will refer as "rescuers" (Fig. 1b). Whereas, for genes that antagonize extraction or are involved in retargeting Cdc42 from the Cdc42-Rdi1 complex to the polar cortex, deletion should exacerbate the Rdi1 over-expression growth defect. These will be referred to as "worse growers" (Fig. 1b). To this end we performed a whole genome screening where Rdi1 was over-expressed in the yeast non-essential gene knock out library and compared growth with respect to wild type cells.

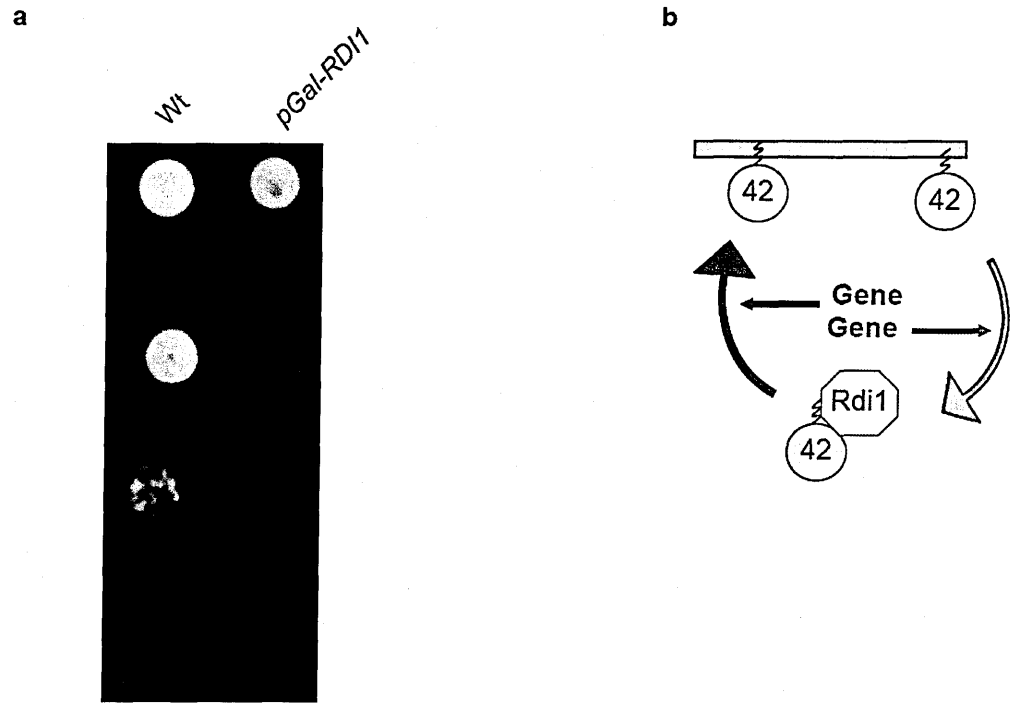

Figure 5-1. Principle of whole-genome screening.

(a) Growth-assay for Wt strain with empty-His vector (pRS313) and Wt strain with pRS313-*pGAL-RDI1* on solid media with over-expression of Rdi1. Cells were spotted with 10 fold serial dilutions from top to bottom and incubated at 23^0C for 5 days. (b) Schematic description of the genome-screening principle. Genes involve in Rdi1 mediated Cdc42 extraction (green), deletion of which should suppress the Rdi1 over-expression growth defect while genes that involve in retargeting Cdc42 from Cdc42-Rdi1 complex (wine) to polar cortex, deletion of those should exacerbate the growth defect.

Result

A centromeric plasmid with Rdi1 under pGal promoter was transformed into yeast nonessential gene knock out library and growth was compared between Rdi1 over-expression strain with the corresponding knock out strain at different time point. A growth-ratio corresponds to the Rdi1 over-expression and the gene deletion itself was obtained by dividing the growth on the Rdi1 over-expression plate by that on the control plate (See methods). Rdi1 over-expression plate (experimental plates) reached saturation after ~122 hr of incubation at 23 °C and therefore to observe the rescuers we used the growth data after 98 hr prior to saturation. While 122hr growth

was used to find worse growers, since gene deletions which enhance the Rdi1 over-expression growth defect should lag while the others will reach to saturation. To study rescuer candidates we set a growth-ratio cut off of maximum to 0.56 by visually inspecting ln(growth-ratio) distribution, a robust statistical analysis to select cut off was not possible (see method) as the distribution did not follow normal distribution (Please see Chapter 4, Figure S1a). ~693 rescuer candidates was obtained within the above range which includes many genes that can be potential regulators of cell polarization process while it also includes many genes unlikely to be a direct regulator of cell polarity such as transcription factors, ribosomal proteins, proteins involve in translation and many mitochondrial genes (gene description checked in Saccharomyces genome database, SGD). Eliminating candidates unlikely to be involved in cell polarity the number reduces to ~277 which is also mentioned in Chapter 4. Candidates for the worse grower was selected based on robust statistical analysis as the ln(growth-ratio) distribution at 122hr followed a near Normal distribution. Candidates were selected with a p-value < 0.002 (corresponding to a false-discovery rate of < 3%) (see method). ~425 candidates obtained within above p-value range without eliminating any candidates that are unlikely to be involved in cell polarity. The list includes worse growers along with the extreme synthetic lethal ones (growth-ratio ~ 0) (see method).

Construction of Modular networks based on physical interactions among rescuers and worse growers candidates

Having large group of candidates in both the list it was difficult to focus on individual candidate to understand a general mechanism that might involve in Rdi1 mediated polarity maintenance process. It was important to find group of genes based on the commonalities in cellular function, we reasoned candidates interact physically most likely to be involved in the same cellular event (for example vesicle trafficking, PAK kinase pathway etc). Here we constructed a modularized physical interaction network for both rescuers and worse growers separately based on maximization of modularity for given partition of nodes (genes) (Guimera and Amaral, 2005) (see methods). However, the modules are yet to be annotated with distinct cellular functions. Interestingly we got a group of rescuers LEM3, CDC50 and DRS2 which share a common mechanism of lipid flipping in one of the modules among rescuers candidates (Fig. 2, pink nodes at lower right) in our preliminary observation. ATP-driven lipid flipping causes asymmetric

phospholipid distribution at plasma membrane (Devaux, 1991), hinting its possible involvement in Cdc42 recycling at polar cortex. Cdc50p forms complex with Drs2p, a P-type ATPase which is required for their endoplasmic reticulum (ER) exit and localization to trans-Golgi network (TGN) (Saito et al., 2004). Drs2p shows ATP-dependent aminophosphilipid translocase (APLT) activity at TGN membrane which is also required for post-golgi vesicle formation (Gall et al., 2002; Natarajan et al., 2004). Drs2 and Cdc50 transiently localize to PM (Saito et al., 2004) hence its effect on Cdc42 extraction from polar cortex is most likely to be indirect. Lem3p, a Cdc50 family protein forms heterodimeric complex with P-type ATPases Dnf1 and Dnf2 which then exits from ER and localize to polarized PM (Saito et al., 2007). The polarized localization of Lem3-Dnf1 or Lem3-Dnf2 (αβ-heterodimeric) complex and its involvement in polarity (Saito et al., 2007) process makes it an important candidate to be studied for its role in Cdc42 extraction from polar cap hence in polarity maintenance. In depth study on Lem3p flippase complexes and their involvement in lipid flipping and polarity maintenance is explained in chapter 4. A detail study on the other lipid flippase candidates like Cdc50, Drs2 and thorough investigation of the other module will be done in the future.

Similar module analysis based on physical interactions was also performed on the worse-grower candidates. Several interesting modules were also obtained from this analysis. Two of the p21-activated kinases (PAK) Ste20 and Cla4 (Fig. 3, upper right green node) seem to be very promising as there is reported involvement for these genes in polarity (Lamson et al., 2002; Wild et al., 2004). One possibility is through phosphorylation of Rdi1, which may play a role in regulating Rdi1 mediated Cdc42 extraction from plasma membrane (Tiedje et al., 2008). It has also been observed that phosphorylated Cdc42 is easily extracted by Rdi1 compared to its non-phosphorylated form (Forget et al., 2002) leading to the possible involvement of PAKs in this process. A detail investigation of the Cla4 protein is underway to understand its role in Cdc42 recycling (please see the Chapter 5).

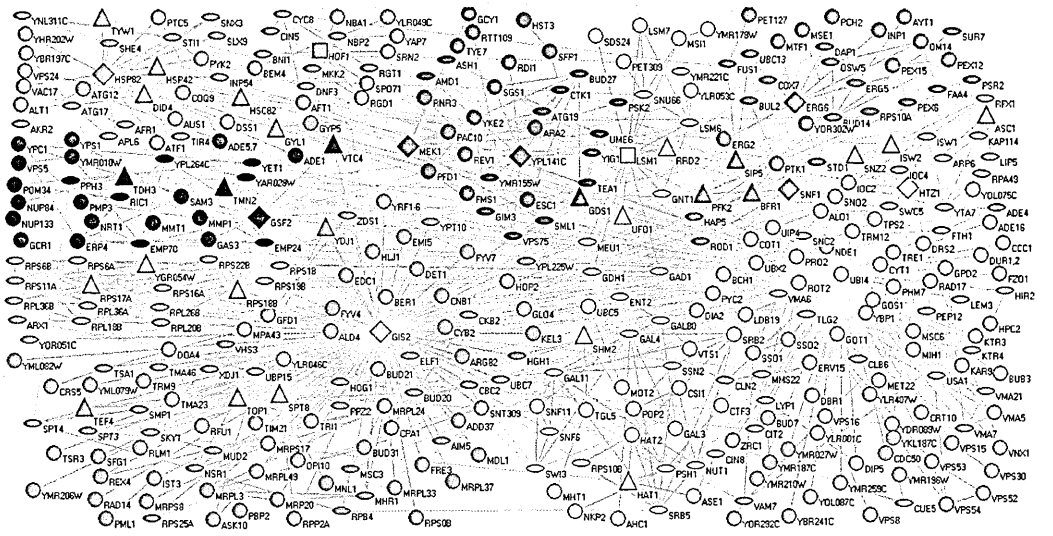

Figure 5-2. Modularization of Rescuer candidate physical interaction network. Visualization of the modularized physical interaction network analysis for rescuer candidates. Network analysis was done among rescuer candidates (~693 genes) within the growth-ratio window of maximum to 0.56 using BioGrid database (version 3.1.80). Each module represented by the nodes with similar color clustered in different areas of the interaction network. This figure was generated with the help of Juntao Tony Gao.

Another set of genes Pkh2 and Sch9 from this module analysis shared common module (Fig. 3, lower right, orange node) also seems to be very important in Cdc42 maintenance at the polar cortex.

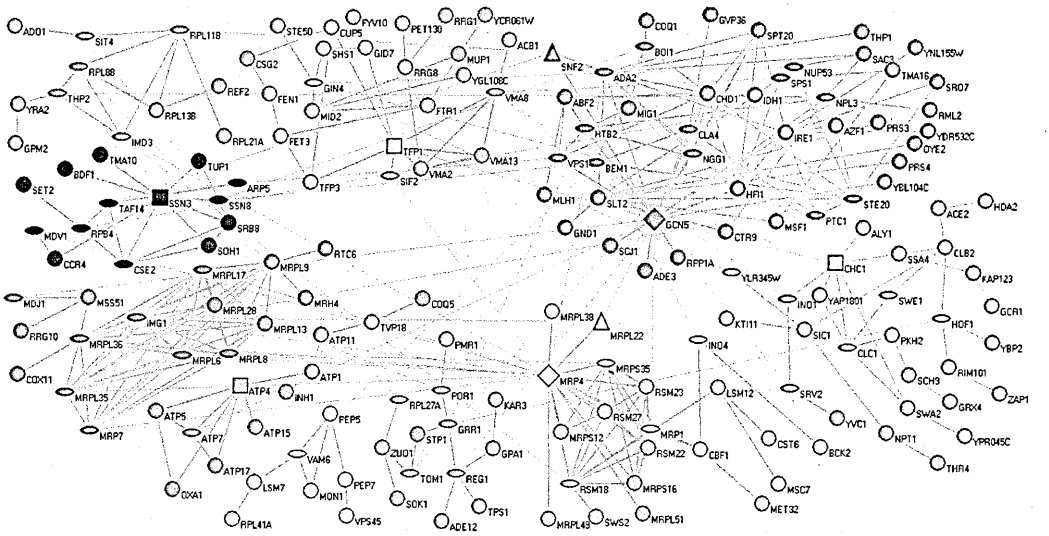

Figure 5-3. Modularization of worse-grower candidate physical interaction network. Visualization of the modularized physical interaction network analysis for worse grower candidates. Modularization was done similarly as explained in (Fig. 2). 426 genes were analyzed for shown interaction network study which includes the genes associated with a p-value < 0.002 (corresponding to a false-discovery rate of < 3% , also see methods) and genes with synthetic-lethal growth phenotype. This figure was generated with the help of Juntao Tony Gao.

A recent study found that aminophospholipid flippase activity is subjected to complex regulation by the Pkh1-Ypk1-Fpk1 kinases associated with the plasma membrane (Roelants et al., 2010). The most upstream kinases, Pkh1 and Pkh2, which ultimately down-regulate the flippase activity, are known to be associated with the membrane microdomain termed eisosomes (Grossmann et al., 2008). The optimal Fpk1 and Fpk2 activity depends upon the sphingolipd content of the eisosomes and the biogenesis of this lipid is dependent on Sch9 (Roelants et al., 2010; Wei et al., 2009). In light of our findings, lipid flipping and Cdc42 recycling at polar cortex (See Chapter 4) it is interesting to speculate that this kinase pathway of flippase regulation also plays an important role in regulating Cdc42 recycling and polarization. A detail investigation of this kinase pathway involving eisosome will be dedicated in the future study.

Materials and methods

The yeast haploid non-essential deletion library was transformed with a centromeric plasmid containing Rdi1 under a galactose inducible promoter (CEN-pGAL-RDI1:His) using robotics (Beckman-Coulter, Biomek FX). As a control, the knockout strains were grown in synthetic complete (Sc) media with 2% raffinose in parallel with the transformed strains, which were grown in Sc-His+2% raffinose. Cells were grown for 2 days at 30 °C so that all the strains reach maximum growth with approximately similar optical density (OD). At this point strains were diluted (1:100) and spotted in quadruplicates on Sc+2% galactose+2% raffinose (for the control) or Sc-His+2% galactose+2% raffinose agar (experimental) for transformed strains using robotics (Singer Instruments, RoTor HDA). The plates were incubated at 23 °C and scanned every 24 hrs. A His^+ wild-type (WT) control strain was included on every plate, allowing normalization of each plate with respect to the growth of this strain. In addition, a WT strain (RLY2530; WT-control) on non-selective raffinose plates and WT strain with Gal-Rdi1 (RLY3811; WT-experimental) were included in several plates throughout the library to cross-check consistency throughout the screen and to obtain the WT reference value. After ~122 hr of incubation at 23 °C the experimental plates reached saturation, and therefore to observe the rescuers we used the growth data after 98 hr prior to saturation. 122hr growth was used to find worse growers, reasoning gene deletions which enhance the Rdi1 over-expression growth defect should lag while the others will reach to saturation. Growth of each spot from the scanned images was quantified as the area and averaged over 4 spots to obtain growth for each strain. Area values were normalized with respect to the WT control strain on the same plate. A growth-ratio for each deletion strain was then obtained by dividing the normalized growth on the experimental plate by that on the control plate. The growth-ratio for the WT control obtained by averaging from several plates was 0.26 after 98 hr and 0.4 after 122 hr of growth. Rescuers candidates after 98hr growth (ln(growth-ratio)) distribution did not follow the normal distribution, so the analysis to have p-value q-ranking as did for 122hr growth (near normal distribution, see below) was not possible for this particular set of data. So the cut-off is set by the visual inspection of the ln(growth-ratio) (rescuers) distribution (Chapter 4, Fig. S1a) and picked away from the central region towards the right side of the distribution and also the

rescuers candidates verified from the growth images. Based on the distribution we used a growth ratio cutoff of 0.56, such that strains with a growth-ratio equal to or above 0.56 were considered as rescuer candidates (see Chapter 4, S1a). The distribution of ln-ratios at 122 hrs of growth approximately followed a Normal distribution, hence robust estimates of mean and standard deviation were used to fit a Normal distribution to the ln-ratio data. Next, a p-value for each ln(growth-ratio) was calculated as the probability to draw such a ln(growth-ratio) from a Normal distribution with the estimated mean and standard deviation. Finally, the p-values were translated into q-values according to Storey JD and Tibshirani R. (2003) (Storey and Tibshirani, 2003). Based on q-value ranking, we selected the first 369 candidates, which were associated with a p-value < 0.002 (corresponding to a false-discovery rate of < 3%), which is a stringent cut-off to select candidates. We made a separate list for candidates with synthetic lethal growth phenotype upon Rdi1 over-expression (growth-ratio ~0) and merged with the candidates obtained from above statistical analysis (combined number of genes ~426) for the network analysis.

Network module analysis

Given a network, for a certain partition P of the nodes into modules, the modularity $M(P)$ is defined as (Newman and Girvan, 2004):

$$M \equiv \sum_{s=1}^{N_M} \left[\frac{l_s}{L} - \left(\frac{d_s}{2L} \right)^2 \right]$$

where N_M is the number of modules, L is the number of links in the network, l_s is the number of links between nodes in module s, and d_s is the sum of the connectivity (degrees) of the nodes in module s. Modules (and the optimal number of modules) are typically identified by selecting the partition P^* that maximizes $M(P)$(Guimerà and Amaral, 2005). House-made program (Gao et al., 2011) was used for this analysis.

Role analysis:

Every node was assigned a role in every network (Guimera and Amaral, 2005; Guimerà and Amaral, 2005; Guimera and Nunes Amaral, 2005; Guimera and Sales-Pardo, 2009; Sales-Pardo et al., 2007). The role is determined by two parameters:

(1) ***Participation coefficient***: For node *i* in module *m,* participation coefficient measures the distribution of connections among the other modules. Nodes with all the connections within their own module have a participation coefficient equal to zero whereas nodes with more connections to several other modules than to its own module have a participation coefficient that is closer to 1.

(2) ***Within module degree z-score***: For node *i* in module *m*, within module degree z-score measures how different the number of connections to other nodes in the same modules with respect to the distribution of within module degrees for all of the nodes in the module.

All of the networks were obtained from BioGrid database (version 3.1.80).

5.2. Lem3 polarization mechanism and existence of other possible mechanisms for phospholipid asymmetry at polar cortex

Lem3 is a plasma membrane protein and it polarizes like Cdc42 (Chapter 4, Fig. S2a). We investigated how polarized localization of Lem3 along with its ATPase components Dnf1 and Dnf2 can create phospholipid asymmetry at polar cortex affecting charge distribution in the plasma membrane leaflets which in turn regulates Rdi1-mediated Cdc42 extraction from the polar cortex. Beyond its mechanistic role in dynamic maintenance of Cdc42 concentration at polar cortex it is important to study how Lem3 itself is localized to the polar cortex. Often time the polarized distribution of plasma membrane protein is achieved through diffusion barrier (Nakada et al., 2003) or dynamically, if the protein is endocytosed and retargeted back before it diffuses to equilibrium (Bretscher and Thomson, 1983; Valdez-Taubas and Pelham, 2003). In yeast polarized distribution of some proteins like SNARE Snc1, Sso1 at the bud tip is achieved through polarized actin cable mediated exocytosis and the formation of septin ring at the bud neck which retains those proteins from diffusing away. However in the absence of septin ring for example prior to bud emergence or during mating response (shmoo), cells still can maintain polarity. In yeast it was observed that polarized distribution during shmoo formation is achieved through localized endocytosis and exocytosis specially under the slow diffusion along yeast plasma membrane compared to animal cells (Valdez-Taubas and Pelham, 2003).

Lem3 diffuses along yeast plasma membrane and polarized distribution is maintained through endocytosis/ exocytosis

We focused on cells at G1 polarized stage prior to bud emergence for our study and at this stage it is possible that Lem3 polarization is maintained through actin mediate recycling. We first studied whether Lem3 diffuses along the yeast plasma membrane. To this end half of the Lem3-GFP distribution at polar cortex was bleached and fluorescence intensity change at the bleached area and the adjacent non bleached area was monitored over time. The rationale was that if

fluorescence intensity recovery at the bleached area is approximately similar to the intensity decay at the non-bleached area it would suggest that protein diffusion occurs along the plasma membrane from the non-bleached to the bleached area. Indeed we observed protein diffuses from non-bleached to bleached area and the corresponding intensity changes are approximately similar (Fig. 4a, b, c). This shows that Lem3 freely diffuses along the plasma membrane. Under this condition the polarized distribution of the protein can be achieved through diffusion barrier or through actin mediated recycling as explained above.

To distinguish these two possibilities we reasoned that if polarization is dependent on diffusion barrier cell can still maintain polarity in the absence of actin structures once it is established or it will depolarize to equilibrium in case of actin mediated recycling. To investigate this we monitored Lem3-GFP polar cortex over time in presence of actin depolymerizing drug LatA or in presence of solvent control DMSO. Interestingly we observed that in presence of LatA lem3 depolarizes while in DMSO control it can still maintain its polarized distribution (Fig. 5). This suggests polarized distribution of this protein is achieved through actin mediated directed exocytosis and endocytosis and in the absence of actin structures it depolarizes due to its intrinsic diffusion along plasma membrane.

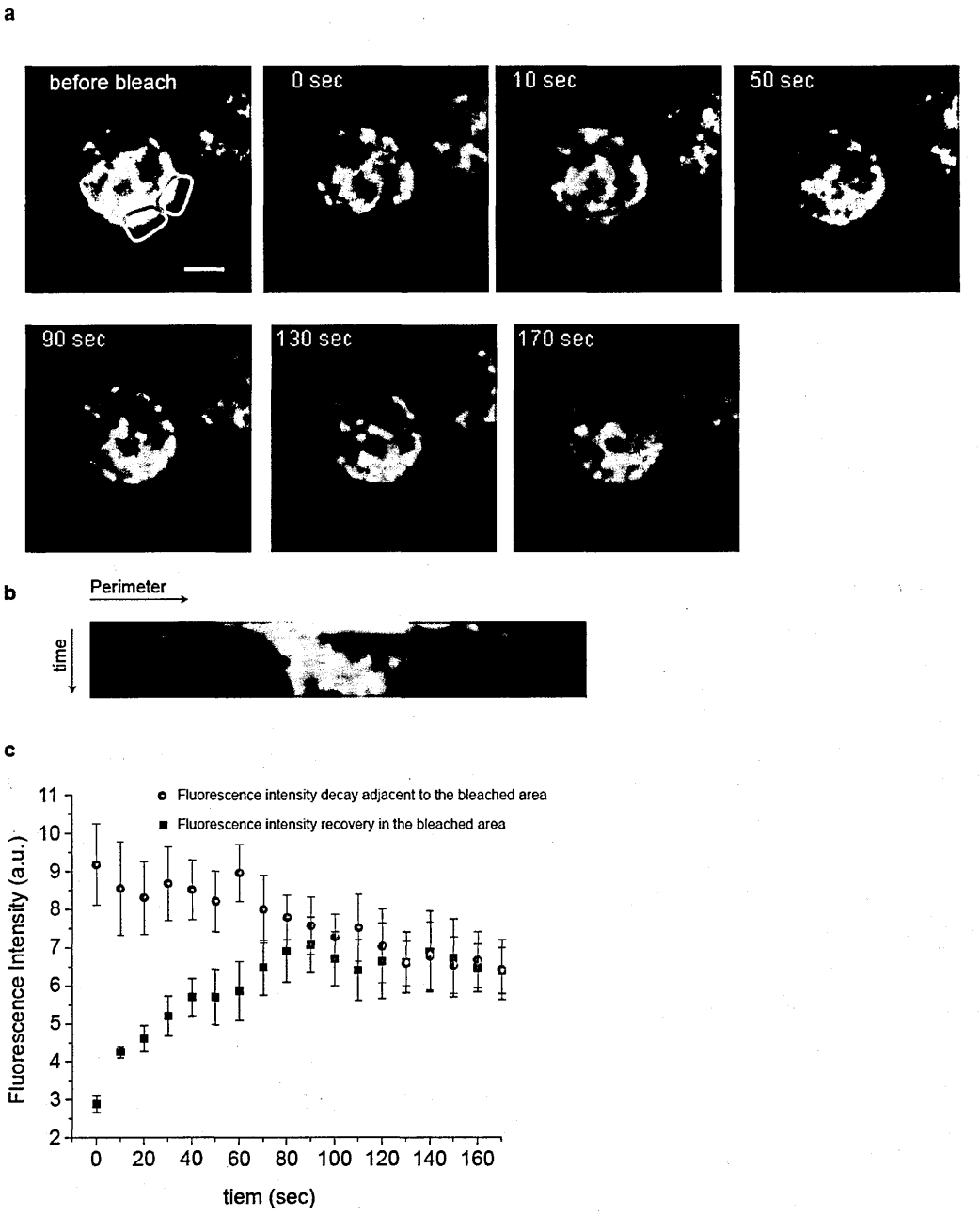

Figure 5-4. Lem3 protein is dynamic at polar cortex.

(a, b) Montage and corresponding kymograph along the cell perimeter of Wt cell expressing Lem3-GFP whose half polar cortex is photo bleached. The bleached and non-bleached areas are marked by red and green respectively. Images and kymograph are weekly smoothed. Scale bar is 2μm. (c) Intensity recovery at the bleached area (red) and decay at the adjacent non-bleached area (green) are shown. Dot represents average intensity (n = 5) while the error bar is SEM.

PS at the inner plasma membrane leaflet can be enriched through the inhibition of outward transporters

In Chapter 4 we have extensively studied how Lem3-Dnf1 and Lem3-Dnf2 complex can create charge asymmetry at the polar cortex. However Dnf1/2 belongs to the P4-ATPase family which selectively translocates aminophospholipids PE and PC from outer to inner leaflet of the plasma membrane (Hanson et al., 2003; Kato et al., 2002; Pomorski et al., 2003; Pomorski and Menon, 2006). It is still an important question how inhibiting PE and PC flipping from outer to inner leaflet increases PS concentration at the inner leaflet.

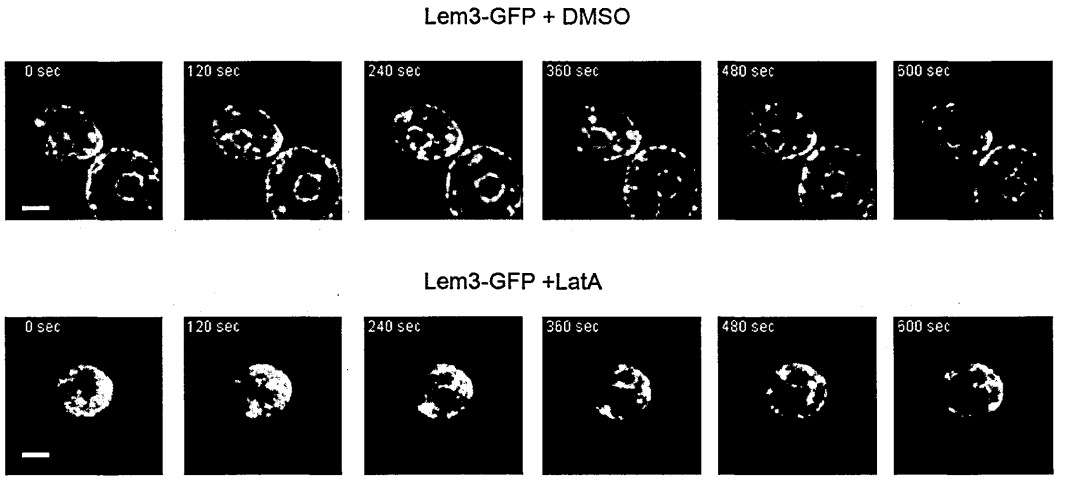

Figure 5-5. Lem3 at polar cortex is maintained through actin mediated endocytosis and exocytosis.
Montage of a time-lapse of a Wt cell expressing Lem3-GFP in presence of DMSO or 100μM LatA. Images are weekly smoothed. Scale bar is 2μm.

It is observed that ABC transporters ABCA1 (Ikeda et al., 2006) in macrophage cell and MDR1 (McGrath and Varshavsky, 1989) in human gastric carcinoma cells transport PS from inner to outer leaflet of the plasma membrane. STE6 is the yeast homologue of mammalian MDR1 (McGrath and Varshavsky, 1989) which is inhibited in presence of pheromone. It is possible to have lipid homeostasis between the leaflets, inward movement of PE and PC is coherent with the outward movement of PS and in the absence of one the other is inhibited. To test if outward movement of PS is dependent on ABC transporter like Ste6 we measured PS concentration at the polar cortex in presence of pheromone for Wt and Δ*lem3* cells. Interestingly in presence of

pheromone PS concentration is significantly enriched at the inner leaflet of Wt cells whereas in Δ*lem3* cells it remained unchanged (Fig. 6a, b quantification done similarly as in chapter 4, Fig. 3c-e). This strongly suggests the possible involvement of MDR genes in regulating PS concentration at the inner plasma membrane leaflet functioning in parallel with Lem3-Dnf1/2 complex. Furthermore we have observed reduced Cdc42 dissociation rate (iFRAP) in presence of pheromone in Wt cells while the effect is insignificant in Δ*lem3*. This also supports the findings in chapter 4 that increased PS concentration at the inner leaflet reduces Cdc42 dissociation rate possibly through increased electrostatic interaction between negatively charged polar head group of PS and COOH-terminal polycationic sequence of Cdc42.

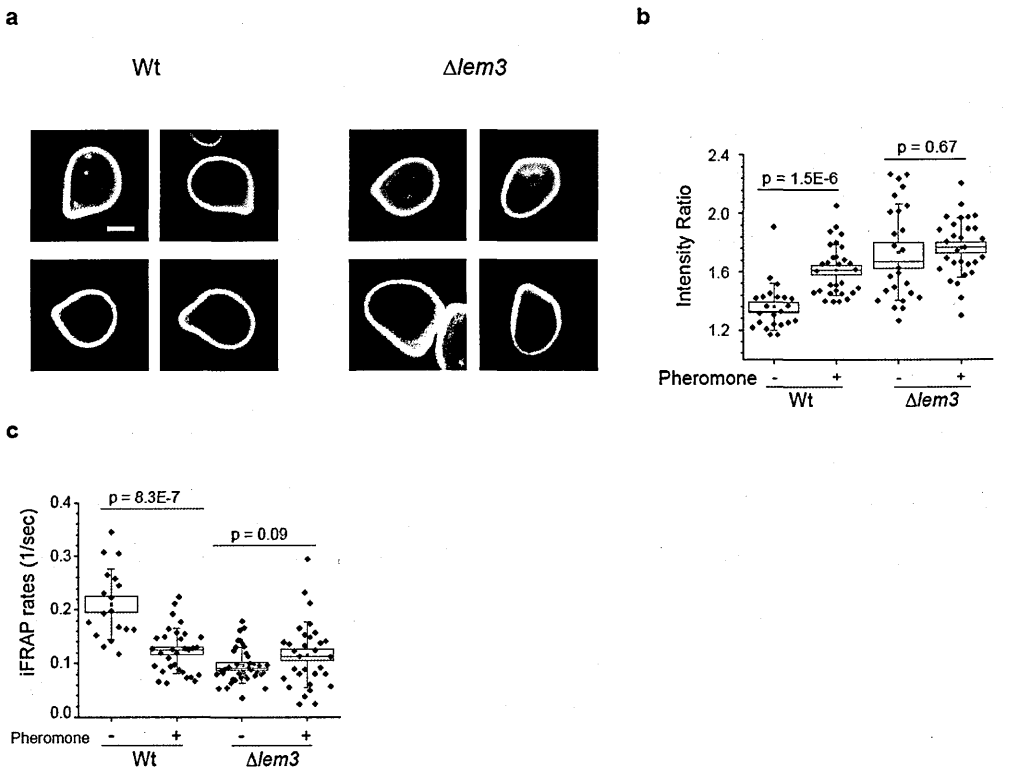

Figure 5-6. Shmooing cell has different phospholipid composition at polar cortex compared to cycling cell.

(a) Representative confocal images of Wt and Δ*lem3* cells expressing GFP-Lact-C2 in presence of pheromone. Scale bar is 2μm. (b) Ratios of GFP-Lact-C2 intensity in the half of the plasma membrane containing the polar cap over that in the rest of the plasma membrane as explained in (chapter 4, Fig. 3e). The small square is the mean; the box range is SEM; whiskers represent standard deviation (SD); line is median. (c)

Internalization rate of GFP-Cdc42 at the polar cap in presence and absence of pheromone measured with iFRAP in Wt and Δlem3 cells. Box as explained in (b).

5.3. Rescuer candidates involve in vesicle trafficking may help in maintaining cell polarity along with Rdi1

From the whole genome screening we obtained a series of candidates that both rescued (rescuers) and exacerbates (worse-growers) the Rdi1 over-expression growth defect. Among the rescuers we got a group of candidates which includes Lem3, Cdc50, Drs2 (Fig. 2), all involved in lipid flipping. Thorough investigation on Lem3-Dnf1 and Lem3-Dnf2 lipid flippase activity and their regulation of Cdc42 recycling at polar cortex was done in my thesis research (chapter 4). Interestingly Drs2 also belongs to the subfamily of P4-ATPases and is involved in PS and PE translocation from luminal to cytosolic leaflet of *trans*-Golgi network (TGN) (Natarajan et al., 2004) in complex with Cdc50 (Saito et al., 2004). Drs2 and Cdc50 complement each other to exit from ER to localize at TGN. It was observed lipid flippase activity of Cdc50-Drs2 complex at TGN is required for the formation and transport of clathrin-coated vesicles (CCVs) from TGN to PM (Gall et al., 2002).

To understand how Cdc42 localization is affected in above mutant we expressed GFP-Cdc42 in Δ*drs2* strain. To our surprise we found Cdc42 is trapped inside some membrane structure as bright puncta in this mutant (Fig. 7b, c). Drs2 and its ATPase function at TGN is required for vesicle formation and target to the PM, however it does not perturb the formation of vesicles targeted to late endosomes (Gall et al., 2002). We asked whether the bright Cdc42 puncta in Δ*drs2* are the endosomal structures. To test this we stained Δ*drs2* strain expressing GFP-Cdc42 with endosomal marker FM 4-64 (Vida and Emr, 1995). Interestingly we found the bright Cdc42 structures are endosomes from the colocalization of bright Cdc42 puncta and FM 4-64 staining (Fig. 7b). To investigate whether this phenotype is dependent on ATP hydrolysis mediated PS flipping at the TGN, we introduced Wt Drs2 and Drs2 ATPase dead mutant ($Drs2^{D560N}$) (Gall et al., 2002) into Δ*drs2* strain. We observed that Drs2 rescued the Cdc42 punctuate localization while the ATPase dead mutant did not (Fig. 7c). This suggests Drs2 mediated lipid flipping at the TGN is required for proper Cdc42 recycling from endosome back to TGN. Similar bright Cdc42 localization was also observed for other rescuers Δ*cdc50,* Δ*vps52,* Δ*vps53,* Δ*vps54,* Δ*tlg2* and Δ*gos1,* also belong to the same physical interaction module (Fig. 2, pink nodes at lower right) and

involve in vesicle trafficking pathway. A detail investigation is required to decipher the Cdc42 trafficking route and its polarized localization based on the above trafficking mutants.

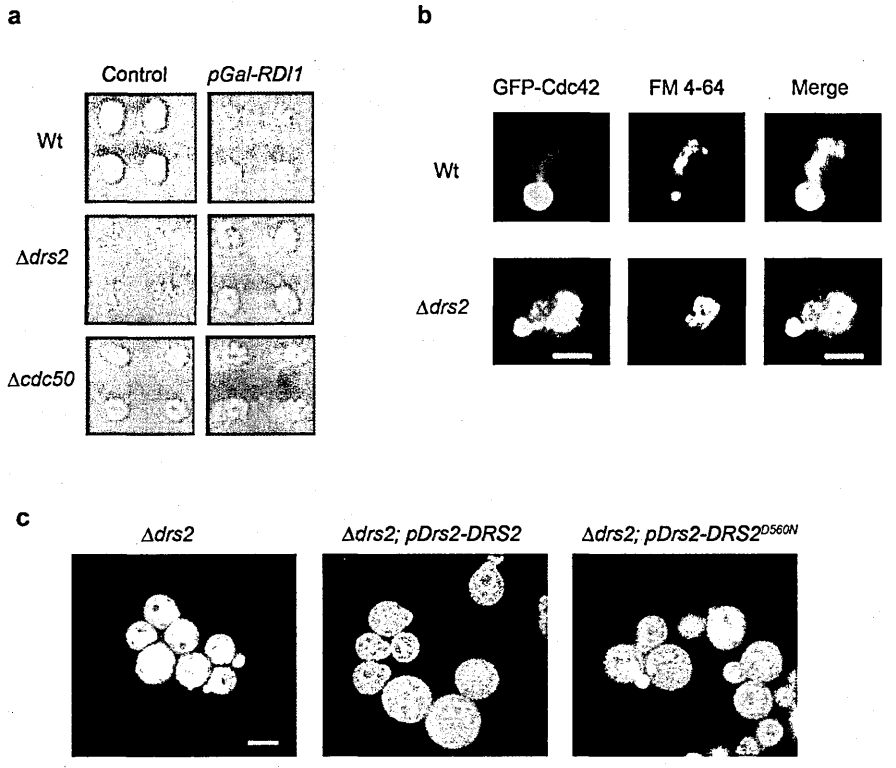

Figure 5-7. Cdc42 trapped in endosomal structures in vesicle trafficking mutants.
(a) Images of Wt, Δ*cdc50* and Δ*drs2* on solid agar media with or without Rdi1 over-expression (pGal-*Rdi1*) from the genome-wide screening. (b) Confocal images of Wt and Δ*drs2* small budded cells expressing GFP-Cdc42 and stained with FM 4-64. Scale bar is 2μm. (c) Confocal images of Δ*drs2* strain expressing GFP-Cdc42 and in presence of pDrs2-*DRS2* and pDrs2-*Drs2D*^{560N} in centromeric plasmid (pRS315). Scale bar is 4μm.

5.4. P21-activated kinase (PAK) regulation of Cdc42 recycling at polar cortex

PAKs are serine/threonine protein kinases (Bokoch, 2003) which are the effectors of active Rac and Cdc42 GTPases. PAKs interact with GTP-bound Cdc42 and Rac through Rac/Cdc24-binding domain (PBD/ CRIB) and turns on several signaling cascades require for cell motility (Bokoch, 2003), cytokinesis (Benton et al., 1997) and cell polarity. Recent evidence suggests Cla4, a yeast PAK can regulate Cdc42-Rdi1 interacting and hence Rdi1 mediated Cdc42 extraction from polar cortex (Tiedje et al., 2008). It is also observed from in vitro assay Pak1 can phosphorylate RhoGDI at Ser101 and Ser174 which disrupts Rac1-RhoGDI complex but interestingly not RhoA-RhoGDI complex (DerMardirossian et al., 2004).

To understand how PAK regulates Cdc42-Rdi1 interaction and Cdc42 recycling at polar cortex we focused on Cla4. Cla4 like other PAKs is a multi-domain protein and apart from its kinase function it can interact with a broad range of molecules, starting from PM phosphoinositides, active Cdc42 and SH3 domain containing proteins like Bem1, Boi1 and Boi2 (Bokoch, 2003) (Fig. 8) to turn on several signaling events required for cellular morphogenesis. It is possible Cla4 can regulate Cdc42 polarization and recycling at polar cortex through the multitude of interactions along with its kinase activity. To decipher the molecular mechanism of Cla4 mediated Cdc42 recycling we developed an over-expression based assay where several Cla4 domains were deleted or mutated to selectively abolish the different modes of interactions as explained above. The goal was to understand the protein function in Cdc42 recycling through gain of function phenotypes under the over-expression of different constructs (Fig. 8).

We studied G1 polarized cells in a dividing population to avoid heterogeneity in data acquisition. We performed FRAP experiment at the polar cortex to study over-expression effect of Cla4 constructs on Cdc42 recycling. Over-expression of Wt Cla4 reduced the recycling rate however the construct with kinase dead mutation ($Cla4^{kd}$) or absence of kinase domain ($Cla4^{\Delta kin}$) reduced the rate even more (Fig. 9a). This suggests elevated level of Cla4 domains other than kinase domain can reduce the overall Cdc42 recycling at polar cortex. Proteins with proline- rich domain like Cla4 can interact with SH3 domain which creates a possibility that excess interaction with above proteins under the over-expression condition might be responsible for slow Cdc42

recycling. To test this, we further deleted Proline-rich domain of Cla4 ($Cla4^{\Delta kin\Delta pro\text{-}rich}$) and interestingly elevated level of $Cla4^{\Delta kin\Delta pro\text{-}rich}$ construct significantly rescued FRAP rate compared to $Cla4^{\Delta kin}$ to an extend similar to the over-expression of only CRIB domain (Cla4-CRIB) (Fig. 9a). Cdc42 recycling rate was also correlated to the growth phenotype under the over-expression of these constructs. While over-expression of Wt Cla4, $Cla4^{kd}$ or $Cla4^{\Delta kin}$ was severely toxic to the cell, elevated level of $Cla4^{\Delta kin\Delta pro\text{-}rich}$ rescued the toxicity significantly (Fig. 9b). We also observed over-expression of $Cla4^{\Delta kin}$ or $Cla4^{kd}$ leads to hyperpolarized Cdc42 distribution and elongated bud morphology (preliminary observation, data not shown). This suggests that the function of proline-rich domain in stable localization of Cdc42 at the polar cortex presumably via interaction with SH3 domain containing proteins. We observed that fast Cdc42 recycling at the polar cortex is dependent on Cdc42-Rdi1 interaction in the cytosol (Chapter 3, Fig. 1c, 3c). Under the over-expression of Wt Cla4, $Cla4^{kd}$ or $Cla4^{\Delta kin}$ we found reduced Cdc42 and Rdi1 interaction from FCCS experiment (Fig. 9c) which further explains slow FRAP rates under these conditions. Over-expression of CRIB domain (Cla4-CRIB) is not toxic (Fig. 10) but reduced FRAP rate and Cdc42-Rdi1 interaction (Fig. 9a, c) albeit less dramatically compared to Wt Cla4, $Cla4^{kd}$ or $Cla4^{\Delta kin}$, presumably via sequestration of more active Cdc42 into cytosol keeping it less accessible to Rdi1.

We next focused on the role of kinase domain in Cdc42 recycling or localization at the polar cortex. To do so we over-expressed the kinase domain (Cla4-Kinase) and found it to be as toxic as the over-expression of Wt Cla4, $Cla4^{kd}$ or $Cla4^{\Delta kin}$ (Fig. 9b, 10). Interestingly we observed that elevated Kinase domain reduced Cdc42 polarization (preliminary observation, data not shown) however increased Cdc42-Rdi1 interaction in cytosol (Fig. 9c) from FCCS experiment. This suggests that excess kinase activity reduced cell polarity presumably through dissociation of Cdc42-Rdi1 complex from the polar cortex rather than disrupting the Cdc42-Rdi1 interaction.

To study the over-expression effect of Cla4 constructs more directly on Cdc42 dissociation rate from polar cortex, we performed iFRAP experiment (see chapter 2 for experimental procedure). Over-expression of Wt Cla4 significantly reduced iFRAP rate which was further enhanced in $Cla4^{kd}$ (Fig. 9d). However introducing mutation at the CRIB domain, defective in Cdc42 interaction ($Cla4^{crib+kd}$) rescued both iFRAP rate and toxicity compared to $Cla4^{kd}$ alone (Fig. 9b, d). This suggests one of the interactions of Cla4 domains that stabilize Cdc42 at the polar

cortex is the CRIB domain. Over-expression of full length protein with mutation at CRIB domain ($Cla4^{crib}$) is less toxic compared to Wt Cla4 (Fig. 9b) with comparable iFRAP rates. This suggests interaction with Cdc42 via CRIB domain contributes to the Cla4 over-expression toxicity while over-expressed along with other domains. Over-expression of CRIB domain alone (Cla4-CRIB) also reduced iFRAP rate albeit less severely compared to the $Cla4^{kd}$ (Fig. 9d) as also observed in FRAP study and the over-expression has no cellular toxicity (Fig. 10). This suggests presumably at the elevated level of CRIB domain active Cdc42 at the polar cortex is mostly shielded from Rdi1 mediated extraction. We next focused on the PH domain which interacts with phosphoinositides at the plasma membrane and found over-expression of PH domain strongly reduced the iFRAP rate (Fig. 9d). However introducing mutation at the PH domain, defective in phosphoinositide interaction in the $Cla4^{\Delta kin}$ ($Cla4^{\Delta kin + PH}$) construct rescued the $Cla4^{\Delta kin}$ over-expression growth defect (Fig. 9b). This suggests elevated level of $Cla4^{\Delta kin}$ makes Cdc42 less dynamic at the polar cortex, a possible factor for toxicity and PH domain contributes significantly in this excess stabilization of the Cdc42 at polar cortex and toxicity.

We found Rdi1 over-expression causes synthetic growth-defect (Chapter 5, genome wide screening) most likely due to excess Cdc42 extraction from the polar cortex (Chapter 4, Fig. 1). In this study we observed over-expression of $Cla4^{kd}$ construct made Cdc42 less dynamic at the polar cortex with severe toxicity. We asked whether Rdi1 over-expression can rescue this toxicity via extracting more Cdc42 from the polar cortex that is blocked in presence of $Cla4^{kd}$ over-expression. Indeed Rdi1 over-expression rescued above toxicity while it did not rescue the Wt Cla4, $Cla4^{crib}$ or kinase domain over-expression toxicity (Fig. 10).

Taking all these results into account it suggests Cla4 can both stabilize Cdc42 at polar cortex and simultaneously induce Rdi1 mediated Cdc42 extraction from polar cortex. The stabilization can be achieved via following interactions: 1) PH domain with PM, 2) CRIB domain with Cdc42, 3) Proline-rich domain that probably stabilizes the interaction between Cdc42 and the SH3 domain containing proteins at the PM. While kinase activity is more into the dissociation of Cdc42-Rdi1 complex from polar cortex together. Similar reduction in iFRAP rate and Cdc42-Rdi1 interaction was also observed under the over-expression of Cdc42 effector with CRIB domain such

as Gic2 (Fig. 9c, d) further validates the conserved nature of these domain interactions and regulation of Cdc42 recycling at polar cortex.

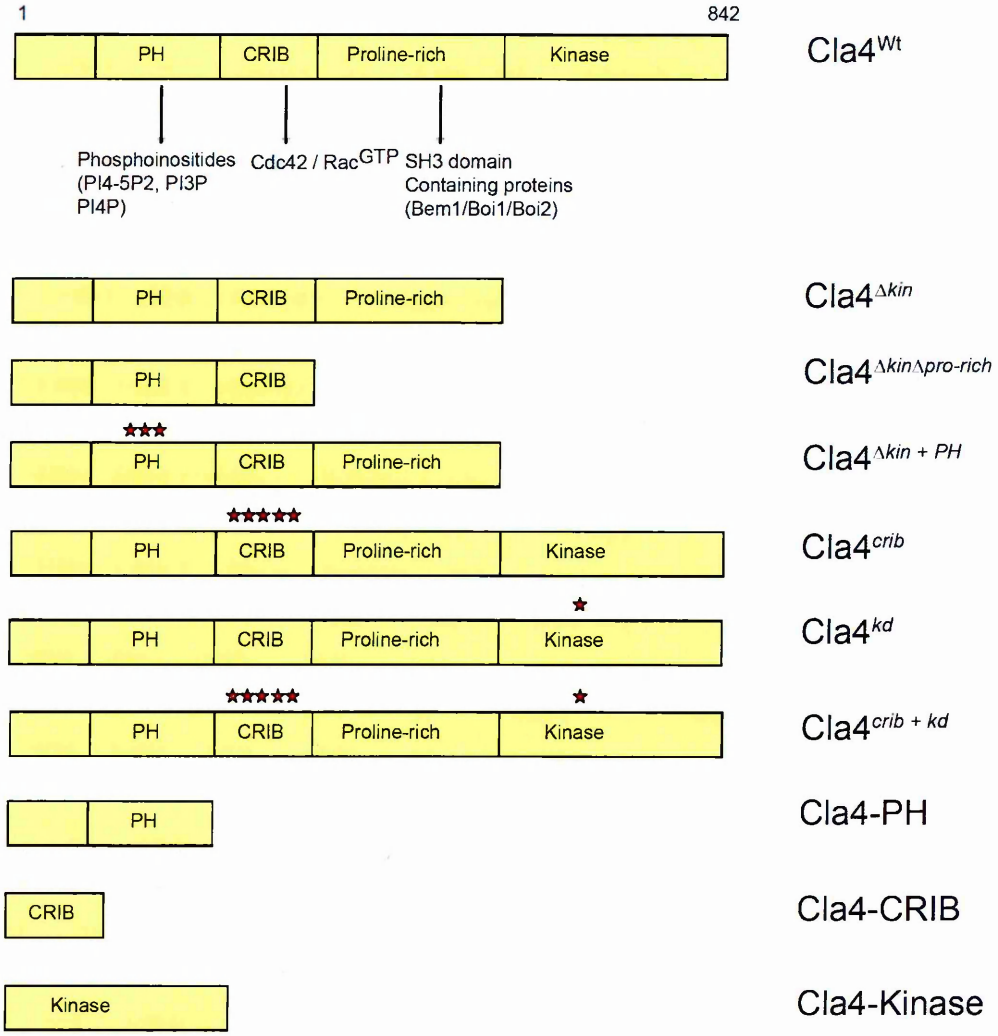

Figure 5-8. Different Cla4 constructs and mutants.

Cla4 constructs and different mutants used in this study are over-expressed under *pGal1* promoter in pRS315 centromeric plasmid. $Cla4^{Wt}$ protein (842 amino acids) with different domains and interacting molecules (Wild et al., 2004). $Cla4^{\Delta kin}$, Cla4 construct (527 amino acid from amino terminal) without COOH-terminal kinase domain (Wild et al., 2004). $Cla4^{\Delta kin\Delta Pro\text{-}rich}$, Cla4 construct (246 amino acid from amino terminal) without COOH-terminal kinase domain and proline-rich domains (Wild et al., 2004). $Cla4^{\Delta kin\ +\ PH}$, Cla4 construct without kinase domain along with the mutation at pleckstrin homology (PH) domain (K71N, K96N, K99N) defective in phosphoinositide interaction (Wild et al., 2004). $Cla4^{crib}$, (V183A, S184A, P186A, H191A, H194A) mutant defective in Cdc42

interaction (Brown et al., 1997). Cla4^{kd}, (K594A) kinase dead mutant of Cla4 (Dobbelaere et al., 2003). Cla4-PH, (amino acid 61-181 from the aminoterminal) (Wild et al., 2004). Cla4-CRIB, (amino acid 181-247 from the aminoterminal) (Wild et al., 2004). Cla4-kinase (amino acid 528-842 at the COOH-terminal) (Wild et al., 2004)

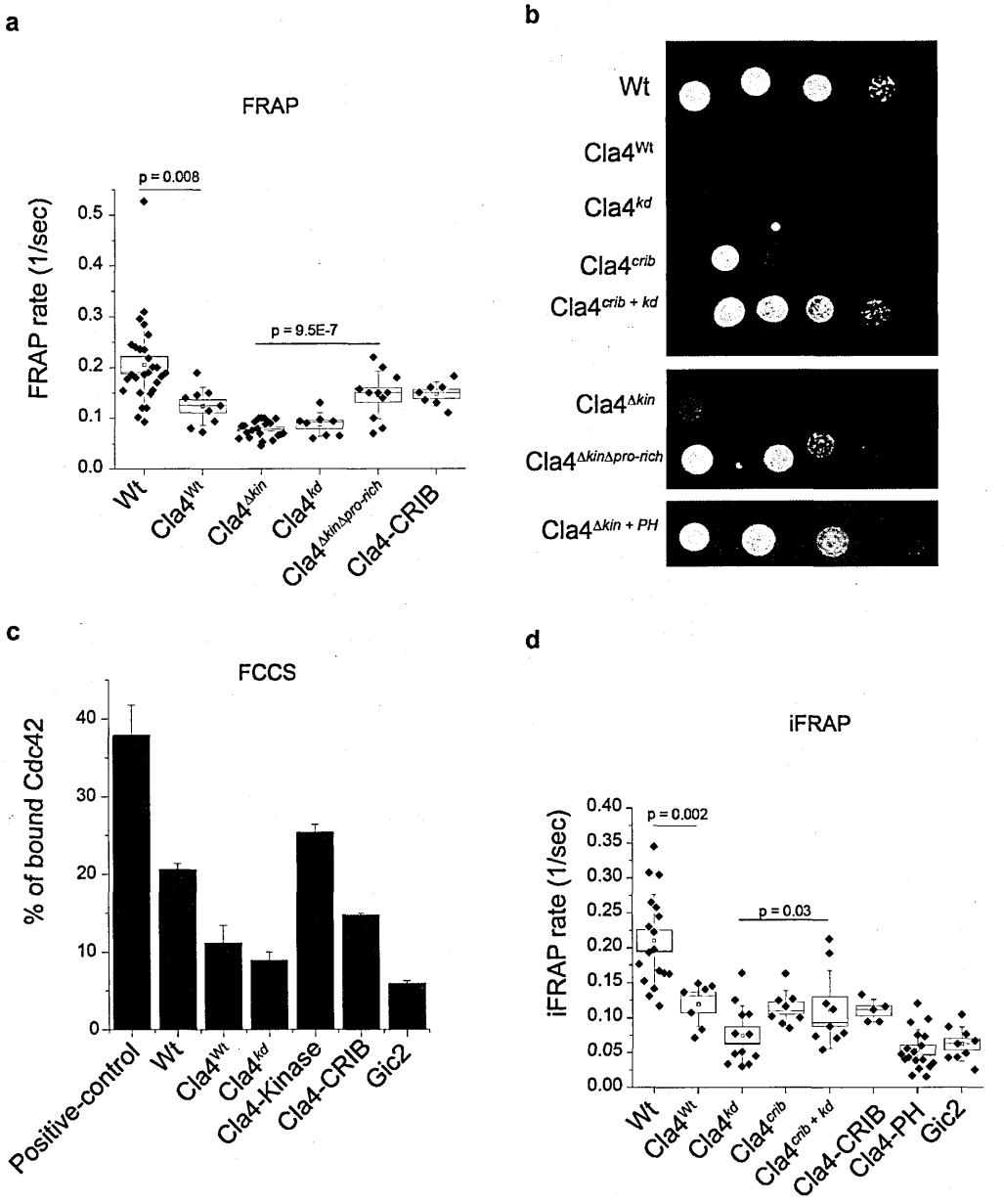

Figure 5-9. Effect of over-expression of Cla4 domains and mutants on Cdc42 recycling and yeast growth.

(a) FRAP rates (1/sec) for strains as indicated conditions. Box represents SEM and the whisker is SD. (b) Serial tenfold dilutions of cultures for the indicated strains were spotted on SGal-Leu plates. Plates were scanned after 3 days incubation at 23^0C. (c) Percentages of bound GFP-Cdc42 with Rdi1-mCherry were quantified under indicated conditions. Positive control is the linked GFP and mCherry at the COOH terminal of Bat2 protein (Slaughter et al., 2009). Column represents average and the error bar is SEM. (d) iFRAP rates (1/sec) for strains as indicated conditions. Box represents SEM and the whisker is SD

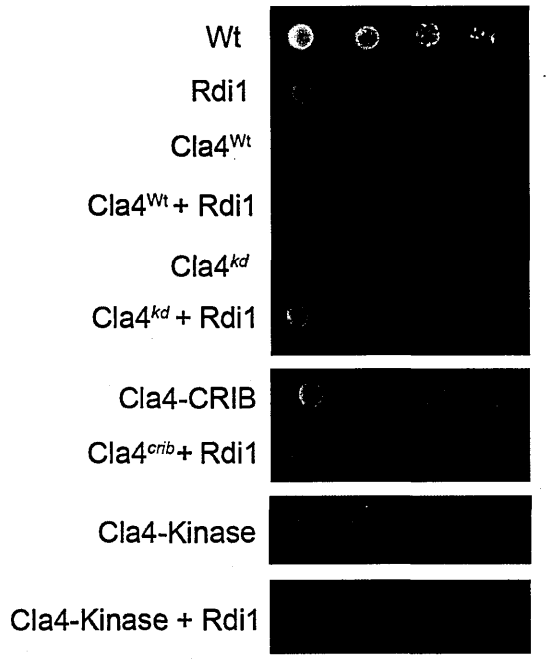

Figure 5-10. over-expression effect of Cla4 domains and mutants on yeast growth. Serial tenfold dilutions of cultures for the indicated strains were spotted on SGal-Leu plates. Plates were scanned after 3 days incubation at 23^0C

Method

Confocal images, FRAP, iFRAP and FCCS were done as explained in chapter 2. Lem3-GFP half cap FRAP and movies with 100μM LatA and DMSO were acquired using the avalanche photodiode (APD) imaging module of a Zeiss Confocor 3, using a 40X, 1.2-NA C-Apochromat water objective.

FM 4-64 staining

Staining was done as explained in (Vida and Emr, 1995). In brief yeast culture at OD ~ 0.5 was harvested and resuspended in fresh media at OD ~ 40. FM 4-64 stain was added at 40μM final concentration and incubated at 23^0c for 15 min under shaking condition. Cells were harvested at 700 X G for 3 min at room temperature and resuspended again in fresh media for another 30 min incubation at room temperature under shaking. Finally harvested at 700 X G for 3 min and resuspended in fresh media for imaging.

Chapter 6. Summary and outstanding questions with conclusion

Summary

The motivation of this work at the beginning was to understand the cell polarity maintenance mechanism at the unicellular level. Existing literature at that point showed Cdc42 at the polar cortex is dynamic from FRAP based study. Two positive feedback loops are coupled for the generation of robust cell polarity: 1) Cdc42 GTPase cycle and actomyosin based transport and 2) Bem1 mediated signaling pathway that recruits or activates Cdc42 GEF Cdc24 at the site of polarized accumulation. Beyond this knowledge we seek to understand what are the pathways through which Cdc42 is recycled and the optimum concentration is maintained at the polar cortex using live cell imaging and spectroscopic based analysis like FRAP, iFRAP, FCS, FCCS and reconstituted in vitro assay involving SLB and TIRF. We found Cdc42 is recycled at the polar cortex via actin dependent slow recycling and Rdi1 mediated fast recycling pathways which are coupled through Cdc42 GTPase cycle. Using mathematical model we further elucidated that both the pathways are required to be spatially overlapping with identical window size, a criteria that is critical to have physiological Cdc42 distribution. At the next level we tried to understand the molecular players involve in Rdi1 mediated Cdc42 recycling. Over-expression of Rdi1 caused synthetic sickness and a genome wide screen in yeast non-essential gene knock out library revealed Lem3, a component of lipid flippase complex Lem3-Dnf1 and Lem3-Dnf2 can rescue the Rdi1 over-expression sickness. In depth study further revealed amino phospholipid flipping at the polar cortex creates asymmetry in charge distribution among the PM leaflets that regulates affinity between Cdc42 polycationic sequence adjacent to the COOH-terminal prenyl group and plasma membrane, an important step of Rdi1 mediated Cdc42 extraction from PM.

How conserved is the charge interaction-mediated Rho GTPase recycling at polar cortex

Our study added an important piece of knowledge, how lipid composition of the PM can regulate Cdc42 recycling via Rdi1 at polar cortex. However apart from Cdc42 yeast has other Rho GTPase such as Rho1, Rho2, Rho3, Rho4 and Rho5 which are also involved in cell polarity. It is interesting to study whether charge interaction mediated regulation of Cdc42 recycling is also applicable for other Rho GTPases. In vitro immunoprecipitation assay showed Rdi1 can pull down Rho1 and Rho4 apart from Cdc42 but not the Rho2, Rho3 and Rho5 (Tiedje et al., 2008). This makes Rho1 and Rho4 an important candidate for Rdi1 mediated recycling. Sequence analysis revealed other than Cdc42; Rho1 and Rho5 also has the polycationic amino acid sequence at their COOH terminal. Our preliminary observation showed indeed Rho1 dissociation rate from polar cortex (iFRAP) is lot slower than wild-type Cdc42 which is close to the $Cdc42^{S185K}$ mutant. This indicates existence of charge interaction mediated regulation of Rho1 at the polar cortex. We are planning to study in depth by changing the amino acid sequence of Rho1 polycationic region to more negative and its effect on dissociation rate. Whether Rho1 is also recycled via Rdi1 will be investigated by iFRAP experiment in Δ*rdi1* background and interaction with Rdi1 in cytosol by FCCS experiment.

Our study (Chapter 4) so far focused on Lipid flippase complex with P4-ATPases (Dnf1/ Dnf2) in generating lipid asymmetry at the PM. This class of ATPases are known to selectively translocate aminophospholipids PE and PC from outer to inner leaflet of the plasma membrane (Hanson et al., 2003; Kato et al., 2002; Pomorski et al., 2003; Pomorski and Menon, 2006). It is still an important question how PE, PC flips back to the outer leaflet and how PS concentration is enriched at the inner leaflet in Δ*lem3* mutant (chapter 4). To investigate these questions we are focusing on a second class of ATP-dependent flippases, ABC transporters which are known to flip amino phospholipid from inner to outer leaflet of PM (Also see Chapter 5). Therefore it is possible these transporters flip lipid from inner to outer leaflet and function along with P4-ATPases. So inhibiting outer to inner leaflet flipping in Δ*lem3* can also inhibit ABC transporters and increase PS concentration in the inner leaflet to maintain the lipid homeostasis. As an evidence to above hypothesis it was found ABC transporter MDR1 in human gastric carcinoma cells transport PS from inner to outer leaflet of the plasma membrane (McGrath and Varshavsky, 1989). The yeast

homolog of human MDR1 is STE6 (McGrath and Varshavsky, 1989) which is inhibited in presence of mating pheromone (Wilson and Herskowitz, 1984). Interestingly our preliminary study showed in presence of pheromone PS concentration is significantly enriched at the inner leaflet of Wt cells with reduced Cdc42 iFRAP rate whereas in *Δlem3* cells it remained unchanged (Chapter 5, Fig. 6a, b, c). This provides an evidence for the involvement of MDR transporter in regulating PS concentration at the inner plasma membrane leaflet possibly in concert with Lem3-Dnf1/2 complex. To have direct evidence next, we plan to delete Ste6 and study Cdc42 recycling at the polar cortex and whether this deletion affects PS concentration at the inner leaflet of polar cortex. If inward and outward lipid flipping is interdependent then it is possible inhibiting outward lipid flipping by *Δste6*, inward flipping (P4-ATPase dependent) will also be inhibited and PE, PC concentration should increase at the outer leaflet. This can be checked by staining cells with Biotinylated-Ro which specifically bind to exposed PE followed by FITC-Streptavidin staining (Iwamoto et al., 2004) in the above condition.

Vesicle trafficking in cell polarity maintenance

From whole genome screening we obtained a series of candidates that rescued Rdi1 over-expression growth defect and also belong to the members of vesicle trafficking pathway (Chapter 5). Among which *Δcdc50, Δdrs2, Δvps52, Δvps53, Δvps54, Δtlg2* and *Δgos1* shared the same physical interaction module (Chapter 5, Fig. 2, pink nodes at lower right) and all belongs to vesicle trafficking pathway. Vps52, Vps53, Vps54, Tlg2, Gos1 involve in vesicle recycling between TGN and early endosomes (Siniossoglou and Pelham, 2001) and also found Ric1 as an rescuers which belong to different interaction module (Chapter 5, Fig. 2, blue node upper left) and involve in trafficking. Among other candidates Drs2 forms complex with Cdc50 which is required for their exit from ER to TGN. Drs2 belongs to the subfamily of P4-ATPases and involves in PS translocation from luminal to cytosolic leaflet of *trans*-Golgi network (TGN) (Natarajan et al., 2004) in complex with Cdc50 (Saito et al., 2004) which is required for the formation and transport of clathrin-coated vesicles (CCVs) from TGN to PM. Interestingly we also found the Snc2 (V-SNARE) and Sso1, Sso2 (PM localized t-SNARE) as rescuer candidates also shared the same physical interaction module (Chapter 5, Fig. 2, pink nodes at lower right) with Drs2. This indicates

Cdc42 is recycled via TGN, PM and endosomes, indeed we observed Cdc42 trapped into endosome in most of the above mutants (Chapter 5). Our preliminary experiment suggests over-expression Rdi1 can extract Cdc42 from these internal structures.

Suppression of Rdi1 over-expression growth defect in above mutants is possibly through releasing trapped Cdc42 into the soluble functional pool. That raises the possibility Rdi1 might extracts Cdc42 from internal membrane structure even in the Wt background. Under this situation deleting both Rdi1 and above trafficking candidates together should cause synthetic sickness. To test this we are planning to create double deletion strains with Rdi1 and each of the above mentioned vesicle trafficking candidates followed by growth assay. We will focus on each of the trafficking candidates to map the trafficking route of Cdc42 between PM and TGN. This will allow us to understand how Rdi1 mediated Cdc42 extraction from internal membrane involves in polarity maintenance together with its detail trafficking route.

Specialized plasma membrane structure can play a role in Cdc42 recycling at polar cortex

Protein distribution in the S. *cerevisiae* plasma membrane is not uniform rather it is reported to be distributed in at least three different structures: 1) concentrated in ~300 nm discrete patch structure, 2) sometime protein concentrates in mesh-shaped structure, or 3) uniformly distributed between two areas (Grossmann et al., 2008). The patches are marked by the localization of proton ATPase , Pma1 and Sur7, presumably involve in endocytosis and regulate PM sphingolipid content (Grossmann et al., 2007; Young et al., 2002) also referred as eisosome (Grossmann et al., 2008). Interestingly we also found Sur7 as an rescuer in the genome screening. Recently it was observed through some complex signaling cascade Pkh1-Ypk1-Fpk1 kinases can regulate aminophospholipid flippase activity in the plasma membrane (Roelants et al., 2010). Pkh1 and Pkh2, the upstream the signaling event down-regulate the flippase activity, also are known to be associated with the membrane microdomain termed eisosomes (Grossmann et al., 2008). Interestingly the optimal Fpk1 and Fpk2 activity depends upon the sphingolipd content of the eisosomes and the biogenesis of this lipid is dependent on Sch9 (Roelants et al., 2010; Wei et al., 2009). We also found Pkh2 and Sch9 as worse grower candidate, which share same interaction module (Fig. 3, lower right, orange nodes).

Above information indicates the involvement of eisosome in cell polarity, possibly a regulator of Rdi1 mediated recycling. We plan to use high resolution confocal microscope and TIRF microscope to see Cdc42 distribution at the PM and whether it localizes within the eisosome. iFRAP study will be performed in the deletion background of Sur7, Pkh2 and Sch9 to see whether Cdc42 dissociation rate is affected. Sur7, involves in regulating PM sphingolipid content (Grossmann et al., 2007; Young et al., 2002) so it is possible sphingolipid content of PM affect Rdi1 mediated Cdc42 recycling. To test this we will pharmacologically inhibit phytosphingosin (PHS) biosynthesis using a drug called myriocin (Roelants et al., 2010). In case of slow recycling the inhibition should be rescued by supplementing the culture with external PSH.

Kinase mediated regulation of Cdc42 recycling

In Chapter 5 we have discussed the ongoing work on PAK, Cla4 and how it is regulating Cdc42 recycling at the polar cortex. It is still an important question how Cdc42-Rdi1 complex is disrupted and Cdc42 is retargeted to the polar cortex. It was speculated from in vitro study that Cla4 might phosphorylate Rdi1 which is required for the Cdc42-Rdi1 complex to break down (Tiedje et al., 2008). However from our study it is indicating Cla4 kinase activity does not disrupt the complex rather dissociates the whole Cdc42-Rdi1 complex together from polar cortex (Chapter 5). Above observation is not much surprising in the context of the finding, Pak1 can phosphorylate RhoGDI which disrupts Rac1-RhoGDI complex but not RhoA-RhoGDI complex (DerMardirossian et al., 2004). We plan to investigate more to find the molecular player that dissociates Cdc42-Rdi1 complex. As a first step we are focusing on kinases that have known interaction with Rdi1 and/ or can phosphorylate Rdi1. Interestingly we found a kinase Yck1, palmitoylated plasma membrane-bound casein kinase which interacts and phosphorylates Rdi1 (Ptacek et al., 2005). Yck1 has a functional redundant Yck2 and together is required for proper bud morphogenesis (Robinson et al., 1993). Importantly we also found Yck1 and Yck2 as mild worse growers from genome screen which fall outside of our stringent cut off (See Chapter 5, Genome wide screening, method) possibly due to the existence of functional redundant. Incase Yck1/2 phosphorylates Rdi1 and disrupts the Cdc42-Rdi1 complex, above result is expected since over-expression of Rdi1 will

extract more Cdc42 from the polar cortex while there is no retargeting due to the absence of Yck1/2, a situation that should exacerbate the Rdi1 over-expression growth defect.

To investigate above possibility we are designing an in vitro kinase assay where purified Yck1 and Yck2 on beads will be added to the purified Rdi1 in presence of γ-32P-ATP and the bands will be studied by autoradiograph. In case of Rdi1 phosphorylation the protein will be sent for mass-spec to analyze the phosphorylated sites. In vivo those phosphorylation sites on Rdi1 will be mutated to phosphomimicking (glutamate) or constitutively dephosphorylated alanine to study the effect on Cdc42 recycling and interaction with Rdi1.

To investigate the effect of Cdc42 recycling (iFRAP) and interaction with Rdi1 (FCCS) in vivo, we need to have a yeast strain where both Yck1/ Yck2 are deleted. However, deletion of both the genes is synthetic lethal. To make this yeast strain Yck2 will be deleted and an analog-sensitive mutant of Yck1 (*as-yck1*) (Blethrow et al., 2004; Levin et al., 2008) will be introduced into that strain followed by deletion of Yck1. Analog sensitive mutation in the kinase allows to accept ATP and keep the protein functional while in presence of ATP analogues (1NM-PP1, 1NA-PP1) ATP-binding pocket is blocked by the analog inhibiting its kinase activity (Blethrow et al., 2004). This provides an opportunity to study the inhibition effect of kinase activity while the kinase activity is essential and deletion of whole gene is not possible. In the above strain we can block kinase activity in presence of ATP analogs and can study the Cdc42 recycling and interaction with Rdi1 in live cell.

Conclusion

Our study has extended the knowledge of cell polarization process specially in the maintenance process by adding following information: 1) Robust cell polarization is obtained via slow actin dependent and fast Rdi1 dependent Cdc42 recycling pathways, 2) Actin and Rdi1 pathways are regulated by Cdc42 GTPase cycle and mathematical modeling predicted to have physiological Cdc42 polarized distribution both the pathways are required to be spatially overlapping with identical delivery window size and 3) Dynamic phospholipid asymmetry at the polar cortex regulates charge interaction between Cdc42 with PM which in turn regulate Rdi1-mediated Cdc42 recycling. While these information helped to understand the mechanistic details

of distinct polarized morphogenesis outcomes and the polarity maintenance process via Rdi1 pathway, future work will be required to understand the molecular interaction modules (obtained from genome screen) those are involved in Rdi1-medaited polarity maintenance. Further work will also be required to better understand how Cdc42 polarized distribution is regulated by the plasma asymmetry in lipid composition and protein distribution in different membrane structures. It is also required to decipher the Cdc42 retargeting mechanism to polar cortex from Cdc42-rdi1 complex, the final step of Rdi1 mediated Cdc42 recycling.

References

Adams, AE, Johnson, DI, Longnecker, RM, Sloat, BF, Pringle, JR (1990) CDC42 and CDC43, two additional genes involved in budding and the establishment of cell polarity in the yeast Saccharomyces cerevisiae. The Journal of cell biology *111*, 131-142.

Aoki, Y, Uenaka, T, Aoki, J, Umeda, M, Inoue, K (1994) A novel peptide probe for studying the transbilayer movement of phosphatidylethanolamine. Journal of biochemistry *116*, 291-297.

Arimura, N, Kaibuchi, K (2007) Neuronal polarity: from extracellular signals to intracellular mechanisms. Nature reviews Neuroscience *8*, 194-205.

Baas, PW, Black, MM (1990) Individual microtubules in the axon consist of domains that differ in both composition and stability. The Journal of cell biology *111*, 495-509.

Bender, A, Sprague, GF, Jr. (1989) Pheromones and pheromone receptors are the primary determinants of mating specificity in the yeast Saccharomyces cerevisiae. Genetics *121*, 463-476.

Benton, BK, Tinkelenberg, A, Gonzalez, I, Cross, FR (1997) Cla4p, a Saccharomyces cerevisiae Cdc42p-activated kinase involved in cytokinesis, is activated at mitosis. Molecular and cellular biology *17*, 5067-5076.

Bevington, P, Robinson, D. K (2003) Data Reduction and Error Analysis for the Physical Sciences, 3rd edn (New York City, McGraw-Hill).

Binder, LI, Frankfurter, A, Rebhun, LI (1985) The distribution of tau in the mammalian central nervous system. The Journal of cell biology *101*, 1371-1378.

Blethrow, J, Zhang, C, Shokat, KM, Weiss, EL (2004) Design and use of analog-sensitive protein kinases. Current protocols in molecular biology / edited by Frederick M Ausubel [et al] *Chapter 18*, Unit 18 11.

Bokoch, GM (2003) Biology of the p21-activated kinases. Annual review of biochemistry *72*, 743-781.

Brandman, O, Ferrell, JE, Jr., Li, R, Meyer, T (2005) Interlinked fast and slow positive feedback loops drive reliable cell decisions. Science (New York, NY *310*, 496-498.

Bretscher, MS, Thomson, JN (1983) Distribution of ferritin receptors and coated pits on giant HeLa cells. The EMBO journal *2*, 599-603.

Brown, JL, Jaquenoud, M, Gulli, MP, Chant, J, Peter, M (1997) Novel Cdc42-binding proteins Gic1 and Gic2 control cell polarity in yeast. Genes & development *11*, 2972-2982.

Butty, AC, Perrinjaquet, N, Petit, A, Jaquenoud, M, Segall, JE, Hofmann, K, Zwahlen, C, Peter, M (2002) A positive feedback loop stabilizes the guanine-nucleotide exchange factor Cdc24 at sites of polarization. The EMBO journal *21*, 1565-1576.

Cannon, JL, Burkhardt, JK (2002) The regulation of actin remodeling during T-cell-APC conjugate formation. Immunological reviews *186*, 90-99.

Caviston, JP, Longtine, M, Pringle, JR, Bi, E (2003) The role of Cdc42p GTPase-activating proteins in assembly of the septin ring in yeast. Molecular biology of the cell *14*, 4051-4066.

Caviston, JP, Tcheperegine, SE, Bi, E (2002) Singularity in budding: a role for the evolutionarily conserved small GTPase Cdc42p. Proceedings of the National Academy of Sciences of the United States of America *99*, 12185-12190.

Chant, J (1999) Cell polarity in yeast. Annual review of cell and developmental biology *15*, 365-391.

Coles, BA, Compton, RG (1983) Photoelectrochemical ESR. Part I. Experimental. Journal of Electroanalytical Chemistry and Interfacial Electrochemistry *144*, 87-98.

Cowan, CR, Hyman, AA (2004) Centrosomes direct cell polarity independently of microtubule assembly in C. elegans embryos. Nature *431*, 92-96.

Daly, PJ, Page, DJ, Compton, RG (1983) Mercury-plated rotating ring-disk electrode. Analytical chemistry *55*, 1191-1192.

Das, S, Dixon, JE, Cho, W (2003) Membrane-binding and activation mechanism of PTEN. Proceedings of the National Academy of Sciences of the United States of America *100*, 7491-7496.

DerMardirossian, C, Bokoch, GM (2005) GDIs: central regulatory molecules in Rho GTPase activation. Trends in cell biology *15*, 356-363.

DerMardirossian, C, Schnelzer, A, Bokoch, GM (2004) Phosphorylation of RhoGDI by Pak1 mediates dissociation of Rac GTPase. Molecular cell *15*, 117-127.

Devaux, PF (1991) Static and dynamic lipid asymmetry in cell membranes. Biochemistry *30*, 1163-1173.

Dobbelaere, J, Gentry, MS, Hallberg, RL, Barral, Y (2003) Phosphorylation-dependent regulation of septin dynamics during the cell cycle. Developmental cell *4*, 345-357.

Drubin, DG, Nelson, WJ (1996) Origins of cell polarity. Cell *84*, 335-344.

Emoto, K, Umeda, M (2000) An essential role for a membrane lipid in cytokinesis. Regulation of contractile ring disassembly by redistribution of phosphatidylethanolamine. The Journal of cell biology *149*, 1215-1224.

Etienne-Manneville, S (2004) Cdc42-the centre of polarity. Journal of cell science *117*, 1291-1300.

Etienne-Manneville, S, Hall, A (2001) Integrin-mediated activation of Cdc42 controls cell polarity in migrating astrocytes through PKCzeta. Cell *106*, 489-498.

Eva, A, Aaronson, SA (1985) Isolation of a new human oncogene from a diffuse B-cell lymphoma. Nature *316*, 273-275.

Ferreira, A, Caceres, A (1989) The expression of acetylated microtubules during axonal and dendritic growth in cerebellar macroneurons which develop in vitro. Brain research Developmental brain research *49*, 205-213.

Forget, MA, Desrosiers, RR, Gingras, D, Beliveau, R (2002) Phosphorylation states of Cdc42 and RhoA regulate their interactions with Rho GDP dissociation inhibitor and their extraction from biological membranes. The Biochemical journal *361*, 243-254.

Fujita, A, Oka, C, Arikawa, Y, Katagai, T, Tonouchi, A, Kuhara, S, Misumi, Y (1994) A yeast gene necessary for bud-site selection encodes a protein similar to insulin-degrading enzymes. Nature *372*, 567-570.

Gall, WE, Geething, NC, Hua, Z, Ingram, MF, Liu, K, Chen, SI, Graham, TR (2002) Drs2p-dependent formation of exocytic clathrin-coated vesicles in vivo. Curr Biol *12*, 1623-1627.

Gao, JT, Guimera, R, Li, H, Pinto, IM, Sales-Pardo, M, Wai, SC, Rubinstein, B, Li, R (2011) Modular coherence of protein dynamics in yeast cell polarity system. Proceedings of the National Academy of Sciences of the United States of America *108*, 7647-7652.

Gibson, RM, Wilson-Delfosse, AL (2001) RhoGDI-binding-defective mutant of Cdc42Hs targets to membranes and activates filopodia formation but does not cycle with the cytosol of mammalian cells. The Biochemical journal *359*, 285-294.

Gladfelter, AS, Moskow, JJ, Zyla, TR, Lew, DJ (2001) Isolation and characterization of effector-loop mutants of CDC42 in yeast. Molecular biology of the cell *12*, 1239-1255.

Goud, B, Salminen, A, Walworth, NC, Novick, PJ (1988) A GTP-binding protein required for secretion rapidly associates with secretory vesicles and the plasma membrane in yeast. Cell *53*, 753-768.

Grossmann, G, Malinsky, J, Stahlschmidt, W, Loibl, M, Weig-Meckl, I, Frommer, WB, Opekarova, M, Tanner, W (2008) Plasma membrane microdomains regulate turnover of transport proteins in yeast. The Journal of cell biology *183*, 1075-1088.

Grossmann, G, Opekarova, M, Malinsky, J, Weig-Meckl, I, Tanner, W (2007) Membrane potential governs lateral segregation of plasma membrane proteins and lipids in yeast. The EMBO journal *26*, 1-8.

Guimera, R, Amaral, LA (2005) Cartography of complex networks: modules and universal roles. J Stat Mech *2005*, nihpa35573.

Guimerà, R, Amaral, LA (2005) Cartography of complex networks: modules and universal roles. J Stat Mech Theor Exp, P02001.

Guimera, R, Nunes Amaral, LA (2005) Functional cartography of complex metabolic networks. Nature *433*, 895-900.

Guimera, R, Sales-Pardo, M (2009) Missing and spurious interactions and the reconstruction of complex networks. Proceedings of the National Academy of Sciences of the United States of America *106*, 22073-22078.

Gundersen, GG, Bulinski, JC (1988) Selective stabilization of microtubules oriented toward the direction of cell migration. Proceedings of the National Academy of Sciences of the United States of America *85*, 5946-5950.

Hanson, PK, Malone, L, Birchmore, JL, Nichols, JW (2003) Lem3p is essential for the uptake and potency of alkylphosphocholine drugs, edelfosine and miltefosine. The Journal of biological chemistry *278*, 36041-36050.

Hao, Y, Boyd, L, Seydoux, G (2006) Stabilization of cell polarity by the C. elegans RING protein PAR-2. Developmental cell *10*, 199-208.

Hart, MJ, Eva, A, Evans, T, Aaronson, SA, Cerione, RA (1991) Catalysis of guanine nucleotide exchange on the CDC42Hs protein by the dbl oncogene product. Nature *354*, 311-314.

Hart, MJ, Eva, A, Zangrilli, D, Aaronson, SA, Evans, T, Cerione, RA, Zheng, Y (1994) Cellular transformation and guanine nucleotide exchange activity are catalyzed by a common domain on the dbl oncogene product. J Biol Chem *269*, 62-65.

Hartwell, LH, Culotti, J, Pringle, JR, Reid, BJ (1974) Genetic control of the cell division cycle in yeast. Science (New York, NY *183*, 46-51.

Hartwell, LH, Mortimer, RK, Culotti, J, Culotti, M (1973) Genetic Control of the Cell Division Cycle in Yeast: V. Genetic Analysis of cdc Mutants. Genetics *74*, 267-286.

Haupts, U, Maiti, S, Schwille, P, Webb, WW (1998) Dynamics of fluorescence fluctuations in green fluorescent protein observed by fluorescence correlation spectroscopy. Proceedings of the National Academy of Sciences of the United States of America *95*, 13573-13578.

Hess, ST, Webb, WW (2002) Focal volume optics and experimental artifacts in confocal fluorescence correlation spectroscopy. Biophysical journal *83*, 2300-2317.

Hoffman, GR, Nassar, N, Cerione, RA (2000) Structure of the Rho family GTP-binding protein Cdc42 in complex with the multifunctional regulator RhoGDI. Cell *100*, 345-356.

Huh, WK, Falvo, JV, Gerke, LC, Carroll, AS, Howson, RW, Weissman, JS, O'Shea, EK (2003) Global analysis of protein localization in budding yeast. Nature *425*, 686-691.

Ikeda, M, Kihara, A, Igarashi, Y (2006) Lipid asymmetry of the eukaryotic plasma membrane: functions and related enzymes. Biological & pharmaceutical bulletin *29*, 1542-1546.

Irazoqui, JE, Gladfelter, AS, Lew, DJ (2003) Scaffold-mediated symmetry breaking by Cdc42p. Nature cell biology *5*, 1062-1070.

Iwamoto, K, Kobayashi, S, Fukuda, R, Umeda, M, Kobayashi, T, Ohta, A (2004) Local exposure of phosphatidylethanolamine on the yeast plasma membrane is implicated in cell polarity. Genes Cells *9*, 891-903.

Johnson, DI (1999) Cdc42: An essential Rho-type GTPase controlling eukaryotic cell polarity. Microbiol Mol Biol Rev *63*, 54-105.

Johnson, JL, Erickson, JW, Cerione, RA (2009) New insights into how the Rho guanine nucleotide dissociation inhibitor regulates the interaction of Cdc42 with membranes. The Journal of biological chemistry *284*, 23860-23871.

Kato, U, Emoto, K, Fredriksson, C, Nakamura, H, Ohta, A, Kobayashi, T, Murakami-Murofushi, K, Kobayashi, T, Umeda, M (2002) A novel membrane protein, Ros3p, is required for phospholipid translocation across the plasma membrane in Saccharomyces cerevisiae. The Journal of biological chemistry *277*, 37855-37862.

Kim, SA, Heinze, KG, Schwille, P (2007) Fluorescence correlation spectroscopy in living cells. Nature methods *4*, 963-973.

Knaus, M, Pelli-Gulli, MP, van Drogen, F, Springer, S, Jaquenoud, M, Peter, M (2007) Phosphorylation of Bem2p and Bem3p may contribute to local activation of Cdc42p at bud emergence. The EMBO journal *26*, 4501-4513.

Kron, SJ, Styles, CA, Fink, GR (1994) Symmetric cell division in pseudohyphae of the yeast Saccharomyces cerevisiae. Molecular biology of the cell *5*, 1003-1022.

Lamson, RE, Winters, MJ, Pryciak, PM (2002) Cdc42 regulation of kinase activity and signaling by the yeast p21-activated kinase Ste20. Molecular and cellular biology *22*, 2939-2951.

Lechler, T, Jonsdottir, GA, Klee, SK, Pellman, D, Li, R (2001) A two-tiered mechanism by which Cdc42 controls the localization and activation of an Arp2/3-activating motor complex in yeast. The Journal of cell biology *155*, 261-270.

Lee, JO, Yang, H, Georgescu, MM, Di Cristofano, A, Maehama, T, Shi, Y, Dixon, JE, Pandolfi, P, Pavletich, NP (1999) Crystal structure of the PTEN tumor suppressor: implications for its phosphoinositide phosphatase activity and membrane association. Cell *99*, 323-334.

Lee, K, Gallop, JL, Rambani, K, Kirschner, MW (2010) Self-assembly of filopodia-like structures on supported lipid bilayers. Science (New York, NY *329*, 1341-1345.

Leslie, NR, Batty, IH, Maccario, H, Davidson, L, Downes, CP (2008) Understanding PTEN regulation: PIP2, polarity and protein stability. Oncogene *27*, 5464-5476.

Levin, SE, Zhang, C, Kadlecek, TA, Shokat, KM, Weiss, A (2008) Inhibition of ZAP-70 kinase activity via an analog-sensitive allele blocks T cell receptor and CD28 superagonist signaling. The Journal of biological chemistry *283*, 15419-15430.

Li, R, Bowerman, B (2010) Symmetry breaking in biology. Cold Spring Harbor perspectives in biology *2*, a003475.

Li, R, Gundersen, GG (2008) Beyond polymer polarity: how the cytoskeleton builds a polarized cell. Nature reviews *9*, 860-873.

Li, R, Zheng, Y, Drubin, DG (1995) Regulation of cortical actin cytoskeleton assembly during polarized cell growth in budding yeast. The Journal of cell biology *128*, 599-615.

Ma, H, Kunes, S, Schatz, PJ, Botstein, D (1987) Plasmid construction by homologous recombination in yeast. Gene *58*, 201-216.

Machacek, M, Hodgson, L, Welch, C, Elliott, H, Pertz, O, Nalbant, P, Abell, A, Johnson, GL, Hahn, KM, Danuser, G (2009) Coordination of Rho GTPase activities during cell protrusion. Nature *461*, 99-103.

Marco, E, Wedlich-Soldner, R, Li, R, Altschuler, SJ, Wu, LF (2007) Endocytosis optimizes the dynamic localization of membrane proteins that regulate cortical polarity. Cell *129*, 411-422.

Martin-Belmonte, F, Gassama, A, Datta, A, Yu, W, Rescher, U, Gerke, V, Mostov, K (2007) PTEN-mediated apical segregation of phosphoinositides controls epithelial morphogenesis through Cdc42. Cell *128*, 383-397.

Martin, BR, Giepmans, BN, Adams, SR, Tsien, RY (2005) Mammalian cell-based optimization of the biarsenical-binding tetracysteine motif for improved fluorescence and affinity. Nature biotechnology *23*, 1308-1314.

Masuda, T, Tanaka, K, Nonaka, H, Yamochi, W, Maeda, A, Takai, Y (1994) Molecular cloning and characterization of yeast rho GDP dissociation inhibitor. The Journal of biological chemistry *269*, 19713-19718.

Matus, A, Bernhardt, R, Hugh-Jones, T (1981) High molecular weight microtubule-associated proteins are preferentially associated with dendritic microtubules in brain. Proceedings of the National Academy of Sciences of the United States of America *78*, 3010-3014.

McGrath, JP, Varshavsky, A (1989) The yeast STE6 gene encodes a homologue of the mammalian multidrug resistance P-glycoprotein. Nature *340*, 400-404.

Motegi, F, Sugimoto, A (2006) Sequential functioning of the ECT-2 RhoGEF, RHO-1 and CDC-42 establishes cell polarity in Caenorhabditis elegans embryos. Nature cell biology *8*, 978-985.

Munro, E, Nance, J, Priess, JR (2004) Cortical flows powered by asymmetrical contraction transport PAR proteins to establish and maintain anterior-posterior polarity in the early C. elegans embryo. Developmental cell *7*, 413-424.

Nakada, C, Ritchie, K, Oba, Y, Nakamura, M, Hotta, Y, Iino, R, Kasai, RS, Yamaguchi, K, Fujiwara, T, Kusumi, A (2003) Accumulation of anchored proteins forms membrane diffusion barriers during neuronal polarization. Nature cell biology *5*, 626-632.

Natarajan, P, Wang, J, Hua, Z, Graham, TR (2004) Drs2p-coupled aminophospholipid translocase activity in yeast Golgi membranes and relationship to in vivo function. Proceedings of the National Academy of Sciences of the United States of America *101*, 10614-10619.

Nern, A, Arkowitz, RA (2000) Nucleocytoplasmic shuttling of the Cdc42p exchange factor Cdc24p. The Journal of cell biology *148*, 1115-1122.

Newman, MEJ, Girvan, M (2004) Finding and evaluating community structure in networks. Phys Rev E *69*, no. 026113.

Onsum, MD, Rao, CV (2009) Calling heads from tails: the role of mathematical modeling in understanding cell polarization. Current opinion in cell biology *21*, 74-81.

Palazzo, AF, Joseph, HL, Chen, YJ, Dujardin, DL, Alberts, AS, Pfister, KK, Vallee, RB, Gundersen, GG (2001) Cdc42, dynein, and dynactin regulate MTOC reorientation independent of Rho-regulated microtubule stabilization. Curr Biol *11*, 1536-1541.

Piekny, A, Werner, M, Glotzer, M (2005) Cytokinesis: welcome to the Rho zone. Trends in cell biology *15*, 651-658.

Pomorski, T, Lombardi, R, Riezman, H, Devaux, PF, van Meer, G, Holthuis, JC (2003) Drs2p-related P-type ATPases Dnf1p and Dnf2p are required for phospholipid translocation across the yeast plasma membrane and serve a role in endocytosis. Molecular biology of the cell *14*, 1240-1254.

Pomorski, T, Menon, AK (2006) Lipid flippases and their biological functions. Cell Mol Life Sci *63*, 2908-2921.

Poste, G, Papahadjopoulos, D., and Vail, W.J. (1976) Lipid Vesicles as Carriers for Introducing Biologically Active Materials into Cells. In Methods in Cell Biology (New York, Academic Press, Inc.).

Pruyne, D, Bretscher, A (2000a) Polarization of cell growth in yeast. Journal of cell science *113 (Pt 4)*, 571-585.

Pruyne, D, Bretscher, A (2000b) Polarization of cell growth in yeast. I. Establishment and maintenance of polarity states. Journal of cell science *113 (Pt 3)*, 365-375.

Ptacek, J, Devgan, G, Michaud, G, Zhu, H, Zhu, X, Fasolo, J, Guo, H, Jona, G, Breitkreutz, A, Sopko, R, McCartney, RR, Schmidt, MC, Rachidi, N, Lee, SJ, Mah, AS, Meng, L, Stark, MJ, Stern, DF, De Virgilio, C, Tyers, M, Andrews, B, Gerstein, M, Schweitzer, B, Predki, PF, Snyder, M (2005) Global analysis of protein phosphorylation in yeast. Nature *438*, 679-684.

Redfern, RE, Redfern, D, Furgason, ML, Munson, M, Ross, AH, Gericke, A (2008) PTEN phosphatase selectively binds phosphoinositides and undergoes structural changes. Biochemistry *47*, 2162-2171.

Richman, TJ, Toenjes, KA, Morales, SE, Cole, KC, Wasserman, BT, Taylor, CM, Koster, JA, Whelihan, MF, Johnson, DI (2004) Analysis of cell-cycle specific localization of the Rdi1p RhoGDI and the structural determinants required for Cdc42p membrane localization and clustering at sites of polarized growth. Current genetics *45*, 339-349.

Rigler, R, Foldes-Papp, Z, Meyer-Almes, FJ, Sammet, C, Volcker, M, Schnetz, A (1998) Fluorescence cross-correlation: a new concept for polymerase chain reaction. Journal of biotechnology *63*, 97-109.

Robinson, LC, Menold, MM, Garrett, S, Culbertson, MR (1993) Casein kinase I-like protein kinases encoded by YCK1 and YCK2 are required for yeast morphogenesis. Molecular and cellular biology *13*, 2870-2881.

Roelants, FM, Baltz, AG, Trott, AE, Fereres, S, Thorner, J (2010) A protein kinase network regulates the function of aminophospholipid flippases. Proceedings of the National Academy of Sciences of the United States of America *107*, 34-39.

Ron, D, Zannini, M, Lewis, M, Wickner, RB, Hunt, LT, Graziani, G, Tronick, SR, Aaronson, SA, Eva, A (1991) A region of *proto-dbl* essential for its transforming activity

shows sequence similarity to a yeast cell cycle gene, cdc24, and the human breakpoint cluster gene, *bcr*. New Biol *3*, 372-379.

Saito, K, Fujimura-Kamada, K, Furuta, N, Kato, U, Umeda, M, Tanaka, K (2004) Cdc50p, a protein required for polarized growth, associates with the Drs2p P-type ATPase implicated in phospholipid translocation in Saccharomyces cerevisiae. Molecular biology of the cell *15*, 3418-3432.

Saito, K, Fujimura-Kamada, K, Hanamatsu, H, Kato, U, Umeda, M, Kozminski, KG, Tanaka, K (2007) Transbilayer phospholipid flipping regulates Cdc42p signaling during polarized cell growth via Rga GTPase-activating proteins. Developmental cell *13*, 743-751.

Sales-Pardo, M, Guimera, R, Moreira, AA, Amaral, LA (2007) Extracting the hierarchical organization of complex systems. Proceedings of the National Academy of Sciences of the United States of America *104*, 15224-15229.

Servant, G, Weiner, OD, Herzmark, P, Balla, T, Sedat, JW, Bourne, HR (2000) Polarization of chemoattractant receptor signaling during neutrophil chemotaxis. Science (New York, NY *287*, 1037-1040.

Shimada, Y, Gulli, MP, Peter, M (2000) Nuclear sequestration of the exchange factor Cdc24 by Far1 regulates cell polarity during yeast mating. Nature cell biology *2*, 117-124.

Siniossoglou, S, Pelham, HR (2001) An effector of Ypt6p binds the SNARE Tlg1p and mediates selective fusion of vesicles with late Golgi membranes. The EMBO journal *20*, 5991-5998.

Slaughter, B, Li, R (2006) Toward a molecular interpretation of the surface stress theory for yeast morphogenesis. Current opinion in cell biology *18*, 47-53.

Slaughter, BD, Das, A, Schwartz, JW, Rubinstein, B, Li, R (2009) Dual modes of cdc42 recycling fine-tune polarized morphogenesis. Dev Cell *17*, 823-835.

Slaughter, BD, Li, R (2010) Toward quantitative "in vivo biochemistry" with fluorescence fluctuation spectroscopy. Molecular biology of the cell *21*, 4306-4311.

Slaughter, BD, Schwartz, JW, Li, R (2007) Mapping dynamic protein interactions in MAP kinase signaling using live-cell fluorescence fluctuation spectroscopy and imaging. Proceedings of the National Academy of Sciences of the United States of America *104*, 20320-20325.

Snaith, HA, Sawin, KE (2003) Fission yeast mod5p regulates polarized growth through anchoring of tea1p at cell tips. Nature *423*, 647-651.

Solecki, DJ, Model, L, Gaetz, J, Kapoor, TM, Hatten, ME (2004) Par6alpha signaling controls glial-guided neuronal migration. Nature neuroscience *7*, 1195-1203.

Stefan, CJ, Audhya, A, Emr, SD (2002) The yeast synaptojanin-like proteins control the cellular distribution of phosphatidylinositol (4,5)-bisphosphate. Molecular biology of the cell *13*, 542-557.

Stevens, HC, Malone, L, Nichols, JW (2008) The putative aminophospholipid translocases, DNF1 and DNF2, are not required for 7-nitrobenz-2-oxa-1,3-diazol-4-yl-

phosphatidylserine flip across the plasma membrane of Saccharomyces cerevisiae. The Journal of biological chemistry *283*, 35060-35069.

Storey, JD, Tibshirani, R (2003) Statistical significance for genomewide studies. Proceedings of the National Academy of Sciences of the United States of America *100*, 9440-9445.

Thompson, NL (1991) Fluorescence Correlation Spectroscopy.Topics in Fluorescence Spectroscopy (New York, Plenum Press).

Tiedje, C, Sakwa, I, Just, U, Hofken, T (2008) The Rho GDI Rdi1 Regulates Rho GTPases by Distinct Mechanisms. Molecular biology of the cell *19*, 2885-2896.

Valdez-Taubas, J, Pelham, HR (2003) Slow diffusion of proteins in the yeast plasma membrane allows polarity to be maintained by endocytic cycling. Curr Biol *13*, 1636-1640.

Vazquez, F, Matsuoka, S, Sellers, WR, Yanagida, T, Ueda, M, Devreotes, PN (2006) Tumor suppressor PTEN acts through dynamic interaction with the plasma membrane. Proceedings of the National Academy of Sciences of the United States of America *103*, 3633-3638.

Vida, TA, Emr, SD (1995) A new vital stain for visualizing vacuolar membrane dynamics and endocytosis in yeast. The Journal of cell biology *128*, 779-792.

Watts, JL, Etemad-Moghadam, B, Guo, S, Boyd, L, Draper, BW, Mello, CC, Priess, JR, Kemphues, KJ (1996) par-6, a gene involved in the establishment of asymmetry in early C. elegans embryos, mediates the asymmetric localization of PAR-3. Development (Cambridge, England) *122*, 3133-3140.

Wedlich-Soldner, R, Altschuler, S, Wu, L, Li, R (2003) Spontaneous cell polarization through actomyosin-based delivery of the Cdc42 GTPase. Science (New York, NY *299*, 1231-1235.

Wedlich-Soldner, R, Wai, SC, Schmidt, T, Li, R (2004) Robust cell polarity is a dynamic state established by coupling transport and GTPase signaling. The Journal of cell biology *166*, 889-900.

Wei, M, Fabrizio, P, Madia, F, Hu, J, Ge, H, Li, LM, Longo, VD (2009) Tor1/Sch9-regulated carbon source substitution is as effective as calorie restriction in life span extension. PLoS genetics *5*, e1000467.

Wiggin, GR, Fawcett, JP, Pawson, T (2005) Polarity proteins in axon specification and synaptogenesis. Developmental cell *8*, 803-816.

Wild, AC, Yu, JW, Lemmon, MA, Blumer, KJ (2004) The p21-activated protein kinase-related kinase Cla4 is a coincidence detector of signaling by Cdc42 and phosphatidylinositol 4-phosphate. The Journal of biological chemistry *279*, 17101-17110.

Wilson, KL, Herskowitz, I (1984) Negative regulation of STE6 gene expression by the alpha 2 product of Saccharomyces cerevisiae. Molecular and cellular biology *4*, 2420-2427.

Witte, H, Neukirchen, D, Bradke, F (2008) Microtubule stabilization specifies initial neuronal polarization. The Journal of cell biology *180*, 619-632.

Wodarz, A, Nathke, I (2007) Cell polarity in development and cancer. Nature cell biology *9*, 1016-1024.

Yeung, T, Gilbert, GE, Shi, J, Silvius, J, Kapus, A, Grinstein, S (2008) Membrane phosphatidylserine regulates surface charge and protein localization. Science (New York, NY *319*, 210-213.

Young, ME, Karpova, TS, Brugger, B, Moschenross, DM, Wang, GK, Schneiter, R, Wieland, FT, Cooper, JA (2002) The Sur7p family defines novel cortical domains in Saccharomyces cerevisiae, affects sphingolipid metabolism, and is involved in sporulation. Molecular and cellular biology *22*, 927-934.